

**STUDIES OF DNA REPAIR BY DNA
PHOTOLYASE**

by

Oliver Ladebeck

**A thesis submitted to
Cardiff University
for the degree of
DOCTOR OF PHILOSOPHY**

**School of Chemistry
Cardiff University
May 2010**

UMI Number: U585345

All rights reserved

INFORMATION TO ALL USERS

The quality of this reproduction is dependent upon the quality of the copy submitted.

In the unlikely event that the author did not send a complete manuscript and there are missing pages, these will be noted. Also, if material had to be removed, a note will indicate the deletion.



UMI U585345

Published by ProQuest LLC 2013. Copyright in the Dissertation held by the Author.
Microform Edition © ProQuest LLC.


All rights reserved. This work is protected against
unauthorized copying under Title 17, United States Code.



ProQuest LLC
789 East Eisenhower Parkway
P.O. Box 1346
Ann Arbor, MI 48106-1346

DECLARATION

This work has not previously been accepted in substance for any degree and is not concurrently submitted in candidature for any degree.

Signed 

Date 21/05/2010

STATEMENT 1

This thesis is being submitted in partial fulfilment of the requirements for the degree of PhD

Signed 

Date 21/05/2010

STATEMENT 2

This thesis is the result of my own independent work/investigation, except where otherwise stated.

Other sources are acknowledged by explicit references.

Signed 

Date 21/05/2010

STATEMENT 3

I hereby give consent for my thesis, if accepted, to be available for photocopying and for inter-library loan, and for the title and summary to be made available to outside organisations.

Signed 

Date 21/05/2010

Acknowledgements

I would like to express my sincere gratitude to Professor Gerald Richter, for providing me an opportunity to perform my Ph.D. study in Exeter and Cardiff. His wide knowledge and logical way of thinking have been of great value for me. His understanding, encouraging and personal guidance have provided a good basis for the present thesis. I am deeply grateful to Professor Rudolf K. Allemann, for providing me laboratory space during my time at Cardiff University, his allowance to use his equipment and chemicals when needed and for his detailed and constructive comments during the Chemical Biology group meetings and half-year vivas.

I wish to express my warm and sincere thanks to Dr. Andrew M. Shaw and Dr. Maxim Rooth from the University of Exeter who introduced me to the field of SPR and EW-CRDS. For their outstanding co-operation, their valuable advices and extensive discussions around our experiments have been very helpful for this study.

I have greatest regards and I wish to extend my warmest thanks to all my colleagues for everything they did to support me: My friends and workmates Piotr Wysoczanski, Thomas Fricke and Dr. Robert Mart. To Dr. Amy Baldwin for proof reading my work, Rhys Charles, Gwen and Robin Batten, Dr. Dave Miller, Dr. Mahmoud Akthar, Dr. Joel Loveridge, Dr. James E. Redman, Nicolas Dellus and last but not least a big thank you to Terry Dumelow.

A very special gratitude is due to my parents for their loving support, without their encouragement and understanding it would have been impossible for me to finish this work.

Abstract

Cyclobutane pyrimidine dimers (CPDs) are the major photo products that can occur in DNA after UV-light exposure. Detrimental effects of CPDs for organisms can be prevented by the DNA repair enzyme DNA photolyase. This protein repairs CPDs by a light induced (300-500 nm) electron transfer involving a non-covalently bound cofactor, FAD. The key role of FAD in the catalytic DNA repair can be investigated by replacing FAD in the enzyme with FAD analogues and compare the activity of wild-type enzyme to the mutant enzyme.

As a part of this study, a stable expression system of photolyase was created and the enzyme was purified in concentrations in the μM range. The FAD analogue roseoFAD was biochemically synthesised from its precursor form roseoflavin. FAD was extracted from photolyase by unfolding the enzyme using the effects of denaturing agents or changes in buffer pH values. The protein was successfully refolded in the presence of roseoFAD and its integration into the proteins active site was confirmed by UV/Vis spectroscopy.

Surface plasmon resonance spectroscopy (SPR) was used to monitor DNA repair by photolyase in real-time. For this purpose photolyase was overexpressed and purified. CPDs, the substrate of photolyase, were produced by UV irradiation of poly-T oligonucleotides. SPR signals were detected for steps of the repair process such as enzyme-substrate complex formation, DNA repair and release of product. Changes in SPR signals were used to obtain the kinetics of DNA repair by measuring the k_{on} and k_{off} rates and calculating the rate constants for substrate binding and product release. According to the data obtained the dissociation constant K_D was calculated and found to be in good agreement with published values obtained by different methods.

Table of contents

1. Introduction	1
1.1 Aim of work described in this thesis	2
1.2 DNA and its sensitivity to mutations	4
1.3 Common mutations in the genome	4
1.4 Ultra Violet (UV) light and its mutagenic potential on DNA	5
1.4.1 Photochemistry of DNA	6
1.4.2 Cyclobutane pyrimidine dimers	7
1.4.3 (6-4) Photoproducts	9
1.5 DNA repair mechanisms	12
1.6 DNA photolyases	18
1.6.1 General background	18
1.6.2 Structure of <i>E. coli</i> CPD photolyase	21
1.6.3 Cofactors of <i>E. coli</i> CPD photolyase	25
1.6.4 Reaction mechanism of DNA repair (photoreactivation)	27
1.6.5 Photoactivation	29
1.7 Two putative electron transfer mechanisms	31
2. Materials and Methods	35
2.1 Materials	36
2.1.1 Instruments	36
2.1.2 Enzymes	38
2.1.3 Media	38
2.1.4 Buffers and solutions	39

2.1.5	Bacterial strains	46
2.1.6	Plasmids	47
2.1.7	Primers	47
2.2	Molecular-biological methods	48
2.2.1	Amplification of DNA using Polymerase Chain Reaction (PCR)	48
2.2.2	Agarose gel electrophoresis	49
2.2.3	Purification of DNA	50
2.2.4	Restricion of DNA	51
2.2.5	Ligation of DNA fragments	52
2.2.6	Preparation of chemical competent cells	53
2.2.7	Heat shock transformation	53
2.2.8	Plasmid isolation	54
2.3	Protein chemical methods	55
2.3.1	Culture preservation	55
2.3.2	Protein expression	55
2.3.3	Testing of protein expression	56
2.3.4	SDS polyacrylamide gel electrophoresis	56
2.3.5	Expression of the DNA photolyase E109A mutant	58
2.3.6	Expression of DNA photolyase containing a 10 x His tag	58
2.3.7	Expression of FAD synthetase from <i>C. ammoniagenes</i>	58
2.3.8	Protein extraction	59
2.3.9	Protein purification	60
2.3.9.1	Purification of <i>C. ammoniagenes</i> FAD synthetase	60
2.3.9.2	Purification of DNA photolyase E109A mutant	60

2.3.9.3 Purification of photolyase with 10x His tag	62
2.3.10 Protein concentration by ultrafiltration	63
2.3.11 Determination of protein concentration	63
2.4 Enzymatic conversion of roseoflavin to roseoFAD	65
2.4.1 Purification of roseoFAD	66
2.4.2 Determination of concentration of roseoflavin and roseoFAD	66
2.4.3 Reconstitution of photolyase with roseoFAD	67
2.4.3.1 Reconstitution of photolyase via Ni-NTA	67
2.4.3.2 Reconstitution of photolyase via dialysis	67
2.4.3.3 Reconstitution of photolyase via phenylsepharose 6 FF	68
2.5 Photolyase purification and substrate preparation for the SPR/ EW-CRDS experiments	69
2.5.1 Substrate preparation	69
2.5.2 Photolyase purification	71
3. FAD exchange in DNA photolyase	77
3.1 Work described in Chapter 3	78
3.2 Reconstitution of apophotolyase with FAD cofactors and cofactor analogs	79
3.3 Roseoflavin as a natural flavin analog	82
3.4 Results and Discussion	85
3.4.1 Production of a stable expression system for <i>E. coli</i> photolyase	85
3.4.1.1 PCR of the <i>phr</i> gene and digestion	85
3.4.1.2 Isolation and digestion of expression vector pET-19b	86

3.4.1.3	Ligation and transformation	87
3.4.1.4	Protein expression and protein purification	91
3.4.2	Purification of FAD synthetase from <i>C. ammoniagenes</i>	97
3.4.3	Catalytic conversion of roseoflavin to roseoFAD	98
3.4.4	Reconstitution of <i>E. coli</i> photolyase with FAD and roseoFAD	101
3.4.4.1	Reconstitution of photolyase with FAD on Ni-NTA Sepharose column	102
3.4.4.2	Reconstitution of photolyase with roseoFAD via dialysis	106
3.4.4.3	Reconstitution of photolyase with roseoFAD using Phenylsepharose 6 FF	108
3.5	Conclusion	113
4.	Surface Plasmon Resonance spectroscopy on DNA photolyase	115
4.1	Work described in Chapter 4	116
4.2	Introduction	117
4.3	Surface Plasmon Resonance spectroscopy (SPR)	118
4.4	Combination of SPR with evanescent wave cavity ring-down spectroscopy (EW-CRDS)	121
4.5	SPR experiments with CPD photolyase and DNA	124
4.5.1	Binding DNA to the SPR sensor chip	125
4.5.2	DNA photolyase-binding to gold nanoparticles with different self-assembled monolayers	131
4.5.3	Photolyase–DNA binding and DNA repair detection in real time	136

4.6 Conclusion	155
5. General conclusions and future work	157
6. References	161

List of figures

Figure 1.1: <i>The molecular structure of FAD</i>	2
Figure 1.2: <i>Spectral wavelength region of sunlight</i>	5
Figure 1.3: <i>Crystal structure of a single CPD (T<>T) lesion in a DNA decamer.</i>	9
Figure 1.4: <i>The crystal structure of a T<>T (6-4) photoproduct in a DNA decamer duplex</i>	11
Figure 1.5: <i>Nucleotides modified by deamination, oxidation or alkylation</i>	14
Figure 1.6: <i>Cofactors associated with photolyases</i>	20
Figure 1.7: <i>Model of crystal structure of CPD photolyase from E. coli</i>	22
Figure 1.8: <i>Model of crystal structure of photolyase solvent exposed surface</i>	24
Figure 1.9: <i>Different redox states of FAD in photolyase</i>	25
Figure 1.10: <i>Two proposed electron transfer pathways based on the orientation of FAD and a thymine dimer in the crystal structure of CPD photolyase from A. nidulans</i>	32
Figure 2.1: <i>Time course of the photodamage of ssDNA oligo-(dT)₁₈</i>	70
Figure 2.2: <i>FPLC-chromatogram of photolyase purification via Blue Sepharose</i>	72

Figure 2.3: 12% SDS-PAGE of eluted protein fractions after Blue Sepharose purification	72
Figure 2.4: FPLC-chromatogram of photolyase purification on a desalting column	73
Figure 2.5: FPLC-chromatogram of photolyase purification via Heparin Sepharose	74
Figure 2.6: 12% SDS-PAGE of eluted protein fractions after chromatography on Heparin Sepharose.	74
Figure 2.7: UV/Vis spectrum of photolyase after protein purification	75
Figure 2.8: Time course of the photo repair of ssDNA oligo-(dT) ₁₈ over a period of 53 min	76
Figure 3.1: Riboflavin derivatives used for reconstitution experiments	80
Figure 3.2: Chemical structures of riboflavin and roseoflavin	82
Figure 3.3: Direct comparison of the absorbance spectra of riboflavin and roseoflavin	84
Figure 3.4: 0.8 % agarose gel of <i>phr</i> PCR products	86
Figure 3.5: 0.8% agarose gel of the linearised vector <i>pET-19b</i>	87
Figure 3.6: 0.8% agarose gel is showing the empty vector <i>pET-19b</i>	88
Figure 3.7: Vector map of <i>pET-19b-phr-5.2</i>	89
Figure 3.8: The vector sequence for the expression vector <i>pET-19b-phr-5.2</i>	91

Figure 3.9: <i>12% SDS-PAGE of photolyase overexpression in BL21 (DE3)</i>	92
Figure 3.10: <i>FPLC chromatogram of photolyase purification via Ni-NTA-Sepharose</i>	93
Figure 3.11: <i>12 % SDS PAGE after photolyase purification by Ni-NTA-Sepharose</i>	93
Figure 3.12: <i>12 % SDS-PAGE of concentrated E. coli photolyase</i>	94
Figure 3.13: <i>UV/Vis spectrum of E. coli DNA photolyase</i>	95
Figure 3.14: <i>Time course of the photo repair of ssDNA oligo-(dT)₁₈ by photolyase</i>	96
Figure 3.15: <i>12 % SDS-PAGE of FAD synthetase from C. ammoniagenes fused to maltose binding protein</i>	97
Figure 3.16: <i>ESI-MS mass spectrum of roseoFAD</i>	100
Figure 3.17: <i>Model of the FAD binding site in DNA photolyase occupied by roseoFAD containing a dimethyl amino group on its C8</i>	101
Figure 3.18: <i>12 % SDS-PAGE of photolyase after denaturation and reconstitution with FAD</i>	103
Figure 3.19: <i>UV/Vis spectrum of photolyase reconstituted with FAD</i>	104
Figure 3.20: <i>12 % SDS-PAGE of apophotolyase after elution from Ni-NTA-Sepharose</i>	107
Figure 3.21: <i>UV/Vis spectrum of apophotolyase in elution buffer containing 8 M urea</i>	107

Figure 3.22: <i>12% SDS PAGE of photolyase after Ni-NTA Sepharose purification</i>	108
Figure 3.23: <i>UV/Vis spectrum of E. coli photolyase</i>	109
Figure 3.24: <i>Absorption spectrum of photolyase fractions</i>	110
Figure 3.25: <i>Absorption spectrum of roseoFAD free in buffer and when bound to photolyase</i>	111
Figure 3.26: <i>Comparison of the absorption spectrum of photolyase containing wild-type cofactor FAD in its oxidised form and absorption spectrum of photolyase containing roseoFAD in its oxidised form</i>	112
Figure 3.27: <i>Absorption spectrum of free roseoFMN and when binding to the LOV 1 domain of C. reinhardtii</i>	113
Figure 4.1: <i>Total internal reflection</i>	118
Figure 4.2: <i>Surface plasmons in a thin metal gold film</i>	
Figure 4.3: <i>The EW-CRDS apparatus designed for SPR experiments</i>	122
Figure 4.4: <i>Shift in the surface plasmon band affecting the extinction</i>	123
Figure 4.5: <i>The prism surface coated with gold nanoparticles</i>	124
Figure 4.6: <i>The detection of a decrease in the refractive index after binding poly-T and UV damaged poly-T to a clean gold surface</i>	127
Figure 4.7: <i>The detection of a decrease in the refractive index after binding damaged poly-T to a cysteine SAM gold nanoparticle surface</i>	128

Figure 4.8: <i>Detection of an increase in the refractive index after binding single stranded salmon sperm DNA to a cysteine SAM gold nanoparticle surface</i>	129
Figure 4.9: <i>L-cysteine, 4-aminothiophenol and thioctic acid utilised for self-assembled monolayers</i>	132
Figure 4.10: <i>SPR response after the binding of photolyase to three different SAM functionalised gold surfaces</i>	132
Figure 4.11: <i>SPR response after the binding of photolyase to plain gold nanoparticle</i>	133
Figure 4.12: <i>SPR sensogram of UV-light damaged ssDNA oligo-(pT)₁₈ binding to photolyase</i>	137
Figure 4.13: <i>The SPR sensogram for the photo-repair of UV light irradiated ssDNA oligo-(pT)₁₈ by photolyase.</i>	139
Figure 4.14: <i>The SPR sensogram of DNA repair by photolyase when binding UV-damaged ssDNA oligo-(pT)₁₈ to gold nanoparticles functionalised with cysteine SAM.</i>	141
Figure 4.15: <i>The SPR Sensogram is showing changes in the refractive index produced by the heating effect of the blue LED used during the SPR experiments.</i>	142
Figure 4.16: <i>SPR sensogram of a repeated experiment showing the photo-repair of UV light irradiated oligo-(dT)₁₈ by photolyase.</i>	144
Figure 4.17: <i>Detailed view on the SPR signal associated with binding of damaged oligo-(dT)₁₈ to photolyase and initialising DNA repair</i>	145

Figure 4.18: <i>The SPR sensogram is showing the variability in changes in the refractive index for the binding of UV-damaged ssDNA oligo-(pT)₁₈ to photolyase</i>	148
Figure 4.19: <i>The SPR sensogram of DNA repair by photolyase binding UV-damaged ssDNA oligo-(pT)₁₈ first to gold nanoparticles modified with a cysteine SAM and then injecting photolyase to the system.</i>	150
Figure 4.20: <i>The sensogram of photolyase with FAD in its oxidised form binding to UV-damaged ssDNA oligo-(pT)₁₈ and illumination with blue light.</i>	153
Figure 4.21: <i>Detailed view on the SPR signal associated with binding of damaged ssDNA oligo-(pT)₁₈ to oxidised photolyase and initialising DNA repair</i>	154

List of schemes

Scheme 1.1: <i>Formation of a (cis-syn) thymine dimer</i>	7
Scheme 1.2: <i>Formation of the 6-4 photoproduct</i>	10
Scheme 1.3: <i>Scheme of the NER pathway</i>	13
Scheme 1.4: <i>Scheme of the BER pathway</i>	15
Scheme 1.5: <i>The postulated mechanism of DNA repair by CPD photolyase</i>	28
Scheme 1.6: <i>Different redox states of FAD</i>	29
Scheme 1.7: <i>Reaction and time scheme of electron transfers during photoactivation</i>	30
Scheme 3.1: <i>Pathway of the enzymatic conversion of roseoflavin to roseoFAD</i>	99

List of tables

Table 1.1: <i>UV absorption maxima of the four nucleotides</i>	6
Table 2.1: <i>E. coli strains</i>	46
Table 2.2: <i>B. subtilis strain</i>	46
Table 2.3: <i>Plasmids</i>	47
Table 2.4: <i>Primers</i>	47
Table 2.5: <i>PCR temperature and time scheme</i>	49
Table: 2.6: <i>Molar extinction coefficients of DNA photolyase from E. coli at different oxidation states</i>	64
Table 4.1: <i>The association rate constants k_a and dissociation constants K_D for photolyase binding to gold nanoparticles functionalised with different SAMs</i>	134
Table 4.2: <i>The association rate constant k_{on} and equilibrium dissociation constant K_d for the binding of UV-light damaged ssDNA oligo-(pT)₁₈ to photolyase in the radical form is listed as well as the dissociation rate constant k_{off} and the equilibrium dissociation constant K_d of DNA after initialising the repair</i>	146
Table 4.3: <i>The association rate constant k_a and equilibrium dissociation constant K_d for the binding of UV-light damaged ssDNA oligo-(pT)₁₈ to photolyase in the oxidised state</i>	154

List of abbreviations

Abbreviations:

8-HDF	8-Hydroxy-5-deazaflavin
Å	Ångstrom
ADP	Adenosine-5'-diphosphate
AMP	Adenosine-5'-monophosphate
APS	Ammonium peroxide sulphate
ATP	Adenosine-5'-triphosphate
bp	Base pair
CPD	Cyclobutane pyrimidine dimers
Da	Dalton
DNA	Deoxyribonucleic acid
dNTP	Deoxynucleotide triphosphate
DTT	Dithiothreitol
EDTA	Ethylenediaminetetraacetic acid
ENDOR	Electron nuclear double resonance
EPR	Electron paramagnetic resonance
ESI-MS	Electrospray ionization mass spectrometry
EW-CRDS	Evanescent wave cavity ring down spectroscopy
FAD	Flavin adenine dinucleotide
FMN	Flavin mononucleotide
FPLC	Fast protein liquid chromatography

h	hour
HEPES	4-[2-Hydroxyethyl]-1-piperazineethanesulfonic acid
IPTG	Isopropyl- β -thiogalactopyranoside
IC	Internal conversion
ISC	Inter system crossing
kDa	kilo Dalton
LB-Medium	Luria-Bertani medium
LED	Light-emitting diode
LOV	Light oxygen voltage
min	Minute
MTHF	Methenyltetrahydrofolate
MWCO	Molecular weight cut off
NADP	Nicotinamide adenine dinucleotide phosphate
NTA	Nitrilotriacetic acid
NMR	Nuclear magnetic resonance
OD	Optical density
PAGE	Polyacrylamide gel electrophoresis
PCR	Polymerase chain reaction
PMSF	Phenylmethanesulphonylfluoride
RNA	Ribonucleic acid
RT	Room temperature
s	Second
SDS	Sodiumdodecyl sulphate
SDS-PAGE	Sodiumdodecylsulphate polyacrylamide electrophoresis
SPR	Surface plasmon resonance

Taq	<i>Thermus aquaticus</i>
TEMED	Tetramethylethylenediamine
Tris	Tris-(hydroxymethyl)-aminomethane
UV	Ultra violet
Vis	visible
TLC	Thin layer chromatography

CHAPTER 1:

Introduction

1. 1 Aim of the work described in this thesis

When this study was begun, the unique reaction mechanism of photo repair by DNA photolyase was still not completely clarified. The contribution of the cofactor FAD, with attention of the role of its C8 α methyl group in the electron transfer during the DNA repair, is still of interest. The purpose of this study was to incorporate FAD analogues into the active site of photolyase, which are predominantly modified on the C8 α . The attempt was to establish an *in vitro* method for replacing the wild-type cofactor FAD with roseoFAD a natural occurring flavin analogue, which carries a dimethyl amino group on its C8 atom (Figure 1.1).

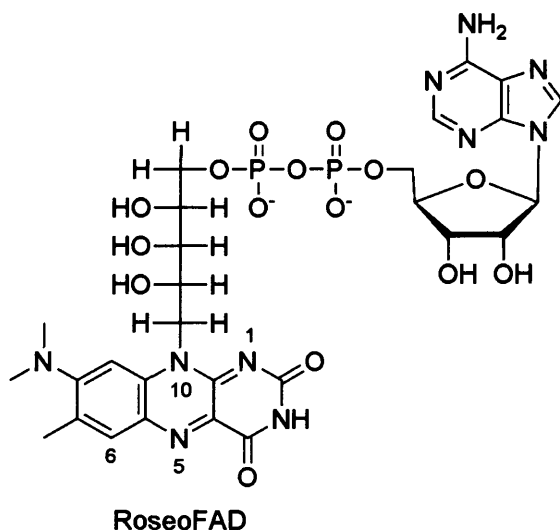


Figure 1.1: *The molecular structure of roseoFAD*

If the cofactor exchange would be successfully performed the comparison of the action spectrum of wild-type photolyase with the modified enzyme would give an updated exploration about the role of FAD during DNA repair. The FADH[•] radical is an essential intermediate step during the catalytic cycle and the influence a modified

C8 α -group would have for radical formation could be observed by utilising radical sensitive spectroscopy methods like EPR and ENDOR.

The second project described in this thesis made use of the spectroscopic method of Surface Plasmon Resonance (SPR). SPR can be applied for the direct observation of molecular interactions in real time. As a part of this thesis, SPR was combined with a second spectroscopic method, evanescent wave cavity ring-down spectroscopy (EW-CRDS) with the attempt to investigate if the combination of these two techniques would result in an increase of sensitivity with respect to the obtained signals indicating for molecular interactions. The interaction of UV light damaged DNA and its repair by the enzyme photolyase was chosen as a promising model to analyse the application of SPR and EW-CRDS. Utilising both spectroscopic methods could firstly result into a more detailed investigation on the rate constants and equilibrium constants of photolyase-DNA interaction by comparing obtained data with existing literature values. Secondly it would establish SPR and EW-CRDS as a new, perhaps more sensitive method for detecting complex biomolecular interactions such as enzyme-substrate interactions.

1.2 DNA and its sensitivity to mutations

Genetic information in prokaryotic and eukaryotic cells is encoded by DNA using the four nucleotide bases: adenine (A), thymine (T), guanine (G) and cytosine (C). The nucleotide sequences exist most commonly as double-stranded DNA and define the configuration of the cell and its proteins. Although DNA is a stable macromolecule it is vulnerable to natural modifications. These mutations are permanent changes in the base sequence of DNA. They are heritable and can arise as spontaneous errors in DNA replication through meiotic recombination or may be induced by mutagenic compounds (Cooper and Grover, 1990), UV-light (Hu, 1990) or ionising radiation (Goodhead, 1989). A certain small mutation rate in the genome is essential to enable evolutionary development of species adapting to their environment. However, a high mutation rate, if unrepaired, is typically detrimental and can even be lethal.

1.3 Common mutations in the genome

There are several types of genetic defects: genome-mutations, chromosome-mutations and gene- or point-mutations (Knippers, 2001). Genome-mutations change the whole genome, for example the number of chromosomes. Chromosome-mutations change the structure and the shape of chromosomes or parts of chromosomes. Structural changes of the DNA nucleotide bases can force DNA polymerases during DNA replication or RNA polymerases during transcription to skip the lesion or to stop the process. Gene or point mutations alter single nucleotides, which change the genetic code and lead to the expression of modified or defective proteins. In “missense

mutations” the original base nucleotide is substituted for a different base, which leads to a different amino acid sequence after translation or to chain termination during transcription if the base change creates a stop codon. Missense mutations can eventually lead to truncated proteins with limited or no function. Conversely, a point mutation can sometimes be “silent” due to the redundancy of the genetic code. If the exchange of a nucleotide base leads to a synonym codon then the amino acid remains unchanged. The addition or deletion of nucleotide bases alters the DNA sequence of all subsequent codon triplets causing the reading frame to shift during transcription, which can result in incompletely synthesized protein fragments.

1.4 Ultra Violet (UV) light and its mutagenic potential on DNA

The UV spectrum can be divided into three categories, UV-A (400-320 nm), UV-B (320-280 nm) and UV-C (280-100 nm), which is shown in Figure 1. 2.

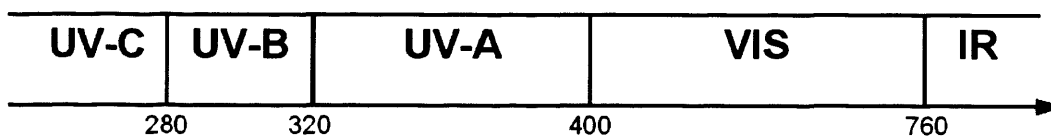


Figure 1.2: *Spectral wavelength region of sunlight in [nm]. VIS= visible light, IR= infra red*

The majority of harmful UV-radiation with wavelength shorter than 320 nm is usually absorbed by the stratospheric ozone layer. In recent years anthropogenic factors such as increased levels of chlorofluorocarbons (CFC’s) and the overproduction of

greenhouse gases such as carbon dioxide and methane (Molina and Rowland, 1974) are responsible for the depletion of the ozone layer. This has resulted in an increase in the amount of UV-radiation reaching the surface of the earth. Consequently, there is a greater risk of DNA mutations due to the fact that the absorption maximum of the four nucleotide bases (Tab.1.1) is around 260 nm (Wang, 1976). UV light irradiation in the short wavelength range can cause sunburn, fast skin aging, cataracts, immune system damage and the resulting photo-lesions are a major factor of DNA damage in cells and can cause skin cancer.

Nucleotide	Absorption maximum [nm]
Adenosine	260.5
Guanidine	246 and 276
Cytidine	267
Thymidine	264.5

Table 1.1: UV absorption maxima of the four nucleotides (Wang, 1976)

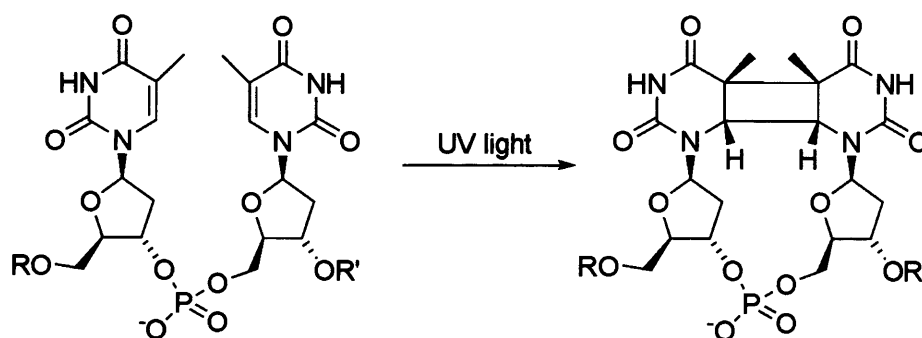
1.4.1 Photochemistry of DNA

The photon energy absorbed by a nucleotide base in its ground state S_0 can promote the molecule into the short-lived first excited singlet state S_1 (lifetime = 10^{-9} to 10^{-7} s) with one electron in a higher orbital with retained spin orientation. Due to internal conversion (IC) the electron normally relaxes back to the ground state by releasing the absorbed energy through heat dissipation. In some cases a small percentage of excited

nucleotide bases can pass via inter system crossing (ISC) into the long lasting first excited triplet state S_3 (lifetime = 10^{-3} to 10^2 s), where they can either transfer their energy to other nucleotide bases, relax to the ground state or react with adjacent nucleotides (Beukers *et al.*, 2008). One of the major UV induced reactions that DNA bases in the excited triplet state undergo is a $[2\pi+2\pi]$ cycloaddition of two adjacent pyrimidine bases.

1.4.2 Cyclobutane pyrimidine dimers

As a result of a cycloaddition, 90 % of these UV radiation photoproducts are cyclobutane pyrimidine dimers (CPDs) (Kao *et al.*, 1993), (Scheme 1.1). The relative efficiency of dimer formation per dinucleotide decreases in the order: $T \diamond T > C \diamond T > C \diamond C$ (Setlow and Carrier, 1966). $T \diamond T$ dimers can theoretically exist as 4 isomers (*cis-syn*, *cis-anti*, *trans-syn* and *trans-anti*) but in double stranded DNA only the *cis-syn* isomer has been identified (Heelis *et al.*, 1993).



Scheme 1.1: Formation of a (*cis-syn*) thymine dimer after UV light irradiation of two adjacent thymines in DNA.

The formation of a cyclobutane ring in double stranded DNA causes a kink of the phosphate backbone (Park *et al.*, 2002), which can act as a barrier to DNA polymerase causing early termination of DNA replication. If replication is not terminated the lesion is skipped and in the majority of the cases two bases are ignored. In some cases only one adenosine is attached during replication to the complementary strand instead of two (Wang and Taylor, 1992). Both cases result in the appearance of frame-shift mutations. It was observed that if C<>C dimers stayed unrepaired, a significant higher rate of deaminations from cytosine to uracil were detected which can result in single C→T or double CC→TT transitions (Peng and Shaw, 1996). The model of the crystal structure of a DNA decamer containing a *cis-syn* thymine dimer is shown in Figure 1.3. on the next page , in which the lesion is responsible for the distortion of the duplex DNA by bending it 30° toward the major groove and unwinding it by 9° (Park *et al.*, 2002).

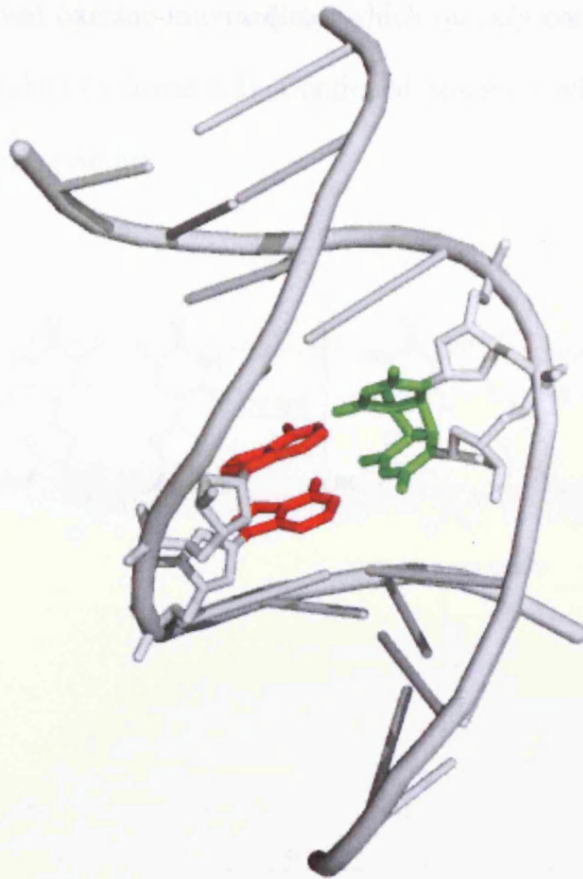
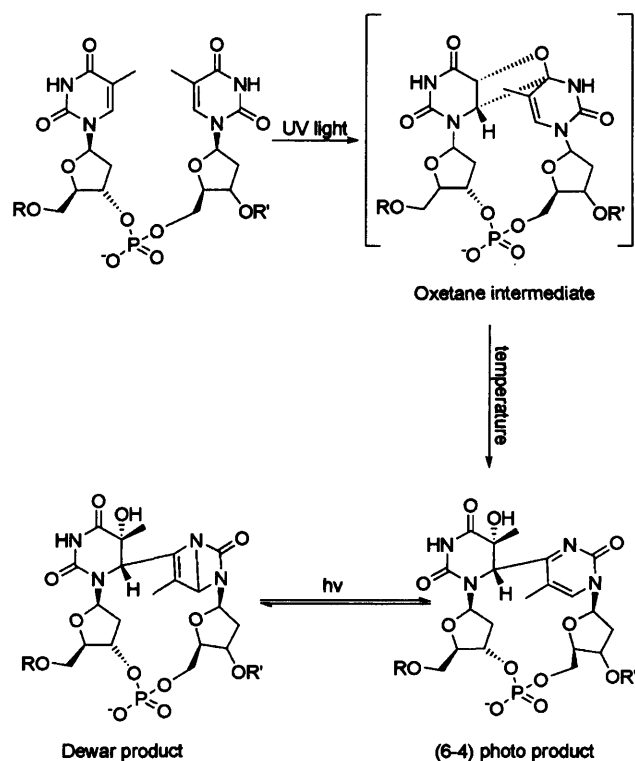


Figure 1.3: Model of the crystal structure of a single CPD ($T \leftrightarrow T$) lesion in a DNA decamer. Both thymines forming a dimer are highlighted in green the corresponding adenines are marked in red; the deoxyribose moieties, other nucleotid bases and the phosphate backbone are kept in grey (Park *et al.* 2002)(PDB ID, 1N4E).

1.4.3 (6-4) Photoproducts

A different kind of photoproduct induced by UV radiation with a 10 % probability (Kao *et al.*, 1993) is the formation of a pyrimidine-pyrimidone (6-4) photoproduct, which is created by a $[2\pi+2\pi]$ -cycloaddition between the C5-C6 double bond of the 3'-thymine and the carbonyl group of the 5'-thymine. The primary product of this

reaction is a short lived oxetane-intermediate, which quickly converts into the more stable (6-4) photoproduct (Scheme 1.2). Continued radiation with UV light finally transfers it into its *Dewar* isomer.



Scheme 1.2: Formation of the 6-4 photoproduct between two thymines via an oxetane intermediate and conversion into its Dewar isomer.

The (6-4) photoproduct is a less frequent photo lesion but compared to CPDs its mutagenic potential is significantly higher (error frequency > 91%) (le Clerc *et al.*, 1991) and it is highly specific in terms of the mutations induced. In DNA containing a thymine-thymine (6-4) photoproduct, adenine was observed to incorporate on the antiparallel strand in response to the 5' thymine of the (6-4) adduct with a frequency of 95%. However guanine was incorporated on the antiparallel strand in response to the downstream 3' thymine with a frequency of 85% while adenine was observed in

just 11% of the cases (Lee *et al.*, 1999). The model of the crystal structure of a DNA decamer duplex containing a T<>T (6-4) photoproduct (Lee *et al.*, 1999) is shown in Figure 1.4 revealing the distorted position of the 3' thymine, which is able to form a stable hydrogen bond between its O2 and the NH1/NH2 of the corresponding guanine. The mutation that occurs is a 3'T→C transition with 85% replication error frequency. While a 3'T→C transition in a T<>T cyclobutane dimer appears with only 4% probability (le Clerk *et al.*, 1991). The high mutagenic potential of (6-4) photoproducts is emphasized by the fact that they are repaired nine times faster by DNA repair enzymes than cyclobutane dimers (Lee *et al.*, 1999).

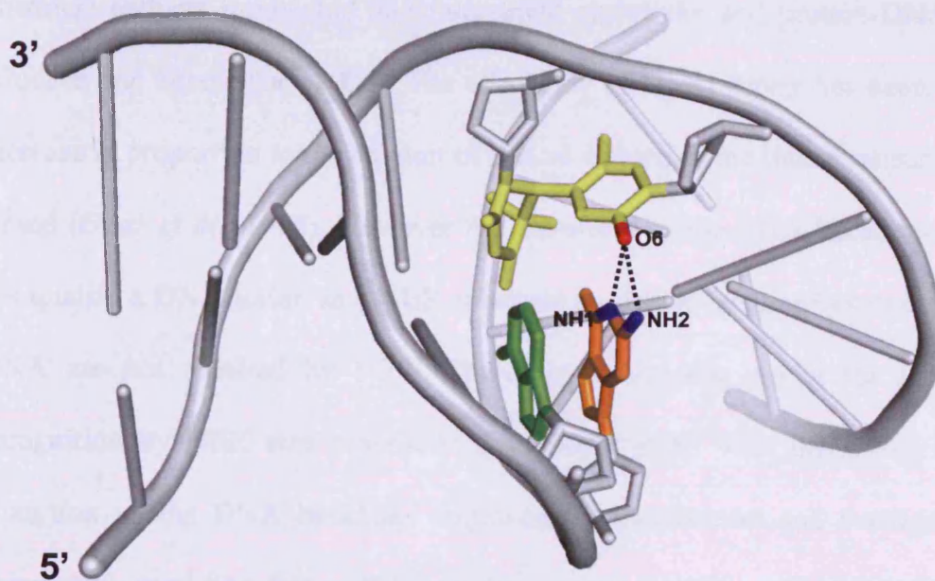


Figure 1.4: Model of the crystal structure of a T<>T (6-4) photoproduct in a DNA decamer duplex (Lee *et al.* 1999). Thymines are coloured in yellow, guanine in orange and adenine in green. H-bonding between the O2 (highlighted in red) of the 3' thymine and the NH1/NH2 (highlighted in blue) of the corresponding guanine is indicated by black dashed lines. The deoxyribose moieties, the phosphate backbone and remaining nucleotide bases shown as sticks, are kept in grey (PDB ID, 1CFL).

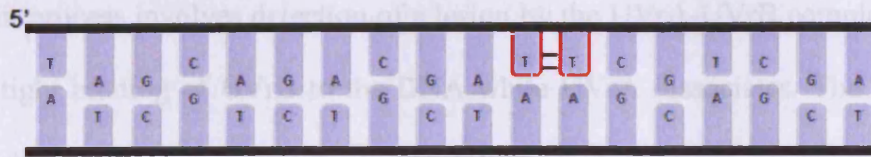
1.5 DNA repair mechanisms

To avoid the detrimental effects of mutations caused by DNA damage and to maintain genetic integrity, several repair mechanisms have evolved. The most important ones are described below.

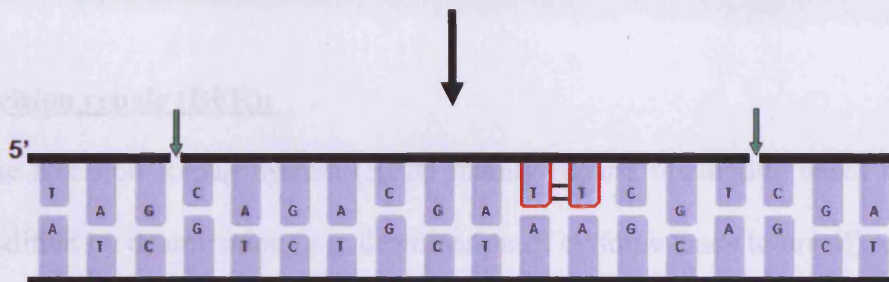
Nucleotide Excision Repair (NER):

The Nucleotide Excision Repair system (NER) is highly conserved in eukaryotes and prokaryotes (Sancar and Sancar, 1988). This repair system shows a broad range of substrate specificity of structurally unrelated lesions that include a large variety of chemical adducts intrastrand and interstrand crosslinks and protein-DNA crosslinks (Goosen and Moolenaar, 2008). The efficiency of lesion repair has been observed to increase in proportion to the amount of helical distortion the lesion causes in the DNA strand (Gunz *et al.*, 1996). However the distortion of the DNA backbone alone does not qualify a DNA lesion as a NER substrate as simple mismatches or bubbles in the DNA are not repaired by NER. Therefore a bipartite model for DNA damage recognition by NER was proposed. This model starts with the recognition of the distortion of the DNA backbone followed by localization and verification of the chemically modified base. This results in the excision of a lesion containing oligonucleotide (Hess *et al.*, 1997).

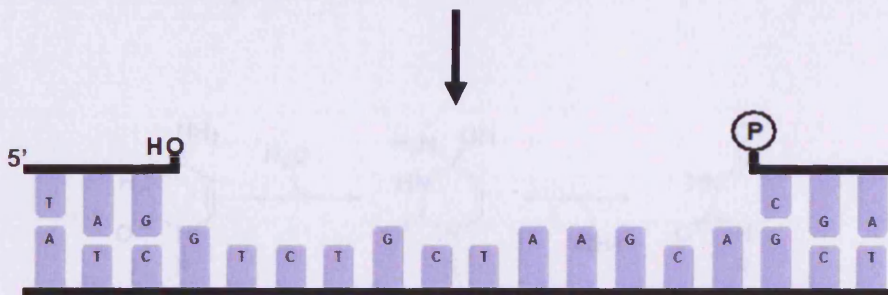
In comparison to eukaryotic NER, which involves approximately 30 proteins (Schaerer, 2003), prokaryotic NER involves only three proteins, namely UvrA, UvrB and UvrC. A general scheme of the prokaryotic NER mechanism repairing a UV-light induced thymine dimer is shown in Scheme 1.3.



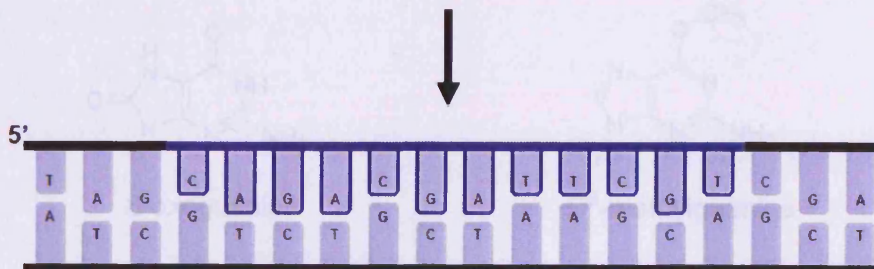
- The UvrAB protein complex is binding to the dimer lesion
- The UvrA protein dissociates; the UvrB protein remains bound to the DNA
- UvrC binds to UvrB to form an UvrBC complex
- Hydrolysis of the fourth phosphodiester bond 3' prime and the eighth phosphodiester bond 5' prime away from the dimer, indicated by green arrows



- The incised 12 bp oligonucleotide is released by DNA helicase II



- DNA polymerase I fills the existing gap
- DNA ligase I seals the nick



Scheme 1.3: Scheme of the NER pathway repairing a UV light induced thymine dimer in DNA.

The repair process involves detection of a lesion by the UVrA-UVrB complex, which initiates tight binding of UVrB to the DNA while UVrA dissociates. The next step involves the association of UVrC to the UVrB-DNA complex by making a first incision at the fourth phosphodiester bond 3' from the damage and a second incision at the eighth phosphodiester bond 5' to the damage. The lesion is excised by helicase II. DNA polymerase I fills the gap using the complementary strand as a template followed by a final ligation by DNA ligase.

Base excision repair (BER):

The Base Excision Repair system (BER) mainly repairs nucleotide bases that have been modified by deamination (*e.g.* deamination of cytidine leads to uracil), oxidation (*e.g.* 8-oxoguanine) or alkylation (*e.g.* *O*⁶-methylguanine) (Lindahl and Wood, 1999).

Examples are shown in Figure 1.5:

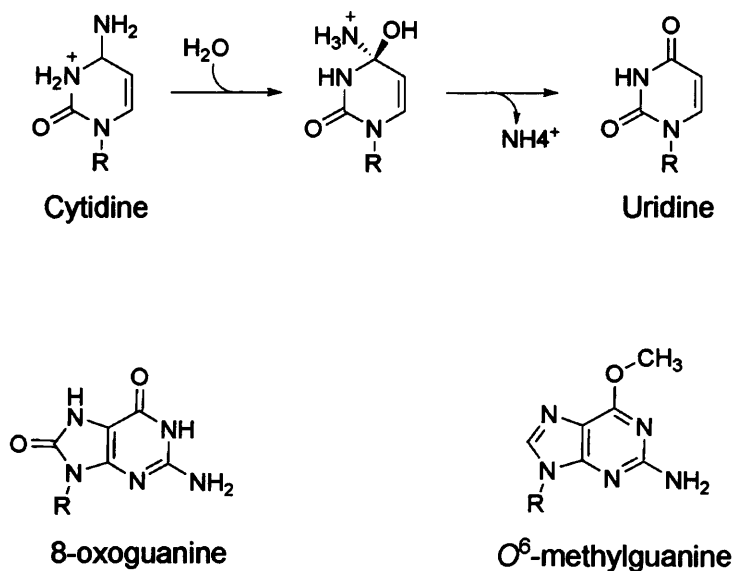
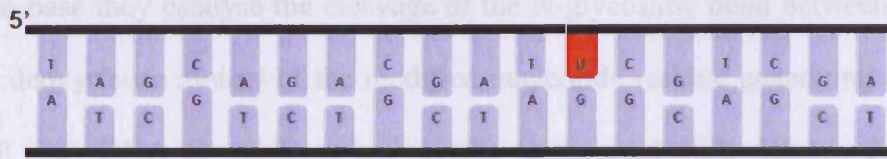
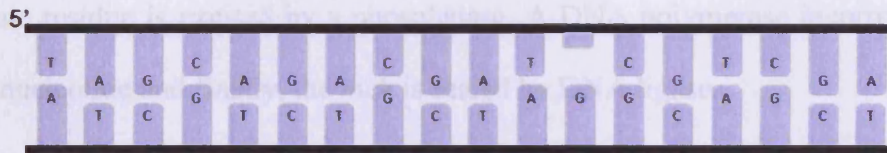


Figure 1.5: Deamination of cytidine by water can lead to uridine formation; oxidation of guanine can give 8-oxoguanine; alkylation of guanine can lead to the formation of *O*⁶-methylguanine.

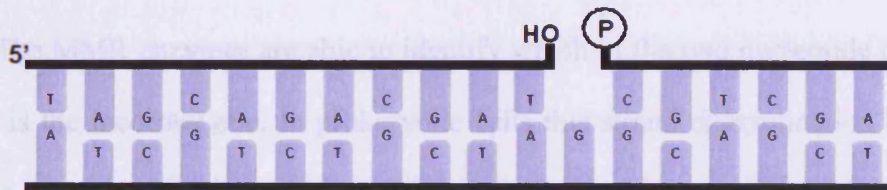
The pivotal steps of BER are shown in Scheme 1.4:



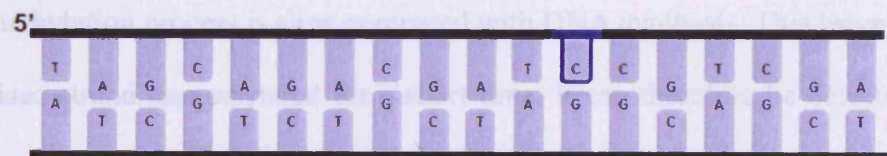
- Recognition of the damaged base by “Uracil DNA glycosylase” and excision from the DNA
- Hydrolysis of the *N*-glycosidic bond between base and deoxyribose moiety generates an abasic site



- AP endonuclease hydrolyses the phosphodiester bond adjacent to the abasic site
- Deoxyribose is removed by deoxyribose phosphatase



- DNA polymerase I fills the existing gap
- DNA ligase I seals the nick



Scheme 1.4: Scheme of the BER pathway repairing a uridine in DNA as a result of a deamination of cytidine.

The key enzymes involved in BER are DNA glycosylases. After recognizing the damaged base they catalyse the cleavage of the N-glycosidic bond between the base and the deoxyribose moiety of the modified nucleotide residue generating an abasic site (AP site). DNA glycosylases are specific to the nucleotide damage they repair (Seeberg *et al.*, 1995). Nine glycosylases have been characterized in human cells, each have its own unique substrate specificity (Schaerer, 2003). The second step is catalysed by AP endonuclease, which creates a nick in the DNA backbone by hydrolyzing the phosphodiester bond 5' to the abasic site. The remaining deoxyribose phosphate residue is excised by a phosphatase. A DNA polymerase incorporates the correct nucleotide and finally, the nick is sealed by DNA ligase.

Mismatch repair:

The mismatch repair system (MMR) eliminates base-base mismatches, nucleotide deletions and insertions, which are accidentally introduced during DNA replication by DNA polymerases despite their high fidelity and proof-reading ability (Schaerer 2003). The MMR enzymes are able to identify which of the two nucleotide bases in a mispair is the incorrect one. In prokaryotic cells this strand discrimination by MMR enzymes can be achieved because parental DNA strands are epigenetically modified by methylation of nucleotide bases at the specific sequence GATC (Modrich, 1991), (Modrich and Lahue, 1996). The new replicated daughter strand is not yet methylated as the methylation process is slow compared with DNA synthesis. This leaves a newly synthesised strand unmethylated for a short time. It can therefore be detected by the MMR system and this is the strand where repair occurs. The mechanism for strand discrimination in eukaryotes is still unknown however it is believed that a close coupling of the MMR system with the replication apparatus allows identification of

the newly synthesized strand (Jiricny, 1998). Initiation of the MMR pathway, which has mainly been investigated in *E. coli* (Modrich, 1991, Modrich and Lahue, 1996, Lahue *et al.*, 1989), starts with the binding of the MutS homodimer to the mismatch or the insertion/deletion loop. MutL binds to the MutS-mismatch complex in an ATP dependent reaction and is subsequently joined by MutH. MutH is an endonuclease that nicks the newly synthesized strand 5' of the non-methylated GATC sequence. Helicase II and endonucleases degrade the nicked strand past the mismatch (Welsh *et al.*, 1987). The gap is filled by DNA polymerase III and sealed by DNA ligase.

Photoreactivation:

In contrast to the previously mentioned multistep pathways of DNA repair involving multiple enzyme complexes, “photoreactivation”, a process to restore UV-light-induced lesions in DNA, is carried out by only one enzyme, DNA photolyase. This enzyme class catalyses the direct reversion of CPDs and (6-4) photoproducts efficiently and with low energy consumption by absorbing near UV- or blue light (300 nm-500 nm) (Sancar, 2008). The next section will present a detailed overview of these enzymes regarding their structure, function and their mechanism of repair.

1.6 DNA photolyases

1.6.1 General background

In 1949, bacteriologist Albert Kelner discovered “photoreactivation” after he recognized that harmful effects of short UV light radiation on *Streptomyces griseus* could be successfully reversed by exposing them to visible light (Kelner 1949). This observation was explained in 1958 by physicist Claud S. Rupert who was able to prove that a light-activated enzyme in a cell free extract of *E. coli* was responsible for the repair of UV irradiated *E. coli* DNA and also of UV damaged DNA extracted from *Haemophilus influenzae*, an organism which showed no photoreactivation ability itself. Rupert named this enzyme “photoreactivating enzyme” (Rupert *et al.*, 1958) and it later became known as photolyase. The DNA photoproducts, serving as substrate for photolyase enzymes were identified in the following years as cyclobutane pyrimidine dimers (CPDs) as the major photoproduct (Beukers and Berends, 1960), (Blackburn and Davies, 1966) and the less frequent (6-4) photoproduct (Varghese and Wang, 1967), (Karle *et al.*, 1969).

In recent years photolyases were discovered to be present in all parts of the kingdom of life. This includes archaeobacteria *i.e.* *Methanobacterium thermoautotrophicum* (Yasui *et al.*, 1994) and eubacteria *i.e.* *Myxococcus xanthus* (O'Connor *et al.*, 1996). Single-celled eukaryota such as *Chlamydomonas* (Petersen *et al.*, 1999), fungi *i.e.* *Neurospora crassa* (Eker *et al.*, 1994) (Yajima *et al.*, 1991), plants *i.e.* *Arabidopsis thaliana* (thale cress) (Ahmad *et al.*, 1997), *Cucumis sativus* (cucumber) (Takahashi *et al.*, 2002) or *Oryza sativa* (rice) (Hirouchi *et al.*, 2003). In the animal

kingdom photolyase was found in insects *i.e.* *Drosophila melanogaster* (fruit fly) (Yasui *et al.*, 1994), in fish *i.e.* *Carassius auratus* (goldfish) (Yasuhira and Yasui, 1994) and *Oryzias latipes* (killifish) (Yasui *et al.*, 1994), in amphibiae *i.e.* *Xenopus laevis* (African clawed toad), in reptiles *i.e.* *Crotalus atrox* and in non placental mammals *i.e.* in *Potorous tridactylis* (rat kangaroo) (Yasui *et al.*, 1994). Photolyase activity was even found in poxviruses (Srinivasan and Schnitzlein, 2001) and baculoviruses (van Oers *et al.*, 2008). Humans and other higher mammals lack the gene for photolyase, however they possess two genes, *Cry1* and *Cry2* with similarity to photolyase sequences (Hsu *et al.*, 1996). These genes encode blue light photoreceptors involved in the circadian rhythm but do not show any DNA repair activity (Sancar, 2003). Today it is commonly accepted that placental mammals, including humans, do not possess photolyases as DNA repair systems (Lee *et al.*, 1993) (Ley, 1993).

Photolyases are classified by their different substrate specificities. CPD photolyase, often referred simply as DNA photolyase binds and repairs CPD photoproducts in single or double stranded DNA, while (6-4) photolyase catalyses the reversion of the (6-4) photoproduct. Additionally CPD photolyases are divided into two sub classes based on their amino acid sequence similarity. These classes are referred to as photolyase I and II (Yasui *et al.*, 1994). Class I photolyases can be found in many microbial organisms, while Class II photolyases have mainly been isolated from higher organisms.

All photolyases identified to date are monomeric proteins with molecular masses in the 53-66 kDa range (454-614 amino acid residues) (Sancar, 1990). Photolyases contain two non-covalently bound cofactors as chromophores. These cofactors are shown in Figure 1.6. :

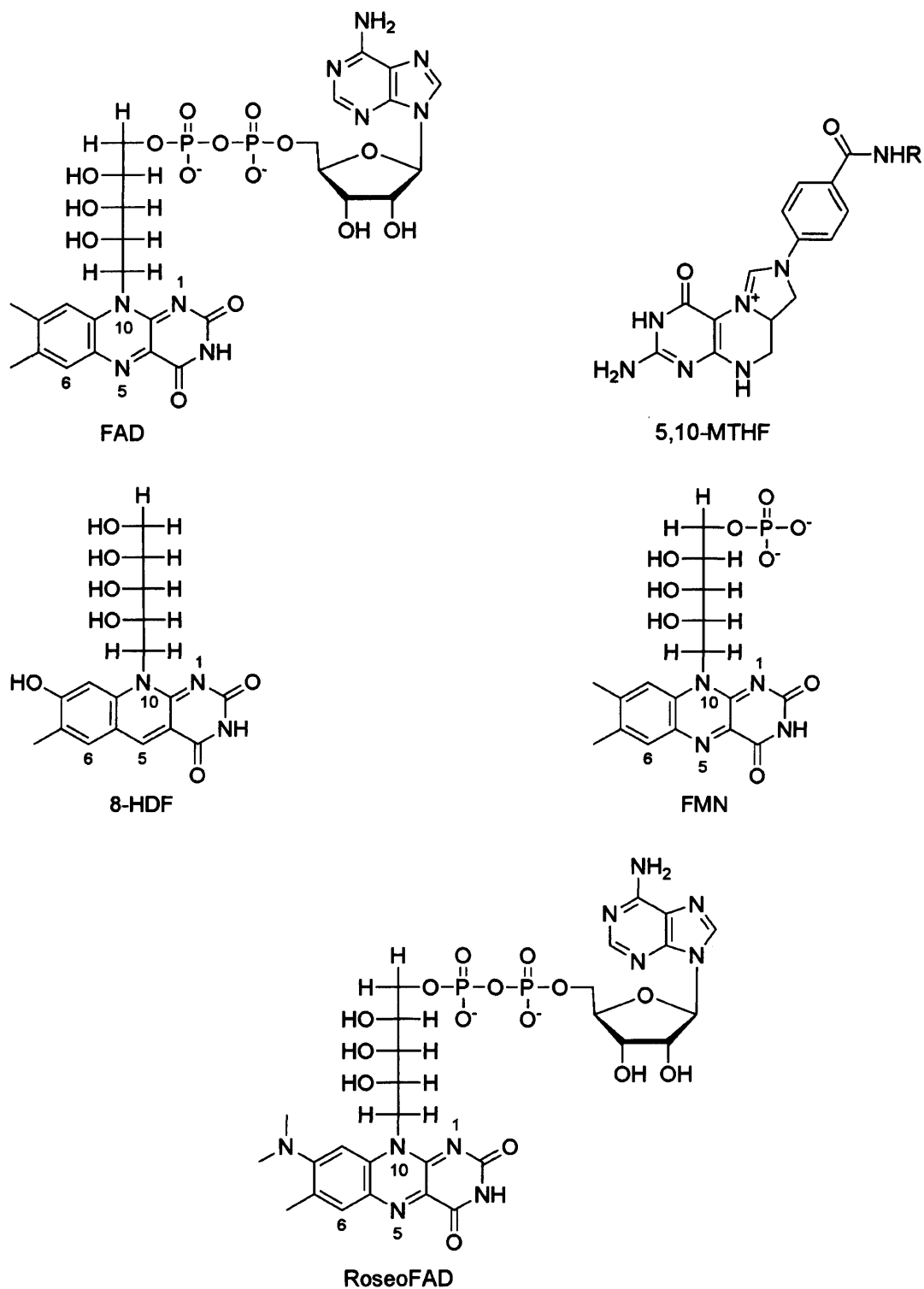


Figure 1.6: Cofactors associated with photolyases: FAD associates with all photolyase enzymes. 5,10-MTHF is found in the folate class and 8-HDF in the deazaflavin class. FMN was only found in *T. thermophilus* photolyase so far. The FAD analogue roseoFAD is able to replace the wild type cofactor FAD in photolyase.

The crucial, redox active chromophore in every known photolyase so far is flavin adenine dinucleotide (FAD) (Carell *et al.*, 2001). The second, light-harvesting cofactor differs between species and is 5, 10-methenyltetrahydrofolate (MTHF) in *E. coli* photolyase (Park *et al.*, 1995), or 8-hydroxy-5-deazaflavin (8-HDF) for example in *Anacystis nidulans* photolyase (Tamada *et al.*, 1997).

Based on the light harvesting cofactor, class I photolyases can be further categorized into either the folate- or the deazaflavin-type. However recent results showed that a second FAD in *Sulfolobus tokodaii* (Fujihashi *et al.*, 2007) and flavin mononucleotide (FMN) in *Thermus thermophilus* (Klar *et al.*, 2006) are the light harvesting cofactors.

1.6.2 Structure of *E. coli* CPD photolyase

Despite the fact that the photolyase family comprises nearly 500 entries in Genbank (Sancar, 2008) the crystal structures of only four different CPD-photolyases are available to date. There are the three dimensional structure of the class-I folate type CPD photolyase from *E. coli* (Park *et al.*, 1995), the crystal structure of the Class I 8-HDF-type CPD photolyase from *A. nidulans* (Tamada *et al.*, 1997), the crystal structure of a thermostable DNA photolyase from the marine bacterium *T. thermophilus* (Komori *et al.*, 2001) and the crystal structure of photolyase from an archeal strain *S. tokodaii* (Fujihashi *et al.*, 2007). An important step forward was made in 2004 by elucidating the crystal structure of *Anacystis nidulans* photolyase binding to a synthetic T\rightleftharpoonsT dimer, giving insight into the enzyme-substrate recognition, the substrate binding as well as the geometric orientation of the thymine dimer and the cofactor FAD in the active site of the protein (Mees *et al.*, 2004). Very

recently the first crystal structure of a DNA (6-4) photolyase from *D. melanogaster* bound to a T\leftrightarrowT was obtained by Maul *et al.*, (2008).

The crystal structure of *E. coli* photolyase (Park *et al.*, 1995) is shown in Figure 1.7.

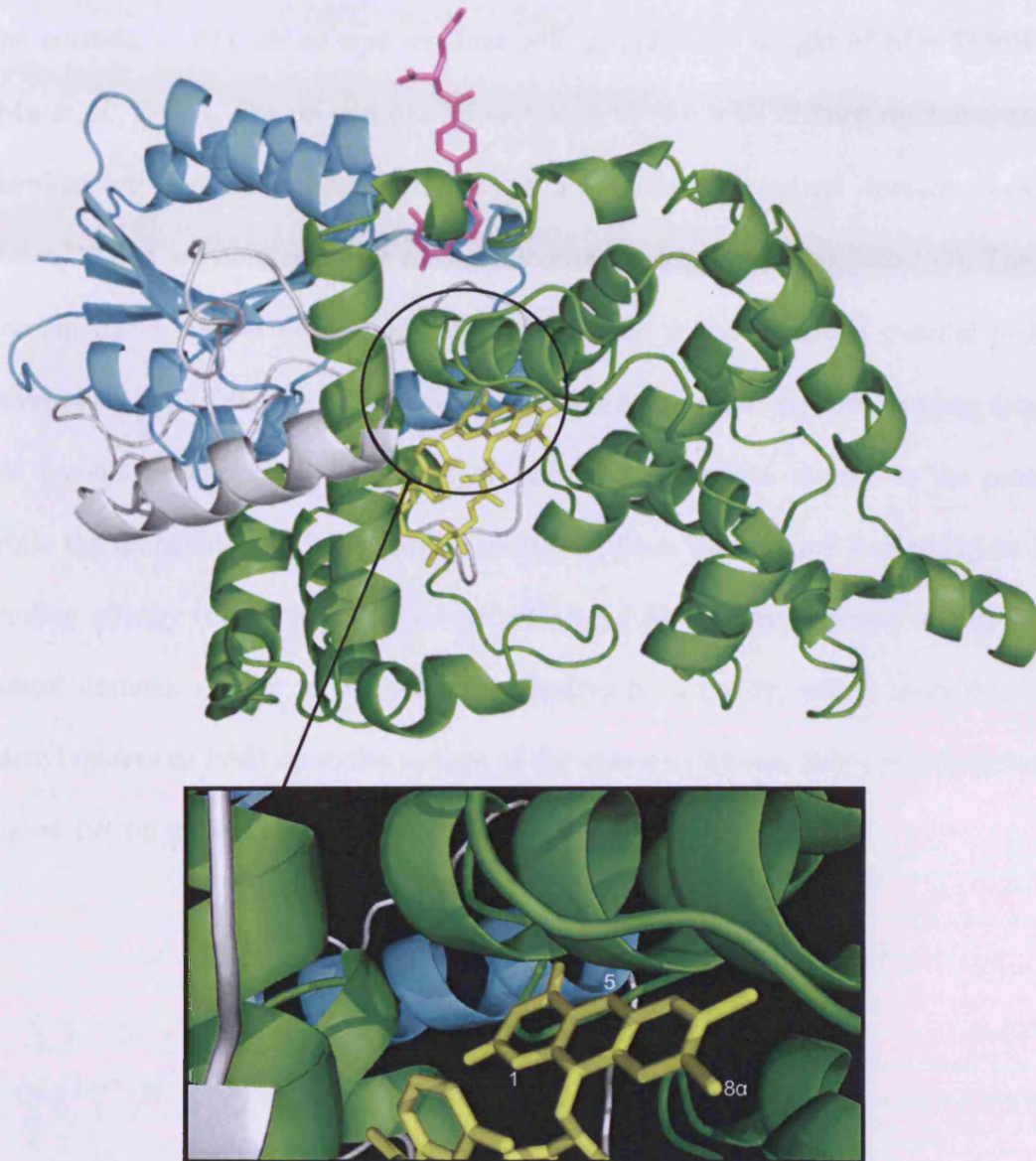


Figure 1.7: Model of the crystal structure of CPD photolyase from *E. coli*. The α/β domain is coloured in turquoise, the interdomain loop in grey and the α -helical domain in green. Cofactors FAD and MTHF are highlighted in yellow and purple (Park *et al.*, 1995) (PDB ID=1DNP). For a better view, the FAD binding pocket is illustrated enlarged.

All CPD photolyases crystallised so far have the same basic architecture, even those containing different second chromophores (Sancar, 2008). *A. nidulans* and *E. coli* photolyases for example have a similar backbone structure, sharing 39% identical residues (Tamada *et al.*, 1997). The photolyase enzyme of *E. coli* is globular in shape and consists of 471 amino acid residues with a molecular weight of $M_r = 53,994$ Da (Mu *et al.*, 2005). The protein can be sectioned in two well defined domains, an N-terminal α/β domain (residues 1-131) and a C-terminal α -helical domain (residues 204-471) that are connected via a long interdomain loop (residues 132-203). The α/β domain has a typical nucleotide-binding fold with a five stranded parallel β -sheet covered on both sides by α -helices and provides the surface exposed binding site for the second chromophore. MTHF binds only with its pterin moiety to the protein, while the glutamate rest is partially sticking out from the enzyme explaining its low binding affinity compared to the flavin cofactor. FAD is deeply buried within the α -helical domain. Access to the solvent is limited by a cavity, which leads from the adenylyl moiety of FAD up to the surface of the enzyme (Weber, 2005) and is shown in Figure 1.8. on the next page.

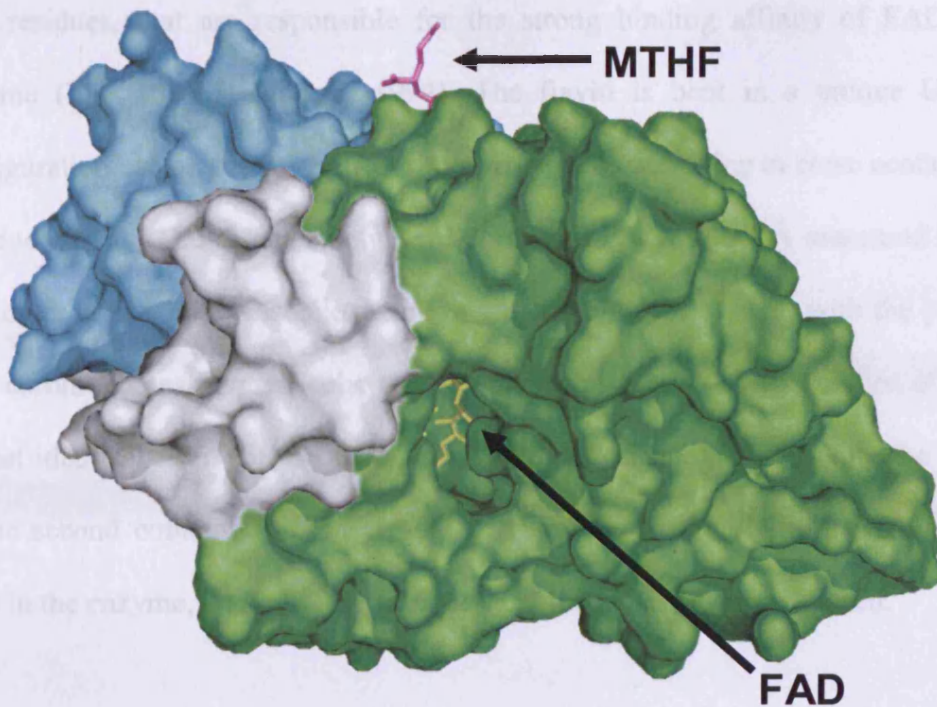


Figure 1.8: Model of the crystal structure of CPD photolyase from *E. coli* is showing the position of FAD (yellow) to be in the core of the enzyme and the position of MTHF (purple) to be on the protein surface with its glutamate moiety sticking out. The α/β domain is coloured in turquoise, the interdomain loop in grey and the α -helical domain in green (Park *et al.*, 1995) (PDB ID=1DNP).

The cavity is wide enough to allow access for the substrate. The thymine dimer is then flipped out of the helix due to weak hydrogen bond interaction with its complementary bases in double stranded DNA (Mees *et al.* 2004). A band of positively charged amino acids residues along the protein surface outside of the cavity favours electrostatic interaction with the negative charged backbone of the substrate DNA. The potential substrate binding side provides hydrophobic amino acid residues on one, and polar residues on the other site of the cavity. This fits well with the asymmetric profile of a CPD. The cyclobutane ring is hydrophobic while the opposite site of the thymine base contains nitrogens and oxygens suitable for H-bond formation. FAD is held tightly in place by interacting with 14 highly conserved amino

acid residues, that are responsible for the strong binding affinity of FAD to the enzyme ($K_D < 10^{-11}M$) (Sancar, 1994). The flavin is bent in a unique U-shaped configuration, which brings the 7,8-dimethyl-isoalloxazine ring in close contact to the adenine moiety. The distance between MTHF and FAD is 16.4 Å measured between the center of the FAD's isoalloxazine ring and the N5 of MTHF, with the planes of both chromophores perpendicular to each other. Position and conformation of FAD is almost identical in *E. coli* photolyase and *A. nidulans* photolyase, while the position of the second cofactors differs greatly. In *A. nidulans* photolyase 8-HDF is buried deep in the enzyme, while MTHF in *E. coli* photolyase is surface exposed.

1.6.3 Cofactors of *E. coli* CPD photolyase

As previously described flavin adenine dinucleotide (FAD) is the redox active cofactor in all photolyases classified so far and can be found in three oxidation states (Figure 1.9), oxidised FAD^{ox} (flavoquinone), radical $FADH^\bullet$ (flavosemiquinone) or fully reduced FAD^{red} (flavohydroquinone).

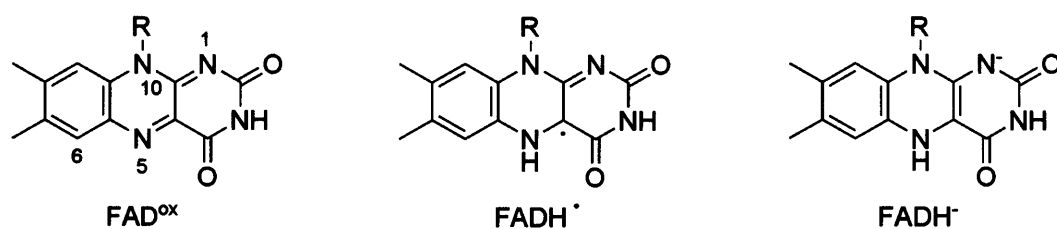


Figure 1.9: The three different redox states of cofactor FAD which can be found in the photolyase enzyme: oxidised FAD^{ox} , semi reduced $FADH^\bullet$ and fully reduced $FADH^-$; R = phosphoribosyl adenosine moiety.

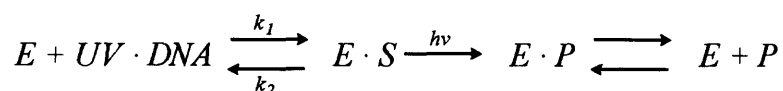
While the substrate binding is redox state independent (Payne *et al.*, 1990) (Sancar *et al.*, 1987), only the fully reduced and deprotonated form FADH⁻ in the enzyme shows catalytic activity by repairing thymine dimers. FAD is not only essential for catalysing DNA repair but also crucial for substrate binding (Sancar, 1994). While absence of the second cofactor, MTHF, does not affect binding affinity to damaged DNA or the DNA repair (Payne *et al.*, 1990). No obvious sequence homology to other flavoproteins can be found, which is explained by the fact that the photoexcited state *FADH⁻ is the catalytic active form, whereas the majority of flavoproteins utilise FAD in its ground state (Massey, 1995).

In photolyase FADH⁻ has its absorption maximum around 360 nm, weak absorbance in the near UV light range and fading absorbance above 400 nm (Jorns *et al.*, 1990). The DNA repair mechanism is a light dependent process in the UV and blue light region (300-500 nm) so the success of dimer repair relies on a high quantum yield. Based on its 5 to 10 times higher extinction coefficient (Payne *et al.*, 1990) compared to FADH⁻, 5,10-methenyltetrahydrofolylpolyglutamate (MTHF) is working as the light harvesting cofactor, increasing quantum yield by absorbing light in the regions near UV and visible wavelengths where FADH⁻ absorbs weakly. In aqueous solution MTHF absorbs light maximally at 358 nm, however at this wavelength the flux of solar radiation is lower as it is at longer wavelengths. When MTHF binds to the photolyase enzyme a bathochromic shift of 25 nm is induced, resulting in a new absorption maximum of the chromophore at 383 nm, leading to a > 5 kcal/mol decrease in transition energy from protein-mediated stabilization of the excited state and/or destabilisation of the ground state of MTHF (Henry *et al.*, 2004).

1.6.4 Reaction mechanism of DNA repair (photoreactivation)

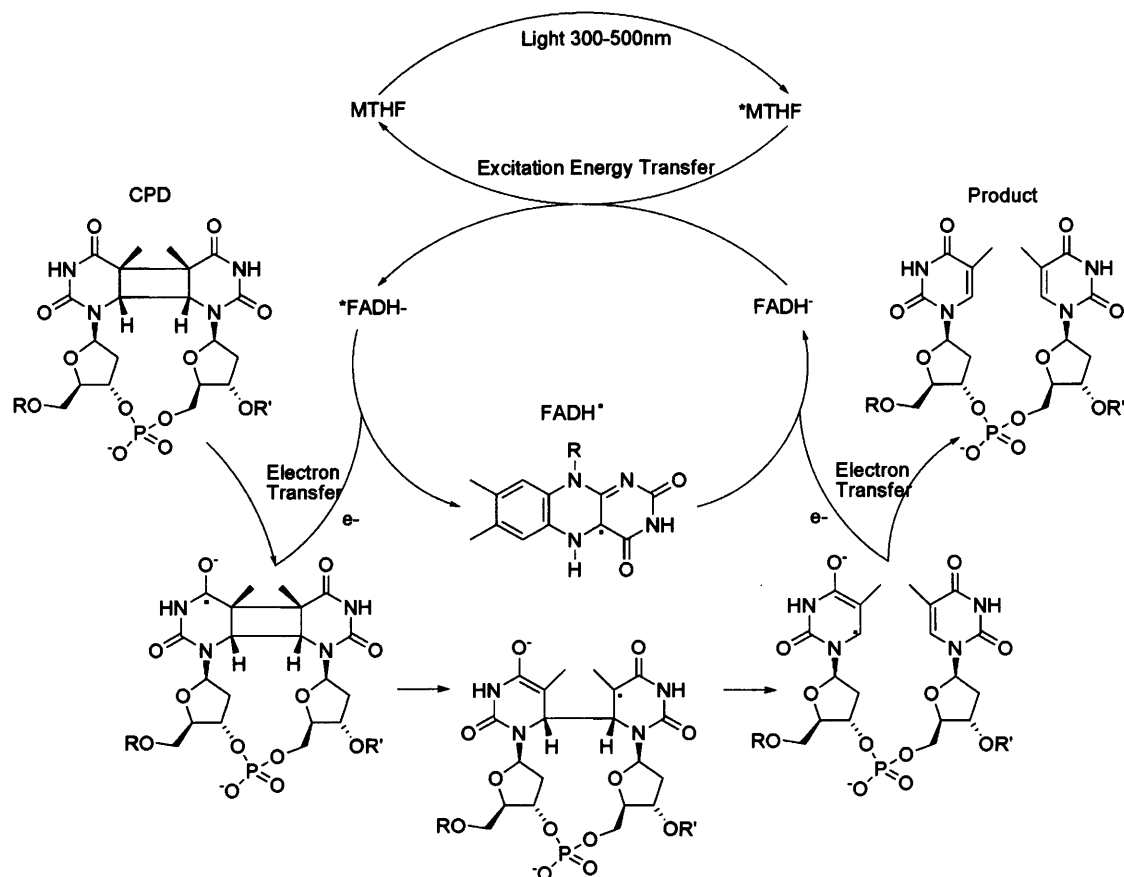
Photolyases are very efficient enzymes taken into account their low copy numbers per cell, which are approximately 10 - 20 molecules in *E. coli* (Harm *et al.*, 1968) and 75-300 in yeast (Yasui and Laskowski, 1975). Photolyase binds to single or double stranded DNA in a light independent step (Sancar *et al.*, 1985) recognising the DNA phosphodiester back bone around the CPDs with an equilibrium association constant for *cis-syn* CPDs of 2.6×10^8 to $2.2 \times 10^9 \text{ M}^{-1}$ (Husain and Sancar, 1987) (Li and Sancar, 1990) or $3.7 \times 10^9 \text{ M}^{-1}$ (Baer and Sancar, 1993). The association constant for undamaged DNA is more than four orders of magnitude lower. The thymine dimer is recognized in the active site by being completely flipped out of the duplex DNA (base flipping) (O'Neil and Wiest, 2007) and bending the DNA by about 50° (Mees *et al.*, 2004). The photolyase-catalysed DNA repair follows Michaelis-Menten kinetics with the important addition that the catalysis strictly depends on light (Rupert, 1962).

The following reaction scheme was introduced by Rupert in 1962:



The enzyme binds to the substrate in a light independent step, to form an enzyme-substrate complex that must absorb a photon as the “second substrate” to start catalysis.

The hypothetical repair cycle introduced by Kim and Sancar in 1993 is shown on the next page in Scheme 1.5



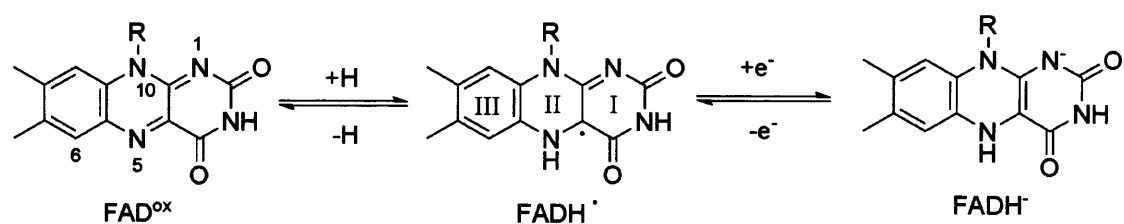
Scheme 1.5: The postulated repair mechanism of a thymine dimer by CPD photolyase (Kim and Sancar, 1993); R = phosphoribosyl adenosine moiety.

The antenna cofactor, which in *E. coli* photolyase is MTHF, absorbs light in the 300-500 nm wave length range and transfers its excitation energy to FADH⁻ resulting in the excited singlet state *FADH⁻ (Lipman and Jorns, 1992). This occurs via a long range dipole-dipole interaction known as Foerster transfer (Kim and Sancar 1993) with an energy transfer (ET) efficiency of $[E_{ET}] = 0.92$ (Ramsey *et al.*, 1992) at rates of $4.6 \times 10^9 \text{ s}^{-1}$ and $3.0 \times 10^{10} \text{ s}^{-1}$ (Kim *et al.*, 1991). Both excitations are singlet $\pi\text{-}\pi^*$ transitions from the highest occupied molecular orbital (HOMO) to the lowest unoccupied molecular orbital (LUMO). In the excited singlet state, *FADH⁻ transfers an electron to the T<math>\text{>T

state FADH^\bullet . The pyrimidine radical anion splits into pyrimidine monomers. The excess electron is transferred back to FADH^\bullet to regenerate the initial redox state of the flavin FADH^- (Weber et al., 2001). The overall quantum yield for $\text{T} \leftrightarrow \text{T}$ splitting is $\Phi = 0.9$ (Sancar, 2004) with the entire DNA repair cycle completed in approximately 2 ns (MacFarlane and Stanley, 2003).

1.6.5 Photoactivation

The photolyase enzyme can contain FAD in three oxidation states. While the enzyme with FAD and FADH^\bullet is catalytic inactive, the reduced form FADH^- is the catalytically active form. Besides photoreactivation the enzyme can carry out a second photoreaction, which is the photoreduction of FAD and FADH^\bullet by absorbing light in the visible wavelength range in presence of a reducing agent, *in vitro* i.e. DTT, resulting in e^- transfer to gain the fully reduced FADH^- as it is shown in Scheme 1.6:

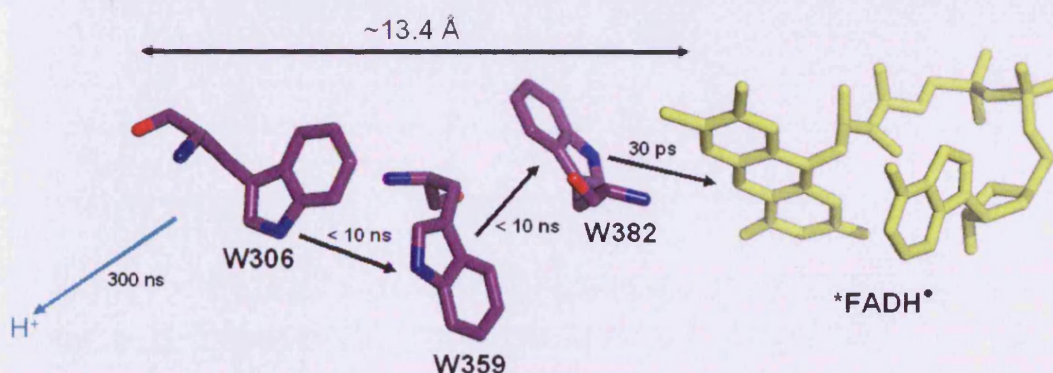


Scheme 1.6: Different oxidation states of FAD. *R* = phosphoribosyl adenosine moiety. Roman numbers I, II and III refer to the pyrimidine-, pyrazine- and xylene-part in the isoalloxazine moiety.

This process is called photoactivation (Sancar, 2003) (Byridin *et al.*, 2003) (Kavakli and Sancar, 2004) (Aubert *et al.*, 2000) and occurs by abstraction of an electron

through a highly conserved triad of tryptophans by the excited $^*FADH^{\bullet}$ over a total distance of 13.4 Å. The following scheme seen in Scheme 1.7 using time resolved absorption spectroscopy was introduced by Aubert *et al.*, (2000).

- Abstraction of an electron from W382 resulting in the reduced $FADH^{\bullet}$ and a tryptophanyl radical cation $W382^{\bullet+}$ in 30 ps
- Radical transfer from W359 to $W382^{\bullet+}$ resulting in $W359^{\bullet+}$ and W382 in less than 10 ns
- Radical transfer from W306 to $W359^{\bullet+}$ resulting in $W306^{\bullet+}$ and W359 in less than 10 ns
- Final deprotonation of $W306^{\bullet+}$ gaining the neutral radical $W306^{\bullet}$ in 300 ns
- Deactivation of $W306^{\bullet}$ by electron abstraction from an exogenous electron donor



Scheme 1.7: Reaction and time scheme of electron transfers during photoactivation over a distance of approx. 13.4 Å via tryptophans 306, 359 and 382 resulting in the reduction of $FADH^{\bullet}$ (Aubert *et al* 2000). For details see text.

1.7 Two putative electron transfer mechanisms

The DNA repair by CPD photolyase is a light induced one-electron transfer reaction, however a distinguished pathway of electron transfer from the excited $^*FADH^-$ to the CPD and the electron back transfer still remains a topic of discussion. The crystal structure of the *A. nidulans* CPD photolyase binding to a T<>T dimer, published in 2004 by Mees *et al.*, can be consulted to predict two electron transfer pathways during the repair cycle (Figure 1.10, next page). They can be distinguished by making use of the orientation, conformation and distance values of FAD and the substrate in the active site of the enzyme (Mees *et al.*, 2004).

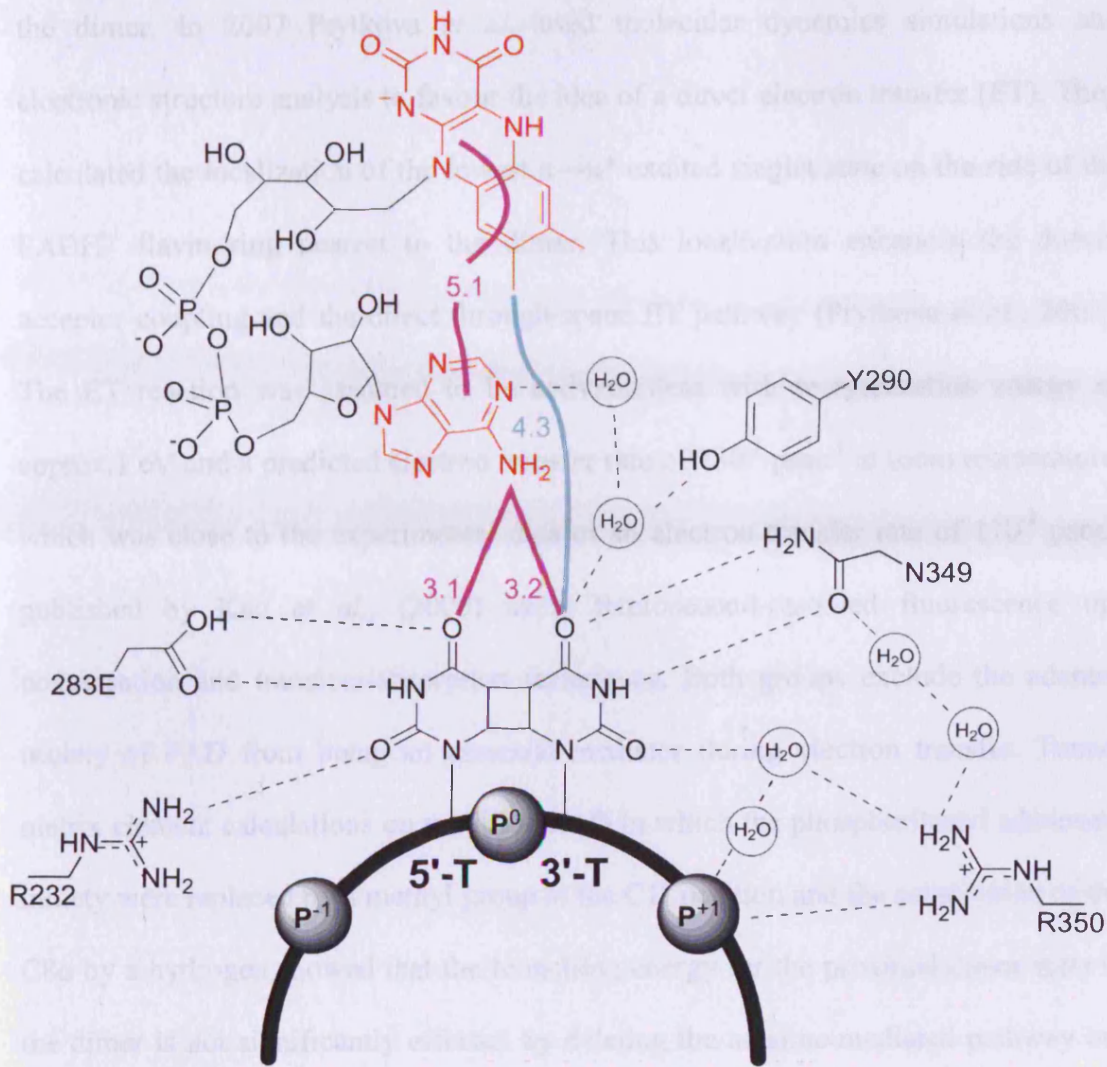


Figure 1.10: Two proposed electron transfer pathways based on the orientation of FAD and a thymine dimer in the crystal structure of CPD photolyase from *A. nidulans*. An indirect electron transfer via the adenine moiety is shown in pink. A direct electron transfer from C8 α of the isoalloxazine moiety to the 3'-T is drawn in turquoise (Source: Mees et al 2004).

The first possibility is a direct single electron transfer (single super exchange) over a distance of approx. 7 Å to the dimer from the center of the electron donating isoalloxazin ring of the flavin. It involves the C8 α group, which points towards the substrate-binding site and is 4.3 Å away from the C4-carbonyl group of the 3'-T of

the dimer. In 2007 Prytkova *et al.* used molecular dynamics simulations and electronic structure analysis to favour the idea of a direct electron transfer (ET). They calculated the localization of the lowest $\pi \rightarrow \pi^*$ excited singlet state on the side of the FADH⁻ flavin ring nearest to the dimer. This localization enhances the donor-acceptor coupling and the direct through-space ET pathway (Prytkova *et al.*, 2007). The ET reaction was assumed to be activationless with reorganization energy of approx. 1 eV and a predicted electron transfer rate of $230^{-1} \text{ psec}^{-1}$ at room temperature, which was close to the experimental data of an electron transfer rate of $170^{-1} \text{ psec}^{-1}$ published by Kao *et al.*, (2005) using femtosecond-resolved fluorescence up-conversion and transient-absorption techniques. Both groups exclude the adenine moiety of FAD from being an essential mediator during electron transfer. Tunnel matrix element calculations on modified FAD in which the phosphoribosyl adenosine moiety were replaced by a methyl group at the C1' position and the substitution of the C8 α by a hydrogen showed that the tunnelling energy for the proximal donor state to the dimer is not significantly effected by deleting the adenine-mediated pathway but reduced by modification on the C8 α (Prytkova *et al.*, 2007). Additionally Kao *et al.* did not measure any intramolecular electron transfer from the isoalloxazine ring to the adenylyl moiety in the absence of substrate.

Both groups rather see the role of the adenine moiety to sterically stabilize the dimer-FADH⁻ conformation in the active site by adenine-dimer hydrogen bond formations. This locates the dimer close to the benzene side of the flavin ring where $\pi \rightarrow \pi^*$ transition for directing the electron to the dimer enhances the donor-acceptor coupling (Prytkova *et al.*, 2007).

A second hypothesis suggests an indirect, superexchange-mediated single electron transfer from the isoalloxazine ring via the adenine moiety to the CPD. In addition,

redox active amino acids can be involved and act as mediators during electron transfer (Weber, 2005). Based on the crystal structure of *E. coli* photolyase, tryptophan 277 is close to the putative substrate-binding site (Park *et al.*, 1995) and could therefore act as potential intermediate electron acceptor. This residue was found of being capable to repair CPD directly when photoexcited by short UV light (≈ 280 nm) (Kim *et al.*, 1992). The involvement of the adenine moiety in a radical transfer is feasible by observing a unique U-shaped conformation of FAD when bound to the enzyme in which the adenine moiety bends over the pyrazine and pyrimidine part of the isoalloxazine ring (Weber *et al.*, 2001). This mechanism is supported by EPR ENDOR and TRIPLE resonance spectroscopy experiments by Weber *et al.* (1999) and computational calculations using density functional theory methods that analyse the electronic structure of the neutral flavin radical FADH^\bullet in photolyase by Kay *et al.* (2001). Firstly, a strong spin density at the N5, C4 α and N10 indicates an increased orbital overlap between the π -system of the isoalloxazine and the adenine moiety of FAD (Weber, 2001). Secondly, the very small spin densities on C8 α and C6 are evidence that the delocalisation of the unpaired electron is shifted mainly towards the central pyrazine and the outer pyrimidine part of the isoalloxazine moiety, which are in close contact to polar amino acids Asp 372 and Arg 344. The xylene part however, points towards the substrate binding site where the absence of any stabilizing amino acid residues does not promote distribution of the unpaired spin over the flavin ring system (Kay *et al.*, 1999). A probable explanation could be that once the electron is transferred from FADH^- to the CPD and the transient FADH^\bullet radical is formed, the rather poor stabilization of the unpaired electron spin over the isoalloxazine moiety might favour electron back transfer from the split dimer to the cofactor.

CHAPTER 2:

Materials and methods

2.1 Materials

All chemicals, if not otherwise stated, were purchased from Fisher, Merck, Sigma-Aldrich, NovaBiochem, New England BioLabs, Quiagen, Fluka or Alfa Aeser. Oligonucleotides were purchased from Operon.

2.1.1 Instruments

Acrylamid gel electrophoresis	SE 250 Mighty Small II (Hoefer Scientific Instruments San Francisco, USA)
Agarose gel eletrophoresis	Multi Sub Choice gel unit with 1x removable, 150x150mm UV gel casting tray 2x1.0mm, 20 samples comb (JENCONS-PLS Staffordshire, UK)
Autoclave	Astell Scientific (Sidcup, Kent, UK)
Balances	Kern ALJ 120-4 (North Fareham, Hampshire, UK) Mettler Toledo AB204-5 (Beaumont Leys, UK)
Centrifuge and rotors	Sorvall RC5C Plus and RC6 Plus with rotors SLA-3000 and SS-34; Thermo Scientific (Waltham, MA, United States)
FPLC	FPLC- <i>ÄKTA</i> Monitor UPC-900, Hg-lamp 280 nm, Pump P 920, Mixer M-925, Valve INV-907, fraction collector Frac-900/901, Software UNICORN 3.10 (former Amersham Biosciences, now GE Healthcare, little Chalfont, UK)
Freeze dryer	Freeze dryer unit Alpha 1-4 (Christ Gefriertrocknungsanlagen GmbH, Osterode am Harz) Controll device LDC-1M; Elekt. Conection 230 V, 50 Hz; Temp. -50°C; pressure 0,200 mbar
Heating block	SB1 mono digital block heater, 2 block model (JENCONS-PLS Staffordshire, UK)

Incubation shaker	New Brunswick Scientific Incubation shaker INOVA 44 (St.Albans, UK)
Incubator	Heraeus Instruments (Buckinghamshire, UK)
pH-Meter	HANNA Instruments pH 209 pH Meter (Woonsocket, USA)
Peristaltic pump Rotational evaporator	101U/R Watson Marlow , (Falmont , Cornwall, UK) Membrane pump and vacuum pump (VAKUUBRAND GmbH & Co, Wertheim) Rotavapor RE 120 (Büchi, Germany), waterbath (Köttermann, Deutschland)
See-saw rocker	Labortechnik KS501 digital (Wasserburg , Germany)
Table top centrifuge	Spectrafuge 24D (JENCONS-PLS Staffordshire, UK)
Thermocycler	TECHNE Touchgene Gradient (JENCONS-PLS Staffordshire, UK)
Ultrasonic device	Vibra cell SONICS (Newtown, USA)
UV -light gel unit	Gene Flash SYNGENE Bio Imaging (Cambridge, UK)
UV/VIS Spectrophotometer	Jasco V-660 Spectrophotometer JASCO CORPORATION 2967-5 Ishikawa-Cho, (Hachioji Tokyo, Japan)
Vacuum pump	MZ 2C (VAKUUBRAND GmbH&Co./Wertheim) For filtration and buffer degassing Roto-Vac 3 (Biotech-Fischer, Reiskirchen, Germany)

2.1.2 Enzymes

Enzyme	Supplier
DNase I	Sigma
Lysozyme	Fisher Scientific
Taq polymerase	New England Biolabs
T4-Ligase	New England Biolabs

Restriction enzymes:

<i>Bam</i> HI	New England Biolabs
<i>Nde</i> I	New England Biolabs

2.1.3 Media

For solid LB plates, 20 g/l agar was added to LB medium. Filter sterilised antibiotics were added to autoclaved medium cooled to approx. 50°C.

LB (Luria Bertani)-Medium	10 g	Trypton
	5 g	Yeast Extract
	5 g	NaCl
per 1 l		H ₂ O
autoclaved		

When applicable, the following antibiotics were added to final concentrations of 180 mg/l ampicillin, 15 mg/l kanamycin, 10 mg/ml erythromycin

2 x YT-Medium	16 g 10 g 5 g per 1 l autoclaved	Trypton Yeast Extract NaCl H ₂ O
SOC-Medium	20 g 5 g 20 mM 10 mM 10 mM 10 mM 2.5 mM per 1 l autoclaved	hydrolyzed Casein Yeast extract Glucose MgSO ₄ NaCl MgCl ₂ KCl H ₂ O
Glycerol-Medium	50 % 50 % autoclaved	LB-Medium Glycerol

2.1.4 Buffers and solutions

Solution- or Buffer name		Compounds
Ethidium bromide solution	1 µg/ml	Ethidium bromide
Ligase buffer	250 mM 50 mM 50 mM 5 mM 25 µg/ml pH 7.5 at 25°C	Tris-HCl, pH 7,6 MgCl ₂ DTT ATP BSA

10 x Polymerase buffer	15 mM 500 mM 100 mM 1 %	MgCl ₂ KCl Tris-HCl, pH 8.8 Triton X-100
Sample buffer for DNA gels	50 % (v/v) 0.25 % (w/v) 0.25 % (w/v) in TE-Buffer	Glycerol Xylenecyanol Bromphenol blue
Saline	0.9 % (w/v)	NaCl
TAE buffer 50 x	2 M 100 mM	Tris-acetate, pH 8.2 EDTA
TE buffer 10 x	100 mM 10 mM	Tris-HCl, pH 8.2 Na ₂ EDTA

Buffers for *E. coli* E109A photolyase purification from host cell *B. subtilis* (vacuum filtered and degassed):

Lysis buffer	50 mM 10 mM 100 mM 10 % (w/v)	HEPES, pH 7.0 DTT NaCl Sucrose
Buffer A _{BS}	50 mM 100 mM 10 mM 10 % (v/v)	HEPES, pH 7.0 KCl DTT Glycerol
Buffer B _{BS}	50 mM 2 M 10 mM 10 % (v/v)	HEPES, pH 7.0 KCl DTT Glycerol

Buffer C _{DS}	50 mM 50 mM 10 mM 10 % (v/v)	HEPES, pH 7.0 NaCl DTT Glycerol
Buffer D _{HS}	50 mM 1 mM 10 mM 10 % (v/v)	HEPES, pH 7.0 KCl DTT Glycerol
Buffer E _{HS}	50 mM 1 M 10 mM 10 % (v/v)	HEPES, pH 7.0 KCl DTT Glycerol

Buffers for purification and reconstitution for *E. coli* photolyase with His tag on Ni-

NTA- Sepharose column (vacuum filtrated and degassed):

Buffer A _{NiS}	50 mM 50 mM 100 mM 10 mM 0.02 % (w/v)	Tris-HCl, pH 7.4 NaCl Imidazole β -mercaptoethanol Azide
Buffer B _{NiS}	50 mM 50 mM 500 M 10 mM 0.02 % (w/v)	Tris-HCl, pH 7.4 NaCl Imidazole β -mercaptoethanol Azide
Buffer A-Urea	50 mM 50 mM 8 M 10 mM 0.02 % (w/v)	Tris-HCl, pH 7.4 NaCl Urea β -Mercaptoethanol Azide
Buffer A ⁻	50 mM 50 mM 10 mM 0.02 % (w/v)	Tris-HCl, pH 7.4 NaCl β -mercaptoethanol Azide

Buffers for reconstitution of *E. coli* photolyase via dialysis

Buffer A _{NIS}	50 mM 50 mM 100 mM 10 mM 0.02 % (w/v)	Tris-HCl, pH 7.4 NaCl Imidazole β-Mercaptoethanol Azide
Buffer A ⁻	50 mM 50 mM 10 mM 0.02 % (w/v)	Tris-HCl, pH 7.4 NaCl β-Mercaptoethanol Azide
Buffer A-Urea	50 mM 50 mM 8 M 10 mM 0.02 % (w/v)	Tris-HCl, pH 7.4 NaCl Urea β-Mercaptoethanol Azide
Buffer B-Urea	50 mM 50 mM 500 mM 8 M 10 mM 0.02 % (w/v)	Tris-HCl, pH 7.4 NaCl Imidazole Urea β-Mercaptoethanol Azide
Buffer C _{Dy}	50 mM 50 mM 10 mM 20% (v/v) with either 4, 2, 1 or 0 M 0.02 % (w/v)	HEPES, pH 7.4 NaCl DTT Glycerol Urea Azide

Buffers for reconstitution of *E. coli* photolyase via Phenylsepharose

Buffer A _{PS}	50 mM 1.7 M 0.5 mM 10 mM 20% (v/v)	KH ₂ PO ₄ , pH 7.0 (NH ₄) ₂ SO ₄ EDTA DTT Glycerol
------------------------	--	--

Buffer B _{PS}	50 mM 1.7 M 0.5 mM 10 mM 20% (v/v) saturated with	KH ₂ PO ₄ , pH 3.5 (NH ₄) ₂ SO ₄ EDTA DTT Glycerol KBr
------------------------	--	---

Buffer C _{PS}	100 mM 0.5 mM 10 mM 50% (v/v)	KH ₂ PO ₄ , pH 7.0 EDTA DTT Ethylene glycol
------------------------	--	--

Buffers for *C. ammoniagenes* FAD-synthetase purification from host cell *E. coli*

(vacuum filtrated and degassed):

Buffer A _A	20 mM 200 mM 1 mM 0.02 % (w/v)	Tris-HCl, pH 7.4 NaCl EDTA Sodium azide
-----------------------	---	--

Buffer B _A	20 mM 200 mM 1 mM 50 mM 0.02 % (w/v)	Tris-HCl, pH 7.4 NaCl EDTA Maltose Sodium azide
-----------------------	--	---

Restriction endonuclease buffers:

NEBuffer 1 (1x)	10 mM 10 mM 1 mM	Tris-HCl, pH 7.0 MgCl ₂ DTT
-----------------	------------------------	--

NEBuffer 2 (1x)	10 mM 50 mM 10 mM 1 mM	Tris-HCl, pH 7.9 NaCl MgCl ₂ DTT
-----------------	---------------------------------	--

NEBuffer 3 (1x)	50 mM	Tris-HCl, pH 7.9
	100 mM	NaCl
	1 mM	DTT
	10 mM	MgCl ₂

NEBuffer 4 (1x)	20 mM	Tris-Ac, pH 7.9
	50 mM	KAc
	10 mM	MgAc ₂
	1 mM	DTT

Buffers and solutions for SDS-Polyacrylamide gel electrophoresis:

Acrylamide solution	38.9 % (w/v)	Acrylamide
	1.2 % (w/v)	Bisacrylamide
Ammonium peroxide sulfaphate solution (APS)	10 % (w/v)	
Bromophenol Blue solution	0.25 % (w/v)	
Coomassie Blue solution	0.25 % (w/v)	Coomassie-Blue R-250
	45 % (v/v)	Methanol
	9 % (v/v)	Acetic acid
Electrophoresis buffer	25 mM	Tris-HCl, pH 8.3
	192 mM	Glycine
	0.1 % (w/v)	SDS
Destainer I	50 % (v/v)	Methanol
	10 % (v/v)	Acetic acid
Destainer II (over night)	5 % (v/v)	Methanol
	7.5 % (v/v)	Acetic acid
Stacking gel buffer	250 mM	Tris-HCl, pH 6.8
	0.2 % (w/v)	SDS

SDS-PAGE sample buffer	5 %	SDS
	30 %	Glycerol
	60 mM	Tris-HCl, pH 6.8
	10 %	Sucrose
	3 %	2-Mercaptoethanol
	0.02 %	Bromphenol blue
Resolving gel buffer	1.5 M	Tris-HCl, pH 8.8
	0.4 % (w/v)	SDS
12 % resolving gel buffer	3.0 ml	Acrylamide
	4.5 ml	H ₂ O
	2.5 ml	stacking gel buffer
	75 µl	APS
	5 µl	TEMED
4 % stacking gel buffer	0.5 ml	Acrylamide
	2.0 ml	H ₂ O
	2.5 ml	stacking gel buffer
	75 µl	APS
	5 µl	TEMED

Ladders for DNA and Protein electrophoresis:

1 kb DNA ladder (NEB)	10 kbp, 8 kbp, 6 kbp, 5 kbp, 4 kbp, 3 kb, 2 kb, 1.5 kbp, 1 kbp 0.5 kbp
Protein marker broad range (NEB)	175 kDa, 83 kDa, 62 kDa, 47.5 kDa, 32.5 kDa, 25 kDa, 16.5 kDa, 6.5 kDa
Protein marker broad range (NEB)	212 kDa, 158 kDa, 116 kDa, 97.2 kDa 66.4 kDa, 55.6 kDa, 42.7 kDa, 34.6 kDa 27 kDa, 20 kDa, 14.3 kDa, 6.5 kDa, 2.4 kDa

2.1.5 Bacterial strains

For molecular biology work, derivatives of the *E. coli* K12 strain were used as listed in table 2.1. The genotype of the *B. subtilis* strain is shown in table 2.2.

E. coli strains:

strain	genotype	source
XL1-Blue	<i>recA1, endA1, gyrA96, thi-1, hsdR17, supE44, relA1, lac, [F', proAB, lac^fZΔM15, Tn10 (tet^r)]</i>	Bullock <i>et al.</i> 1987
BL 21 (DE3)	<i>F⁻, ompT, hsdS_B(r_B⁻, m_B⁻), dcm, gal, λ(DE3)</i>	Promega
M15[pGB3]	<i>lac, ara, gal, mtl, recA⁺, uvr⁺, [pGB3, lacI, bla^r]</i>	Qiagen

Table 2.1: *E. coli* strains

B. subtilis strain:

strain	genotype	source
BR151[pBl1][p602E109A]	<i>trpC2, lys-3, metB10 [pBL1, lacI, ery^r]</i> <i>[p602, lacI, kan^r, phrE109A]</i>	Schleicher, 2001

Table 2.2: *B. subtilis* strain

2.1.6 Plasmids

The expression plasmids used are listed in table 2.3.

plasmid	size [kbp]	resistance	source
p602E109A	5.8	Kanamycin	Schleicher 2003
pET 19b-phr-5.2	7.2	Ampicillin	Ladebeck 2008
pMalribF-CA	7.6	Ampicillin	Kemter 2003

Table 2.3: *Plasmids*

2.1.7 Primers

Primers were synthesized by Operon Biotechnologies[©]:

Primer	Sequence
OL_phr-NdeI-fwd	GGAGAAA <u>CATATG</u> ATGACTACCCATC <i>NdeI</i>
OL_phr-BamHI-reverse	TCACGCC <u>GGATCC</u> GGCATCTG <i>BamHI</i>

Table 2.4: *Primers; (Restriction sites are underlined)*

2.2 Molecular-biological methods

2.2.1 Amplification of DNA using Polymerase Chain Reaction (PCR)

PCR (Mullis *et al.*, 1990) is a well-established method in biochemistry used to increase the amount of a short DNA fragment *in vitro*. It requires four main components: the template DNA, a set of short oligonucleotide primers specific to known sequences on the template strand, deoxynucleotide triphosphates (dNTPs) of adenine, thymine, cytosine and guanine and a thermostable DNA polymerase *e.g.* Taq. The reaction proceeds in repeated cycles at three temperatures. In the initial step, 94-96°C, the template DNA double strand is denatured to give two DNA single strands. At the second temperature, which depends on the sequence and the length of the primers and varies usually between 45-60°C, the primers hybridize to the complementary sequences on the parent strand. The primers are extended in step three by the addition of individual deoxynucleotides by DNA polymerase to synthesise the new DNA strand at 72°C. Repeating this three temperature process allows an exponential amplification of the template DNA with an average rate of 1000 nucleotides per min. A final incubation time between 10 to 20 min at 72°C ensures the completion of the DNA copying by the DNA polymerase. The following protocol was used:

Template DNA (5-25 ng)	2 μ l
dNTPs (25 mM each)	0.8 μ l
Primer forward (100 pmol)	0.5 μ l
Primer reverse (100 pmol)	0.5 μ l
Polymerase buffer (10 x)	10 μ l
Taq-DNA-Polymerase (1 U)	1 μ l
dH ₂ O (sterile)	85.2 μ l
<hr/>	
Total volume	100 μ l

Step	Temperature[°C]	time[s]	function
1	94	30	Separation of DNA double strands
2	54-62	30	Primer hybridisation
3	72	30	Primer elongation
4	72	600-1200	Final elongation

Table 2.5: PCR temperature and time scheme (Steps 1-3 repeated 25 times)

2.2.2 Agarose gel electrophoresis

For analytical and preparative separation of DNA fragments, agarose gel electrophoresis was used. Negatively charged DNA molecules move in the electrical field towards the anode and smaller molecules move faster in agarose gels than larger molecules. Thus, this method can be used to determine the size of DNA fragments,

their purity and their concentration in a sample by comparing to a known DNA ladder. To determine the size of DNA fragments DNA molecular weight markers with definite sizes can be used. Agarose gels are usually prepared at concentrations between 0.8-1 % (w/v). Agarose gels were prepared by suspending agarose powder in TAE buffer and boiling the mixture until a clear solution formed. The solution was poured onto the gel caster equipped with a gel comb. After a rigid agarose gel was formed, it was placed in an electrophoresis chamber and filled with TAE buffer so that the gel was completely submerged. The gel comb was removed from the gel and DNA samples (5–20 μ l) mixed with DNA sample buffer, as well as suitable molecular weight marker were pipetted into the wells of the gel. The electrophoresis chamber electrodes were connected to a constant voltage power supply (145 V) for 45–90 minutes. The colour marker bromophenol blue present in the sample buffer makes the progress of electrophoresis visible. The gel was then incubated 20 minutes in ethidium bromide solution (1 μ g/ml) in the dark. Ethidium bromide can intercalate into double stranded DNA and becomes highly fluorescent under UV light (366 nm) and therefore makes nucleic acids visible upon UV excitation.

2.2.3 Purification of DNA

For concentration and purification of DNA, either PCR fragments, restriction- or ligation samples, “QIAquick PCR Purification kit” from (QIAGEN, West Sussex, UK) was used. The purification buffers contain chaotropic salts, which dehydrate the DNA so that the negatively charged phosphate groups interact via salt bridges with hydroxyl groups of a silica gel matrix attached to a microcentrifuge tube (spin

column). Polysaccharides and proteins do not bind the matrix and can be eluted under high salt conditions. An elution with water or low salt buffers will re-hydrate and elute the DNA from the silica gel matrix. Binding buffer was mixed with DNA in the ratio 5:1, placed on a silicagel containing spin column and centrifuged (1 min, 16,000 x g). The flow-through was discharged and the column was washed with 750 µl wash buffer (1 min, 16,000 x g). Residual wash buffer was removed by another centrifuge step (1 min, 16,000 x g). The DNA was eluted using 50 µl of sterile water. The average yield of DNA was approx. 90 %. Agarose gel electrophoresis was carried out to visualise the products of purification.

2.2.4 Restriction enzyme digestion of DNA

DNA digesting enzymes, so-called restriction endonucleases, recognise specific sites in the DNA by short palindromic sequences. These enzymes cut DNA either within that recognition site or a few nucleotides upstream or downstream. Three kinds of restriction cuts are possible: cuts with a 5' end or 3' end overhang (sticky ends) or with no overhang (blunt ends). Restriction endonucleases were obtained from New England BioLabs[®] *Inc.* For analytical digestions 100-300 ng of DNA, 2 µl of reaction buffer (10 x) and 0.5- 1 units (U) restriction endonuclease in a total volume of 20 µl were used. 1 U is defined as the amount of enzyme required to completely digest 1 µg of substrate DNA in a total reaction volume of 50 µl in one hour (New England BioLabs., 2006). Reaction mixtures were incubated for 1 h at 37°C. The results were examined by agarose gel electrophoresis. For preparative digestions, 1-5 µg DNA, 10 % (v/v) of reaction buffer and 4-8 U of restriction enzyme were used. The total

reaction volume was between 100-130 μ l. Samples were incubated for 3-4 h at 37°C, and subsequently transferred to an agarose gel, electrophoretically separated, incubated for 10 min in ethidium bromide and excised from the gel under UV light. The recovery of DNA from agarose fragments was undertaken using the “QIAquick Gel Extraction kit” (QIAGEN, West Sussex, UK). Three volumes of “binding buffer” were added to the gel fragment and incubated at 65°C with regular mixing until the agarose was melted. The solution was transferred to a spin column, centrifuged for 1 min at 16,000 x g and the flow-through was discharged. The DNA was washed and recovered in an identical manner to the procedure used in 2.2.3.

2.2.5 Ligation of DNA fragments

DNA fragments were ligated using the “Quick Ligation Kit” from New England BioLabs[®] *Inc.*. Briefly, DNA ligase isolated from T4 bacteriophage catalyses the ATP dependent phosphodiester bonding between the 3'-hydroxyl and the 5'-phosphate group of double stranded DNA. Vector DNA and the DNA fragment with the gene of interest (insert) were used in the molar ratio of 1:3.

Typical protocol was used:

1-6 μ L	50 ng Vector DNA
1-6 μ L	150 ng Insert DNA
	Adjusted to a total volume of 10 μ l with sterile water
10 μ L	2 x Quick ligation buffer
1 μ L	Quick T4 DNA ligase

The reaction was incubated for 5 min at room temperature and used to transform chemical competent cells via heat shock.

2.2.6 Preparation of chemical competent cells

Chemical competent cells were prepared by inoculating 100 ml of Luria Bertani media with 1 ml of an overnight culture of *E. coli* strains XL1-Blue or BL21 (DE3). The culture was incubated at 37°C on a shaker at 145 rpm. The culture was grown to an optical density (OD) of 0.6 at 600 nm and then cooled on ice to 4°C. A 100 ml volume of the culture was then transferred to a 250 ml centrifuge tube and the culture was centrifuged for 30 min at 2,700 x g at 4°C. The pellet was resuspended with 50 ml of cold (4°C) 50 mM CaCl₂ buffer. The resuspended cells were put on ice for 10 min and then centrifuged again (30 min, 2,700 x g, 4°C). The pellet was resuspended with 30 ml of cold (4°C) 50 mM CaCl₂ buffer containing 15 % (v/v) glycerol. The suspension was dispensed as small aliquots of 100 µl in sterile eppendorf tubes, snap frozen in liquid nitrogen and stored at -80°C. The transformation efficiency was approx. 3×10^7 transformants/µg of DNA.

2.2.7 Heat shock transformation

An aliquot of 100 µl chemical competent cells was incubated on ice for 10 min. Either ligation reaction or plasmid DNA was added to the competent cells and incubated for 30 min on ice. Then the DNA was transferred into the batch of competent cells and

incubated for 30 min on ice. The cell–DNA mix was incubated at 42°C for 1 min in a heating block, returned to ice for 2 min and then 1 ml of SOC medium was added. The cells were then incubated for one hour at 37°C in a shaking incubator before being streaked out on agar plates containing the appropriate selective antibiotic(s).

2.2.8 Plasmid isolation

Fresh overnight culture (10 ml) bearing the desired plasmid was centrifuged (15 min, 16,000 x g) and the supernatant discarded. Plasmid isolation was performed using the Qiagen Plasmid Mini Kit (QIAGEN, West Sussex, UK). The pellet was resuspended in 250 µl of solution I and transferred to a microcentrifuge tube. In order to lyse the cells, 250 µl solution II was added, mixed gently by repeatedly inverting the tube until the solution became viscous and slightly clear. Lastly 350 µl of solution III was added, and mixed by gentle and thorough inverting the tube. The solution became cloudy. Subsequently the microcentrifuge tube was centrifuged (10 min, 16,000 x g). The supernatant was pipetted carefully in a spin column and centrifuged to allow the DNA to bind to the column matrix (1 min, 16,000 x g). The flow-through was discarded. The spin column was washed by adding 500 µl of HB buffer and subsequent centrifugation (1 min, 16,000 x g). Thereafter it was washed with 750 µl of DNA wash buffer, centrifuged (1 min, 16,000 x g), and the flow-through was discarded. For complete removal of residual DNA wash buffer, the spin column was centrifuged for an additional 1 min at 16,000 x g. To elute the plasmid DNA, the spin column was placed in a clean microcentrifuge tube, 50 µl of sterile water was added

and centrifuged (1 min, 16,000 x g). By this method up to 20 µg of plasmid DNA can be isolated from 10 ml of cell culture.

2.3 Protein chemical methods

2.3.1 Culture preservation

Bacterial cultures were streaked on agar plates with appropriate antibiotics, incubated over night at 37°C and then stored at 4°C. Every four weeks, the new subcultures were prepared on fresh medium. For long-term storage of stock cultures, 10 ml over night cultures were centrifuged (10 min, 2,700 x g, 4°C) and the supernatant discarded. The cell pellet was resuspended in 1 ml LB media containing 50 % glycerol (v/v) transferred to sterile eppendorf tubes, snap frozen in liquid nitrogen and stored at -80°C.

2.3.2 Protein expression

Bacteria were cultured in Luria Bertani (LB) media with the appropriate antibiotic(s). Culture media supplemented with appropriate antibiotics was inoculated with an over night culture of bacterial strain in the ratio 1:100 and incubated at the desired temperature (25°C, 30°C or 37°C) in a shaking incubator until reaching an optical

density (OD) of 0.5-0.7 at 600 nm. Gene expression was induced by the addition of IPTG to a final concentration of 1 mM, and the cells were incubated (25°C, 30°C or 37°C) for 4 h or overnight. The cells were harvested by centrifugation (20 min, 2,700 x g, 4°C), the pellet was washed with 0.9 % saline, centrifuged (30 min, 2,700 x g, 4°C), and stored at -20°C till protein purification.

2.3.3 The testing of protein expression

LB media (5 ml) supplemented with the appropriate antibiotics was inoculated with bacteria cells from a single colony grown overnight at 37°C. 20 µl of this over night culture was used to inoculate a 200 ml LB culture with appropriate antibiotics. The culture was incubated at 37°C with shaking. Cells were grown to an optical density (OD) of 600 nm of 0.5-0.7 and IPTG was added to a final concentration of 1 mM to induce expression. Cells were incubated for a further 4 h or over night. To break open the cells, the cell pellet (in lysis buffer) was disrupted by ultrasonification, centrifuged (10 min, 48,000 x g, 4°C), and supernatant checked for protein expression by means of SDS polyacrylamide gel electrophoresis.

2.3.4 SDS polyacrylamide gel electrophoresis

The purity of protein fractions was determined using discontinuous sodium dodecylsulfate polyacrylamide gel electrophoresis (SDS-PAGE) according to the system of Laemmli (1970). SDS is an anionic detergent, which denatures proteins and

confers net negative charges to proteins. The proteins have mobility that is inversely proportional to their size.

The gel was prepared using the SDS-PAGE discontinuous buffer system. The components of the resolving gel solution were mixed together and then loaded into the slab deposited between two glass plates on the gel caster. The gel was covered with isopropanol. Polymerisation of acrylamide was completed after 10 min and isopropanol was removed. The stacking gel solution was prepared, and loaded on top of the resolving gel in the presence of a 10-15 well comb. Polymerisation of stacking gel was completed after 10 min. The slab gel was placed on the SE 250 Mighty Small II electrophoresis system (Hoefer, San Francisco, USA), which was connected to a cooling system. Protein samples were mixed with SDS-sample buffer in a ratio of 1:1. The mixtures were incubated at 95°C for 10 min. The protein samples were then loaded into the wells of the gel. Standard proteins were used as molecular-weight markers. Proteins were separated by passing 50 mA across the gel. After approx. 1 h, the gel was removed from the support plates and stained in staining solution for 30 min. The gel was destained with destaining solution for 1 hour. The following discontinuous buffer system recipe for two gels was used:

Resolving Gel (12%):

3.0 ml acrylamide

4.5 ml H₂O

2.5 ml resolving gel buffer

75 µl APS

5 µl TEMED

Stacking Gel (4%):

0.5 ml acrylamide

2.0 ml H₂O

2.5 ml stacking gel buffer

75 µl APS

5 µl TEMED

2.3.5 Expression of the DNA photolyase E109A mutant

DNA photolyase from *E. coli* was expressed in the recombinant *B. subtilis* strain BR151 harbouring plasmids pBL1 and p602E109A. Cells were cultured in baffled 2 l Erlenmeyer flasks containing 800 ml LB medium supplemented with 15 mg/l kanamycin and 10 mg/l erythromycin. The cultures were incubated at 28°C while shaking. At an optical density of 0.6 (600 nm), IPTG was added to a final concentration of 1 mM, and incubation was continued for 14 h. The cells were harvested by centrifugation and stored at -20°C.

2.3.6 Expression of DNA photolyase containing a 10 x His tag

The recombinant *E. coli* strain BL21 (DE3) harbouring the plasmid pET-19b-phr-5.2 was cultured in baffled 2 L Erlenmeyer flasks containing approx. 800 ml of 2x YT medium supplemented with 150 mg/l ampicillin. The cultures were incubated at 25°C with shaking. At an optical density of 0.7-0.8 (600 nm), IPTG was added to a final concentration of 1 mM, and incubation was continued at 20°C for 14 h. The cells were harvested by centrifugation (20 min, 2,700 x g, 4°C), and stored at -20°C.

2.3.7 Expression of FAD synthetase from *C. ammoniagenes*

The recombinant *E. coli* strain XL1-Blue harbouring the plasmid pMalribF-CA containing the genes for FAD synthetase and the maltose binding protein *MalE* as

fusion-tag, was cultured in baffled 2 L Erlenmeyer flasks containing 500 ml LB media supplemented with 150 mg/l ampicillin. The cultures were incubated at 37°C while shaking. At an optical density of 0.6 (600 nm), IPTG was added to a final concentration of 1 mM, and incubation was continued for 4 h at 37°C. The cells were harvested by centrifugation (20 min, 2,700 x g, 4°C) and stored at -20°C.

2.3.8 Protein extraction

The first step of a typical protein isolation procedure consists of cell disruption, which releases the protein in soluble form from its intracellular compartment. For cell disruption, thawed cell pellet (5-10 g wet cell mass) were suspended in respective buffer (10 ml per g of wet cell mass). Lysozyme (1 mg-5 mg/g of cells), 1 mM PMSF and DNaseI (0.1 mg/g of cells) were added.

The mixture was incubated at room temperature for 30 min while stirring. Sonification was performed for cell lysis. The extract obtained after lysis, termed homogenate, was centrifuged (30 min, 48,000 x g, 4°C). The subsequent supernatant, called the crude extract was used for protein purification.

2.3.9 Protein purification

2.3.9.1 Purification of *C. ammoniagenes* FAD synthetase

The purification of the enzyme FAD synthetase from *C. ammoniagenes* was carried out by utilising the strong affinity of the fusion tag protein, maltose binding protein, to the polysaccharide amylose. The crude extract in buffer A was applied to an amylose drip column (volume 10 ml; amylose resin from New England Biolabs[®]) previously equilibrated with buffer A. The column was washed with buffer A till the Abs_{280nm} was less than 0.1. The protein was eluted with buffer B containing 50 mM maltose. Fractions (5 ml) were collected and analysed by SDS-PAGE.

2.3.9.2 Purification of DNA photolyase E109A mutant

DNA Photolyase tends to self-aggregation under oxidative conditions. The catalytic cofactor FAD can be present in three different oxidation states and their interconversion is dependent upon light and oxygen. All purification work with this enzyme, when possible, was therefore accomplished under argon atmosphere in order to prevent a change of oxidation state. The recombinant DNA photolyase E109A mutant was isolated in its blue radical form by the following sequence of three chromatographic steps:

Dye affinity chromatography:

The principle of the dye affinity chromatography is based on the interaction of colouring materials with protein, which is mainly due to the binding of proteins with

adenyl containing cofactors (such as ATP, NADH and NADPH) to the dye. Since the binding effect of the dye to the protein decreases with an increasing salt concentration, protein can be eluted from the column. The column of Blue Sepharose (colouring material: Cibacron-Blue; Amersham Biosciences; column volume 10 ml) was first equilibrated with 5 column volume of buffer A_{BS} and the crude cell extract was applied to the column. The column was washed with a minimum of 10 column volumes of buffer A_{BS} ($Abs_{280nm} < 0.1$). Protein was then eluted with an increasing salt gradient of potassium chloride in buffer B_{BS} . All steps were accomplished with a flow rate of 2 ml/min. The fractions containing the protein were combined. To exchange the buffer two different methods were used: first of all the ammonium sulphate precipitation and secondly a desalting column.

Ammonium sulphate precipitation:

The solubility of a protein in aqueous environment strongly depends on the concentration of dissolved salts. At high ionic strength, the solubility of a protein decreases due to competition between salt ions and protein around the solvated molecules. Thus the protein concentration can be altered while simultaneously exchanging the buffer through a fast and simple method termed "salting out". Ammonium sulphate is commonly used due to its good solubility in water and high ionic strength. The combined photolyase fractions were incubated with ammonium sulphate (0.43 g/ml) which was added over a time period of 30 min with stirring and then centrifuged (10 min, 27,000 x g, 4°C). The precipitate, which could be stored at -80°C if necessary, was dissolved in 5 ml buffer C_{DS} for the next desalting step.

Desalting column:

The desalting column HiPrep 26/10 (Amersham Biosciences) was used with an exclusion volume of 5 kDa. The column was equilibrated with 3 column volume of buffer C_{DS}. The protein sample was applied to the column with a maximum volume of 10 ml and eluted with a flow rate of 5 ml/min. Fractions containing protein were combined.

Affinity chromatography:

For affinity chromatography Heparin Sepharose CL-6B (Amersham Bioscience) was used as the column material. It consists of 6% high cross linked agarose, which contains 3 mg heparin/ml column volume. This material exhibits an affinity for oligonucleotide binding proteins. The column was equilibrated with 3 column volume of buffer D_{HS}. The protein solution (in buffer C_{DS}) was applied to the column, washed with a minimum of 10 column volumes of buffer D_{HS} and then eluted with increasing salt concentrations of 0.001-1 M of KCl in buffer E_{HS}. All steps were accomplished with a flow rate of 2 ml/min. Protein containing fractions were identified by SDS-PAGE and combined. A second desalting column step was used to transfer the protein in the desired storage buffer C_{DS}. The enzyme could be stored without loss of activity at -80°C.

2.3.9.3 Purification of photolyase with 10 x His tag

Nickel chelating chromatography:

Photolyase protein was purified by immobilised metal affinity chelating chromatography (IMAC). To immobilise the metal ions on Chelating Sepharose Fast

Flow, a solution of 200 mM NiSO₄ was passed through the column. The column was washed with distilled water containing 0.02 % azide to remove excess NiSO₄. The column was then equilibrated with 10 column volumes of buffer A_{NiS} with the flow rate of 2 ml/min. The crude extract in buffer A_{NiS} was applied to the column of Nickel Chelating Sepharose Fast Flow (column volume 10 ml). The column was washed with at least 10 column volumes of buffer A_{NiS}, and was then switched to a linear gradient increasing the concentration of imidazole from 100 mM (buffer A_{NiS}) to 500 mM (buffer B_{NiS}).

2.3.10 Protein concentration by ultrafiltration

Ultrafiltration was used to concentrate protein. The protein solution was added to a stirred cell with a volume of either 10 ml or 50 ml (AMICON, Witten, Westphalia) and passed through a cellulose filter with a molecular weight cut off of 30 kDa (Millipore Corporation, Bedford, MA, USA).

Concentration of small volumes of protein (300-500 µl) was achieved using Microcon centrifugal filter devices (Millipore Corporation) according to the supplier's protocol. The exclusion limit of the membrane was selected to retain the target protein.

2.3.11 Determination of protein concentration

Protein concentration was determined photometrically by UV/Vis spectroscopy, which obeys Beer-Lambert's law:

$$A = \epsilon_{\lambda} \cdot c \cdot d$$

Where A is the absorbance, ϵ the molar extinction coefficient at the specific wavelength λ with units of $M^{-1} \cdot cm^{-1}$, c is the concentration of the absorbing sample expressed in $mol \cdot L^{-1}$ and d the path length of the cuvette in cm.

Determination of the concentration of DNA photolyase:

The concentration of DNA photolyase could be determined by characteristic UV/Vis spectrum absorption signals of its cofactor FAD in its three oxidation states: reduced, radical and oxidised. The following table shows the different molar extinction coefficients for maxima of the three oxidation states (Jorns et al., 1990).

Wavelength (nm)	Oxidation state of FAD		
	oxidised	radical	reduced
380	11000	6000	5680
443	11200	--	--
580	--	4800	--

Table: 2.6: Molar extinction coefficients of DNA photolyase from *E. coli* at different oxidation states

Determination of concentration of DNA photolyase under denatured conditions:

The concentration of protein under denatured conditions was determined using the molar extinction coefficient for apophotolyase $\epsilon_{280nm} = 103630 M^{-1} \cdot cm^{-1}$ (Xu et al., 2006).

Determination of the concentration of FAD synthetase (in fusion with maltose binding protein):

The concentration of FAD synthetase in fusion with maltose binding protein was determined using the sum of the molar extinction coefficient $\epsilon_{280\text{nm}} = 28500 \text{ M}^{-1} \text{ cm}^{-1}$ for FAD synthetase (Efimov *et al.*, 1998) and $\epsilon_{280\text{nm}} = 66350 \text{ M}^{-1} \text{ cm}^{-1}$ for maltose binding protein. The sequence for the maltose binding protein was provided from supplier New England BioLabs[©] *Inc.*, the molar extinction coefficient at 280 nm was calculated using the ProtParam tool from Expasy (<http://www.expasy.ch/>).

2.4 Enzymatic conversion of roseoflavin to roseoFAD

The phosphorylation and adenylation of roseoflavin to roseoFAD is a two-step reaction, catalyzed by the bifunctional enzyme FAD synthetase from *C. ammoniagenes*. It takes place at physiological pH and at 37°C and was performed using a modified protocol from Manstein and Pai (1986). 160 nmol roseoflavin (Supplier: MP Biomedicals, Ohio, USA) and 5.28 μmol ATP was diluted in 20 ml FAD-synthetase-reaction buffer (50 mM Tris-HCl, pH 7.5, 15 mM MgCl_2) at room temperature. The solution was then incubated for 20 min at 37°C and the pH was readjusted to 7.5 before 7.5 mg of enzyme was added. The solution was incubated in the dark at 37°C for 14 h with shaking. The conversion was confirmed by thin layer chromatography (TLC) with solvent of *n*-butanol, acetic acid and dH_2O in the ratio 3:1:1 and electrospray ionization mass spectrometry (ESI-MS).

2.4.1 Purification of roseoFAD

To separate FAD synthetase and MgCl_2 from roseoFAD the reaction mixture was purified via anion exchange chromatography (Q-Sepharose, column volume 70 ml). The column was equilibrated with 3 column volumes of buffer A^- . RoseoFAD did not bind to the column and was collected in the wash fractions. FAD synthetase, which did bind to the column, was eluted from the column by a constant gradient of NaCl (50 mM to 1 M) in buffer A^- . Further purification of roseoFAD was performed as followed.

RoseoFAD was applied on a florisil column (Acros Organics, volume 50 ml) and washed with 3 column volumes dH_2O and then eluted from the column with 50 % (v/v) acetone in water. The eluate was concentrated to half of its original volume in a Buechi rotavapor under reduced pressure and subsequently lyophilised. The lyophilised roseoFAD could be stored in the dark at 4°C .

2.4.2 Determination of concentration of roseoflavin and roseoFAD

The concentration of roseoflavin or roseoFAD was determined by measuring the absorbance at 505 nm (molar extinction coefficient $\epsilon_{505\text{nm}} = 31500 \text{ M}^{-1} \text{ cm}^{-1}$) (Otto et al. 1981).

2.4.3 Reconstitution of photolyase with roseoFAD

2.4.3.1 Reconstitution of photolyase via Ni-NTA

The crude extract was passed through a Nickel Chelating Sepharose Fast flow drip column (volume 10 ml or 2 ml), which had been equilibrated with buffer A_{NiS}. The column was washed with buffer A_{NiS} till Abs_{280nm} was less than 0.1, then switched to buffer A⁻ and washed with at least 5 column volumes. The column was then washed with buffer A-urea, containing 8 M urea until the flow-through was colourless (to visual inspection via UV-A lamp (366 nm) and UV/Vis spectroscopy), and then constantly washed with buffer A⁻ containing 0.5 mM FAD or 40 μM roseo-FAD for 14 h at 4°C. The column was subsequently washed with buffer A⁻ till unbound cofactor or cofactor analogues were completely washed off and the reconstituted protein was then eluted with buffer B (500 mM imidazole). The collected fractions were analysed by SDS-PAGE and UV/Vis spectroscopy to confirm reconstituted protein.

2.4.3.2 Reconstitution of photolyase via dialysis

Crude extract was passed through a Nickel Chelating Sepharose fast flow drip column (Volume 10 ml or 2 ml) equilibrated with 5 column volumes of buffer A. The column was washed with buffer A until the absorbance at 280 nm of the collected fractions was less than 0.1, then washed with buffer A⁻ for at least 5 column volumes. The

column was then washed with buffer A-urea, containing 8 M urea until the flow-through was colourless (to visual inspection via UV-A lamp (366 nm) and UV/Vis spectroscopy). The protein was eluted under denatured conditions using buffer B-urea (500 mM imidazole and 8 M urea). Fractions containing protein were analysed by SDS-PAGE, combined and concentrated using the AMICON system at room temperature to prevent crystallisation of urea in the protein solution. The concentration of denatured protein was determined by UV/Vis spectroscopy. 300 μ l photolyase (12 μ M) in buffer B-Urea and 300 μ l roseoFAD (110 μ M) in buffer A⁻ were transferred to a cellulose ester (CE) dialysis tube (Supplier: Spectra/Por[®], California, USA), with a molecular weight cut off of 100-500 Da. The mixture was dialysed for at least 12 h under argon atmosphere against buffer C_{Dy} (25 mL) containing decreasing urea concentrations: 4 M 2 M, 1 M and no urea. Results were analysed by UV/Vis spectroscopy.

2.4.3.3 Reconstitution of photolyase via phenylsepharose 6 FF

Reconstitution of photolyase with roseoFAD was carried out according to a modified protocol by Jorns *et al.* (1990). 900 μ l of 31 μ M photolyase solution were diluted in 3 ml buffer A_{PS} and passed on a phenylsepharose 6 FF drip column (bed volume 1 ml) which was equilibrated with buffer A_{PS}. The column was washed with 6 column volumes of buffer A_{PS}. Native FAD was removed by continuously washing with buffer B_{PS} at pH 3.5 until the flow through was FAD-free by visual inspection via UV-A lamp (366 nm) and UV/Vis spectroscopy. The pH was readjusted to 7 by washing with buffer A_{PS}. 40 μ M roseoFAD in buffer A⁻ containing 1.7 M (NH₄)₂SO₄

was passed through the column and cycled for at least 14 h at a flow rate of 0.25 ml/min. Reconstituted protein was eluted from the column with buffer C_{PS} and fractions were analysed by UV/Vis spectroscopy.

2.5 Photolyase purification and substrate preparation for the SPR/ EW-CRDS experiments.

2.5.1 Substrate preparation

Lyophilised single stranded DNA (10 μ mol of oligo-(dT)₁₈; supplier: OPERON[®]) was dissolved in SPR-buffer (50 mM Tris-HCl, pH 7.0, 50 mM NaCl, 20 % glycerol(v/v)) to give a final concentration of 2.2 μ M. The concentration was calculated using Beer-Lambert's law after measuring the absorption of DNA at 260 nm. The extinction coefficient for a single thymidine at 260 nm is $\epsilon_{260\text{nm}} = 8700 \text{ M}^{-1} \text{ cm}^{-1}$ (value taken from <http://www.operon.com>). The extinction coefficient of 18 thymidines at 260 nm was calculated to be $\epsilon_{260\text{nm}} = 156600 \text{ M}^{-1} \text{ cm}^{-1}$. 2.2 μ M oligo-(dT)₁₈ in 5 ml SPR-buffer were placed in a flat petri dish on ice. UV radiation at 256 nm using a UV lamp (model: UVG-11, 25 W, Upland; USA) was performed under constant stirring of the DNA-buffer solution for 20 min. The UV-damage of DNA was observed by following spectrophotometrically the decrease in absorption of DNA at 260 nm (Figure 2.1) until a constant value was reached. Detection of a decrease of the absorbance at 260 nm can be used to monitor photoproduct formation for the

following reason. The formation of a cyclobutane ring between two adjacent thymines is the dominant photoreaction induced by UV light that can occur in DNA. The covalent linkage results in the loss of aromaticity in the pyrimidine heterocycle, which results in a decrease of the absorbance at 260 nm. After 15 min of UV radiation a constant absorbance signal was observed. DTT was added to the irradiated sample to give a final concentration of 10 mM and the prepared samples were stored at 4°C prior to the experiment.

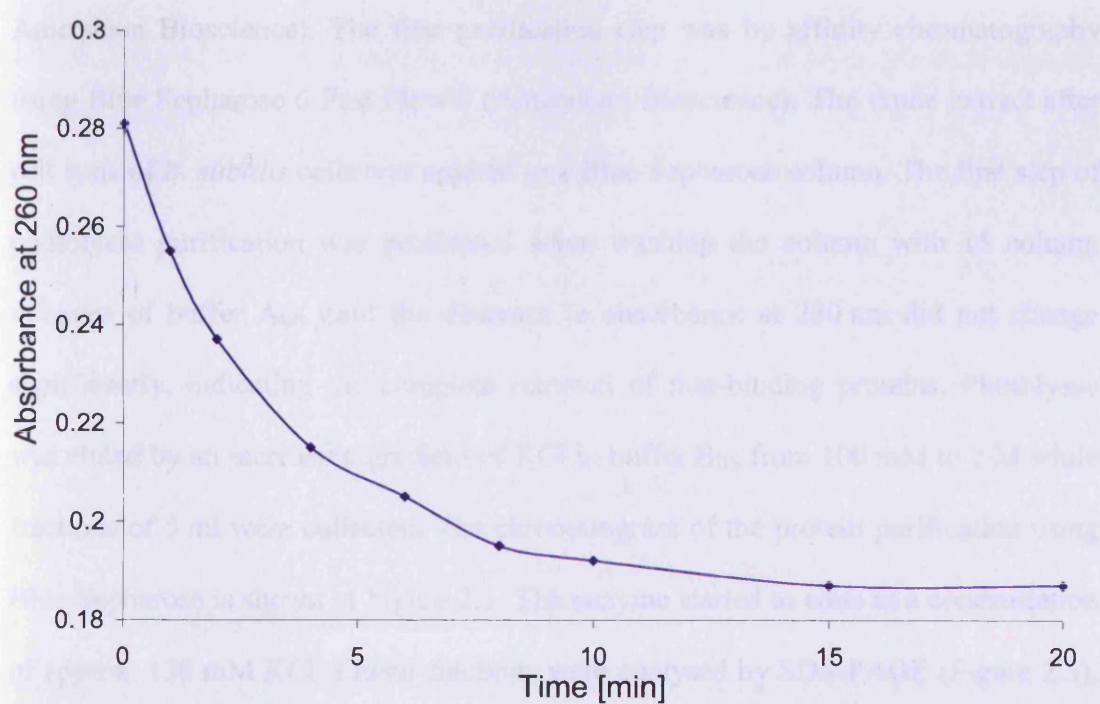


Figure 2.1: Time course of the photodamage of ssDNA oligo-(dT)₁₈ by 254 nm UV-light. The decay in absorbance at 260 nm was followed over the period of 20 min.

2.5.2 Photolyase purification

CPD Photolyase from *E. coli* was overexpressed in the *B. subtilis* host strain BR151[pB11] harbouring the expression vector p602, which contains the E109A-*phr* gene coding for *E. coli* photolyase. The *phr*-gene carries the E109A mutation in which the codon for glutamate 109 was replaced by a codon for alanine. Therefore the enzyme was expressed without the second cofactor MTHF. All chromatography steps were performed using fast protein liquid chromatography (FPLC, AKTA-System, Amersham Bioscience). The first purification step was by affinity chromatography using Blue Sepharose 6 Fast Flow© (Amersham Bioscience). The crude extract after cell lysis of *B. subtilis* cells was applied to a Blue Sepharose column. The first step of photolyase purification was performed when washing the column with 15 column volumes of buffer A_{BS} until the decrease in absorbance at 280 nm did not change significantly, indicating the complete removal of non-binding proteins. Photolyase was eluted by an increasing gradient of KCl in buffer B_{BS} from 100 mM to 2 M while fractions of 5 ml were collected. The chromatogram of the protein purification using Blue Sepharose is shown in Figure 2.2. The enzyme started to elute at a concentration of approx. 130 mM KCl. Eluted fractions were analysed by SDS-PAGE (Figure 2.3). Figure 2.3 shows that fractions 2-5 contain a high concentration of protein with a molecular weight of approx. 50 kDa corresponding to photolyase, and these fractions were combined. Fractions 3-5 contained higher photolyase concentration compared to the fraction in lane 2 but with a higher contamination of background proteins.

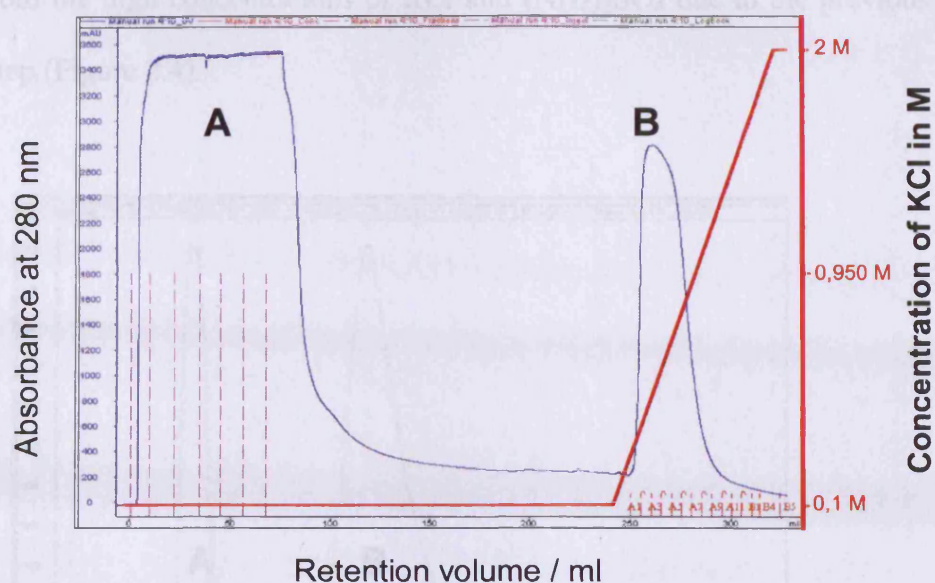


Figure 2.2: FPLC-chromatogram of photolyase purification via Blue Sepharose. A = unbound protein, flow through, B = photolyase elution peak; blue signal = absorbance at 280 nm; red signal = increasing concentration of KCl in M.

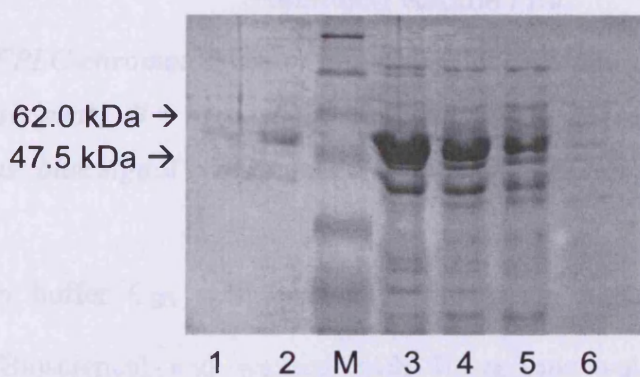


Figure 2.3: 12% SDS-PAGE of eluted protein fractions after Blue Sepharose purification. Lane 1-6 = eluted fractions; Fractions 2-5 containing photolyase were combined. M = protein marker

Proteins were precipitated from the combined fractions from the previous purification step (20 ml) by addition of 8.6 g $(\text{NH}_4)_2\text{SO}_4$. Protein was pelleted by centrifuging for 10 min at 27,000 $\times g$ at 4°C. The protein pellet was resuspended in 5 ml buffer C_{DS} and applied to a desalting column (HiPrep 26/10, Amersham Bioscience) to separate

the protein from the high concentrations of KCl and $(\text{NH}_4)_2\text{SO}_4$ due to the previous purification step (Figure 2.4).

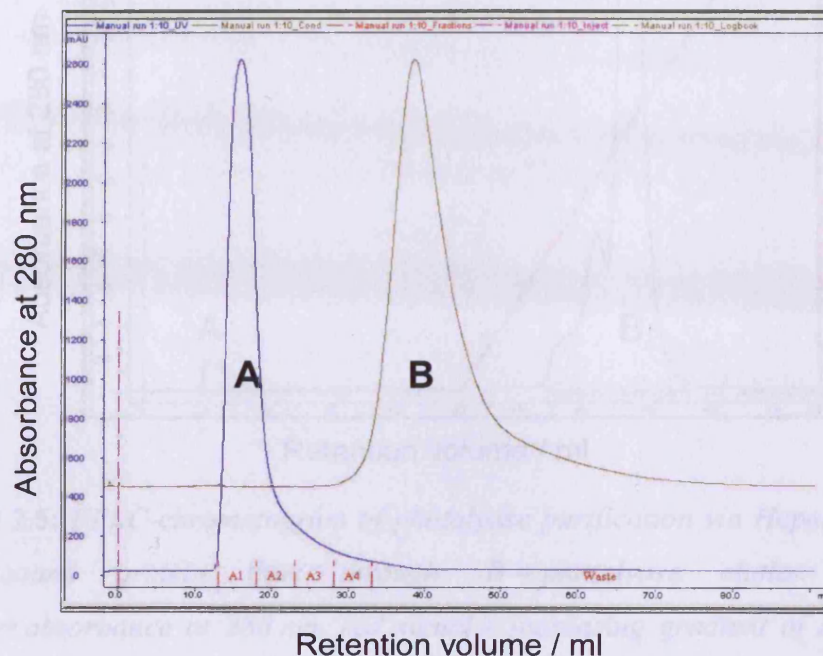


Figure 2.4: FPLC-chromatogram of photolyase purification on a desalting column. *A* = photolyase peak; *B* = high signal in conductivity as indication for high salt concentrations; blue signal = absorbance at 280 nm, grey signal = conductivity

Photolyase in buffer C_{DS} was applied to a Heparin Sepharose CL-6B column (Amersham Bioscience) and washed with 10 column volumes of buffer D_{HS} . Photolyase was eluted by increasing the concentration of KCl with buffer E_{HS} from 1 mM to 1 M. The chromatogram of photolyase purification via Heparin Sepharose is shown in Figure 2.5. The protein elutes at a concentration of approx. 450 mM KCl. Eluted fractions were collected and analysed by SDS-PAGE as shown in Figure 2.6.

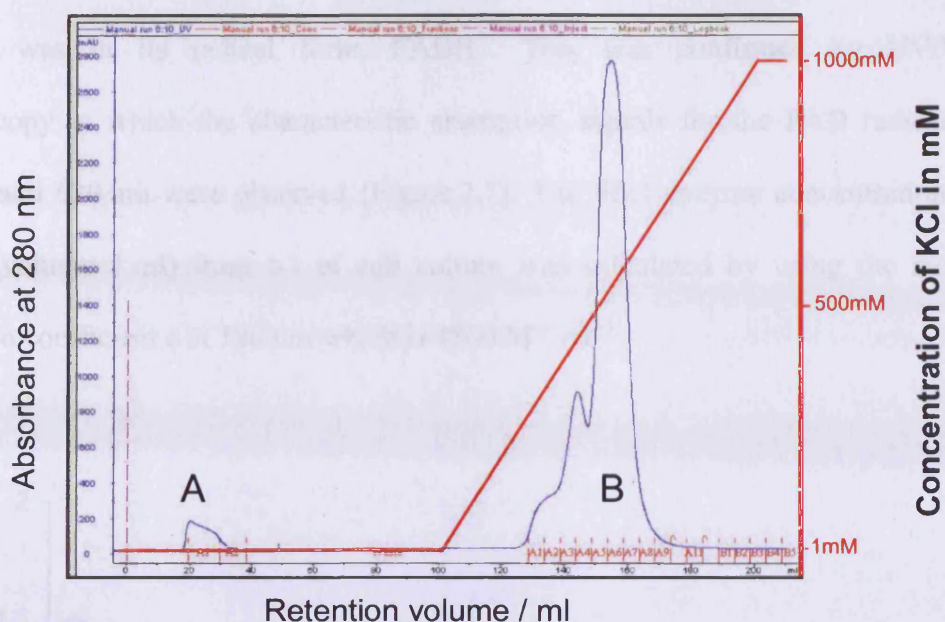


Figure 2.5: FPLC-chromatogram of photolyase purification via Heparin Sepharose. A = unbound protein flow through, B = photolyase elution peak; blue signal = absorbance at 280 nm, red signal = increasing gradient of KCl in elution buffer in M.

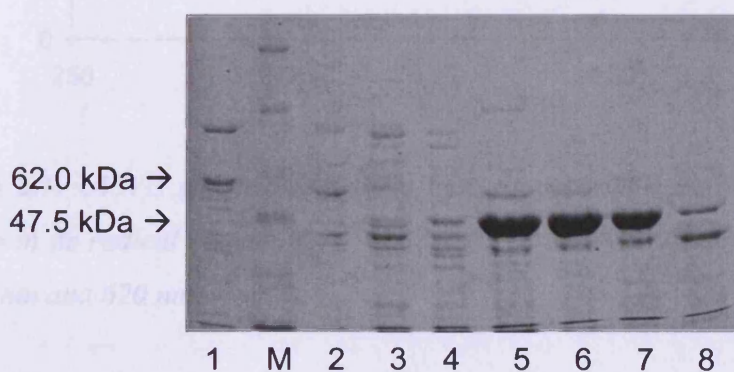


Figure 2.6: 12% SDS-PAGE of eluted protein fractions after chromatography on Heparin Sepharose. Lane 1-8 are fractions of the eluent; Fractions 5-7 containing photolyase were combined. M = protein marker

Following the Heparin Sepharose, a second $(\text{NH}_4)_2\text{SO}_4$ precipitation was performed on combined fractions 5-7 containing photolyase and the pellet was resuspended in 5 ml of buffer C_{DS}. The enzyme was finally concentrated using AMICON centrifugal

filter units. The colour of the enzyme solution was blue, which indicated that the FAD cofactor was in its radical form, FADH^\bullet . This was confirmed by UV/Vis spectroscopy in which the characteristic absorption signals for the FAD radical at 580 nm and 620 nm were observed (Figure 2.7). The final enzyme concentration of $68 \mu\text{M}$ (volume 1 ml) from 6 l of cell culture was calculated by using the molar extinction coefficient ϵ at 580 nm which is $4800 \text{ M}^{-1} \text{ cm}^{-1}$.

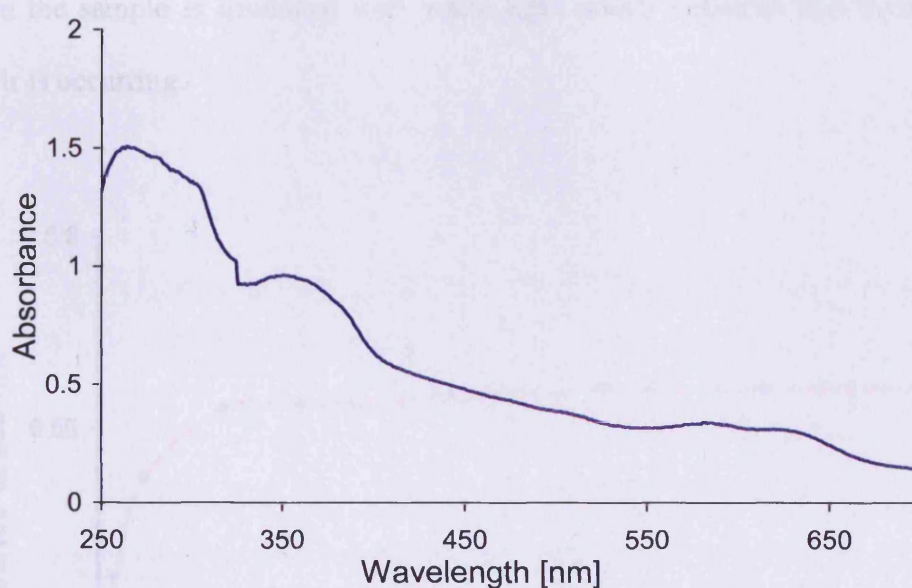


Figure 2.7: UV/Vis spectrum of photolyase after protein purification. The cofactor FAD is in its radical form FADH^\bullet indicated by the characteristic absorption signals at 580 nm and 620 nm.

The DNA repair ability of purified photolyase can be tested by adding the enzyme to UV irradiated DNA and exposing the sample to white light. A decrease in the absorbance at 260 nm upon irradiation of ssDNA oligo-(dT)₁₈ with UV light can be associated with thymine dimer formation, as mentioned in 2.5.1. By adding photolyase to UV light damaged DNA and subsequently white light exposure an increase in the absorbance at 260 nm would indicate for a thymine dimer repair.

135 nM enzyme (volume = 2 μ l) were transferred to 2.2 μ M UV-irradiated ssDNA oligo-(dT)₁₈, in reaction buffer (50 mM Tris-HCl, pH 7.0, 50 mM NaCl, 10mM DTT 20 % glycerol). The absorbance of the sample at 260 nm was measured and the sample was then kept for 10 min in a photon resistant container. The photolyase-UV irradiated DNA mix was then exposed to white light for a total time of 53 min while the absorbance at 260 nm was measured in 1 min, 2 min, 5 min and 10 min steps. An increase in the absorbance at 260 nm shown in Figure 2.8 (orange signal) is detected when the sample is irradiated with white light which indicates that thymine dimer repair is occurring.

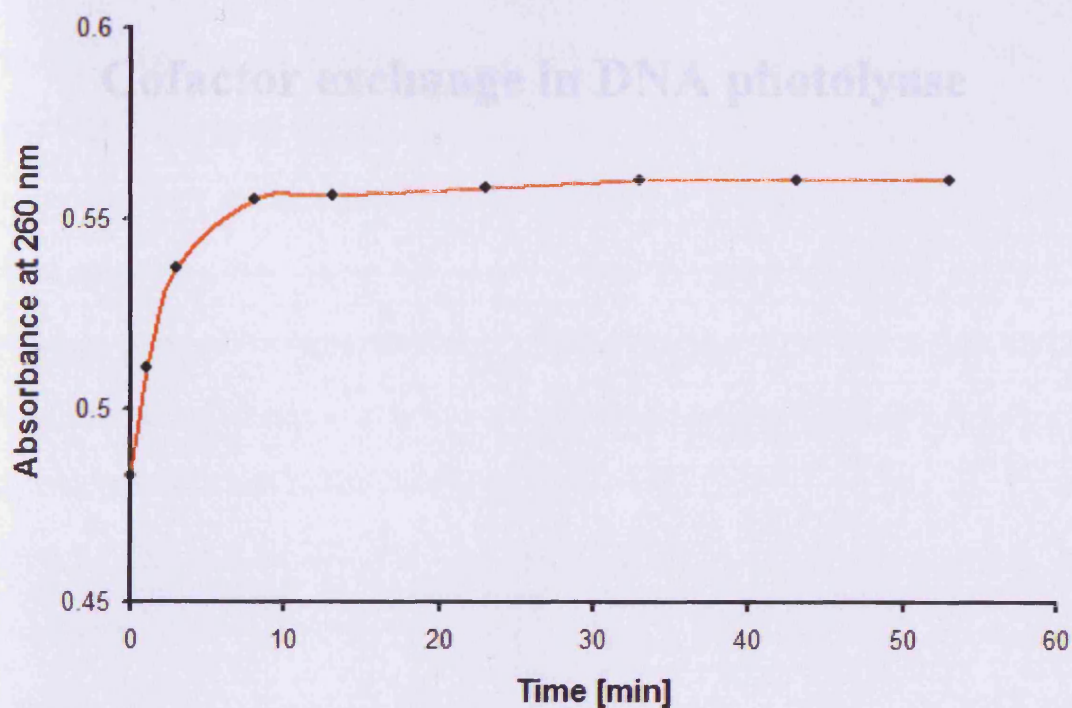


Figure 2.8: Time course of the photo repair of ssDNA oligo-(dT)₁₈ over a period of 53 min. The orange signal is showing an increase in the absorbance at 260nm after white light exposure. After approx. 30 min the signal has reached its maximum.

CHAPTER 3:

Cofactor exchange in DNA photolyase

3.1 Work describe in Chapter 3

The following chapter is about the replacement of the wild-type cofactor FAD in *E. coli* photolyase with the FAD analogue roseoFAD. RoseoFAD was chosen for the following purposes. Roseoflavin, a precursor of roseoFAD, is one of a few natural occurring riboflavin analogues (Otani *et al.*, 1974) and therefore easier commercial available than other non-natural flavin analogues. Secondly, the potential role of the C8 α -methyl group of FAD during DNA repair by photolyase is of interest, a modification such as a dimethyl-amino group on the C8-atom as in roseoFAD could have a significant impact on the redox potential of this flavin compound. The effects could influence the DNA repair ability of photolyase could therefore be directly linked to the modification on the C8 α .

To replace FAD in the photolyase enzyme with an alternative cofactor a stable photolyase expression system was created. The *phr* gene, containing an E109A mutation that results in the expression of a MTHF-free photolyase was cloned into the pET 19-b expression vector, which would express photolyase with a 10 x N-terminal His-tag. Therefore protein purification was performed via a single purification step on a Ni-NTA Sepharose column. This was carried out with the predominantly attempt to bind photolyase to a Ni-NTA sepharose column and to perform cofactor exchange on the immobilised enzyme. RoseoFAD was biochemically synthesised from its precursor form roseoflavin by a FAD synthetase from *Corynebacterium ammoniagenes*. FAD replacement with roseoFAD in photolyase was tried utilising three different methods: 1. Photolyase was immobilised on a Ni-NTA Sepharose column due to its high affinity of the additional His-tag to Ni²⁺-ions. Protein was denatured with a high urea concentration in the wash buffer resulting in the loss of

FAD. The incorporation of roseoFAD should then be achieved by refolding the protein in presence of roseoFAD when bound to the column while removing the urea.

3. Denatured apophotolyase was renatured in the presence of roseoFAD by removing the denaturing agent via dialysis. 3. The protein was immobilised via hydrophobic interaction to a phenylsepharose column and the extraction of FAD was achieved by lowering the pH in the wash buffer. RoseoFAD incorporation was carried out while adjusting the pH back to its physiological value in the presence of roseoFAD.

3.2 Reconstitution of apophotolyase with FAD cofactors and cofactor analogues

The replacement of an original cofactor with suitably modified cofactor analogues is a prevalent procedure to study its biological role and catalytic function in an enzyme. As FAD plays the key role in the enzymatic process of DNA repair in photolyase, it is of major interest to analyse its role and function in this enzyme. Reconstitution experiments were not only focused on FAD but also included the second cofactor MTHF, and were intensively carried out by several groups during recent years.

Payne *et al.*, 1990; Jorns *et al.*, 1990; Ramsey and Jorns, 1992, Xu *et al.*, 2006 published the replacement of FAD with the flavin analogue 5-deazaFAD (Figure 3.1) and the original cofactor in different oxidation states. The publications also included the attempt to recombine apophotolyase with riboflavin, FMN, Coenzyme F₄₂₀ and 1-deazaFAD (Figure 3.1). Jorns *et al.* (1990) also used MTHF derivatives differing in the number of glutamate residues for reconstitution experiments.

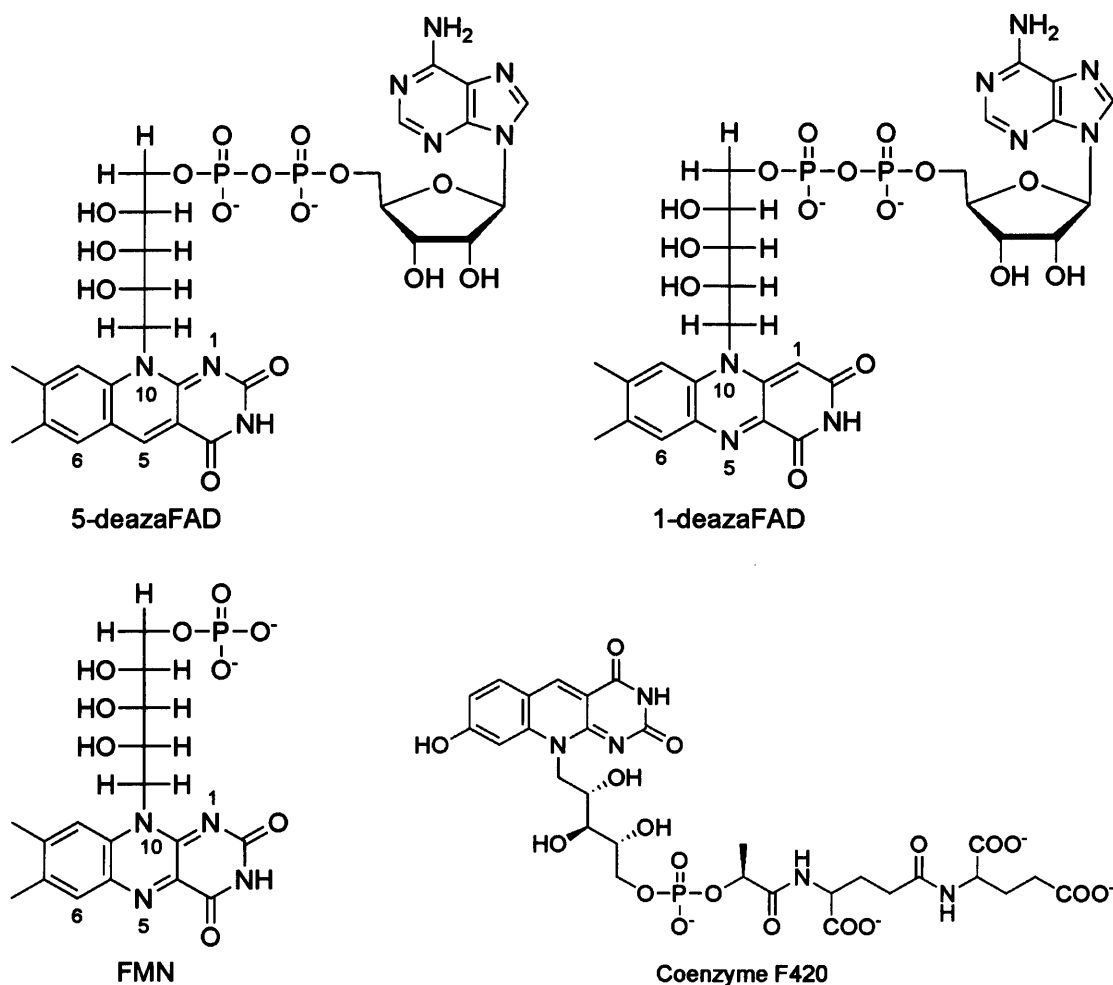


Figure 3.1: Riboflavin-related compounds used for reconstitution experiments. The chemical structure of riboflavin is shown in Figure 3.2.

Several fundamental aspects focusing on the protein structure around the catalytic centre and substrate binding abilities, which involved kinetic distributions of enzyme-cofactor and enzyme substrate interaction, were investigated.

FAD as well as 5-deazaFAD binds stoichiometrically to apophotolyase ($14.3 \mu\text{M}$ FAD/ $12 \mu\text{M}$ apoenzyme and $21.6 \mu\text{M}$ 5-deaza FAD/ $19.2 \mu\text{M}$ apoenzyme (Payne *et al.* 1990). This result is supported by Xu *et al.* (2006) who estimated that 0.95 mol of FAD^{ox} is bound per 1 mol apoprotein. Photolyase binds its FAD cofactor in all FAD oxidation states, but with different affinities. Xu *et al.* 2006 calculated K_D values based on fluorescence measurements of $\sim 20 \text{ nM}$ for enzyme-FADH⁻ and only $2.3 \pm$

0.9 μM for enzyme-FAD^{ox}. Interestingly, this difference in the dissociation constant was entirely due to a difference in on-rates, with the reduced flavin having a forward rate two orders of magnitude faster ($k_{1\text{red}} \approx 3000 \text{ M}^{-1} \text{ s}^{-1}$) than the oxidised form ($k_{1\text{ox}} \approx 34 \text{ M}^{-1} \text{ s}^{-1}$).

Substrate binding was restored after the enzyme was reconstituted with FADH⁻, FAD^{ox} or FADH[•]. After photoreduction of the latter two the enzyme was fully active in catalysing DNA repair (Jorns *et al.*, 1990) (Payne *et al.*, 1990). The presence or absence of MTHF in the enzyme neither affected substrate binding nor DNA repair. MTHF was therefore considered to be a light harvesting but not a catalytic chromophore. The incorporation of 5-deazaFAD by Payne *et al.* (1990), Jorns *et al.*, (1990) and Ramsey and Jorns, (1992) gave evidence that the N5 atom of the isoalloxazine is not important for binding FAD to apophotolyase (Payne *et al.*, 1990). However, N5 is able to form a hydrogen bond with Asn 378, which was argued to be crucial for stabilizing the neutral flavin radical during catalysis of DNA repair by Xu *et al.* (2008). The reconstituted protein with 5-deazaFAD showed DNA repair ability when fully reduced but to a significant lower extent compared to wild-type photolyase (Ramsey and Jorns, 1992). The inability to replace FAD with FMN and riboflavin (Payne *et al.*, 1990), both precursors of FAD (Massey, 2000) (Fischer and Bacher 2005) (Moertl *et al.*, 1996), emphasizes the importance of the diphosphate linker and the adenine ring in binding FAD to the apoenzyme. The failure to incorporate F₄₂₀ (Payne *et al.*, 1990) (Jorns *et al.*, 1990), which is considered being either a flavin- or a folate analogue with respect to its tricyclic ring structure and its polyglutamate tail may rely on two reasons. Firstly, the polyglutamate moiety is not essential for binding F₄₂₀ to the MTHF binding site. Secondly, it might be obstructive for binding to the FAD pocket.

3.3 Roseoflavin as a natural flavin analogue

The synthesis of flavin derivatives is time consuming and expensive. A more convenient way, if available, is the use of naturally occurring flavin analogues *e.g.* 7-methyl-8-dimethylamino-10-(1'-D-ribityl)-isoalloxazine. Commonly known as roseoflavin, this molecule differs from riboflavin by having the methyl group on C8 replaced by a dimethyl-amino group (Figure 3.2)

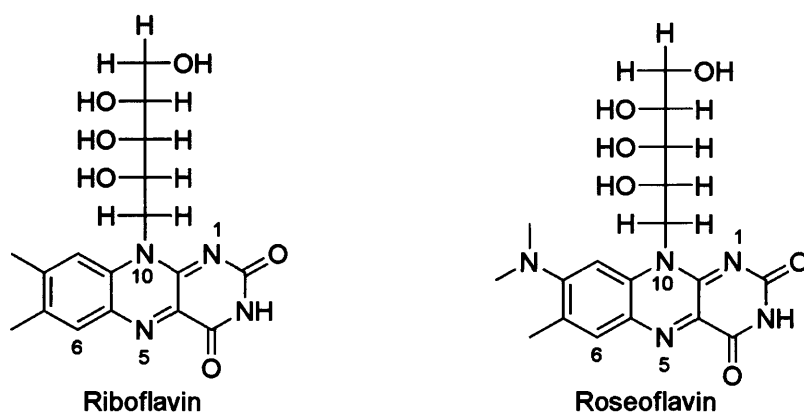


Figure 3.2: Chemical structures of riboflavin and roseoflavin.

This compound was first isolated in 1974 from *Streptomyces dawawensis* as a reddish pigment that showed antimicrobial activity against gram-positive bacteria including *Staphylococcus aureus* (Otani *et al.*, 1974). Rat feeding experiments with roseoflavin demonstrated that it acts as a B₂ vitamin antagonist *in vivo* by influencing the activity of drug metabolizing enzymes (Horvath *et al.*, 1978). A reasonable explanation for its antibiotic character is the fact that FMN kinase and FAD synthetases accept roseoflavin as substrate and therefore it acts as a competitive inhibitor. After roseoflavin is metabolised, roseoFMN and roseoFAD can replace FAD and FMN in their role as prosthetic groups and cofactors in flavoproteins with the result in

reducing or deactivating their function (Grill *et al.*, 2008). Compared to riboflavin, roseoflavin shows different characteristic features with respect to the dimethyl-amino group at the 8 position of the isoalloxazine (Cooke *et al.*, 2004). The reduction potential of roseoflavin was estimated to be -0.466 V and therefore it is harder to reduce than riboflavin (reduction potential = -0.428 V) (Kasai *et al.*, 1975). If roseoflavin binds to an apoenzyme it is postulated that protonation of the nitrogen in the dimethyl-amino group by an acidic residue would decrease the reduction potential of roseoflavin by transforming the electron donating amino group (*e.g.* Hammett σ value for $p\text{-NH}_2 = -0.66$) to an electron withdrawing ammonium group (*e.g.* Hammett σ value for a $p\text{-NH}_3^+ = +0.60$) (Cooke *et al.*, 2004). The absorption spectrum of roseoflavin (Figure 3.3) in aqueous solution shows a characteristic absorption peak in the long wavelength range with a maximum at 505 nm compared to riboflavin, which has a maximum at 445 nm. Furthermore roseoflavin has an absorption minimum near 380 nm whereas riboflavin has a maximum (Otto *et al.*, 1980). The replacement of FMN by roseoFMN was carried out *in vivo* (Otto *et al.*, 1980) by supplying roseoflavin in the micromolar range to *Phycomyces* cultures. Roseoflavin was taken up into the mycelium and translocated to the sporangiophore where it was phosphorylated to roseoFMN by a riboflavin kinase. In 2008 Mathes *et al.* developed an *in vivo* method for the incorporation of flavin derivatives via a riboflavin-auxotrophic *E. coli* strain, which expresses a riboflavin transporter from *Corynebacterium glutamicum* to import flavin from the medium. Using this method it was possible to integrate roseoFMN into the FMN-specific LOV1 domain of phototropin from *Chlamydomonas reinhardtii* (Mathes *et al.*, 2009).

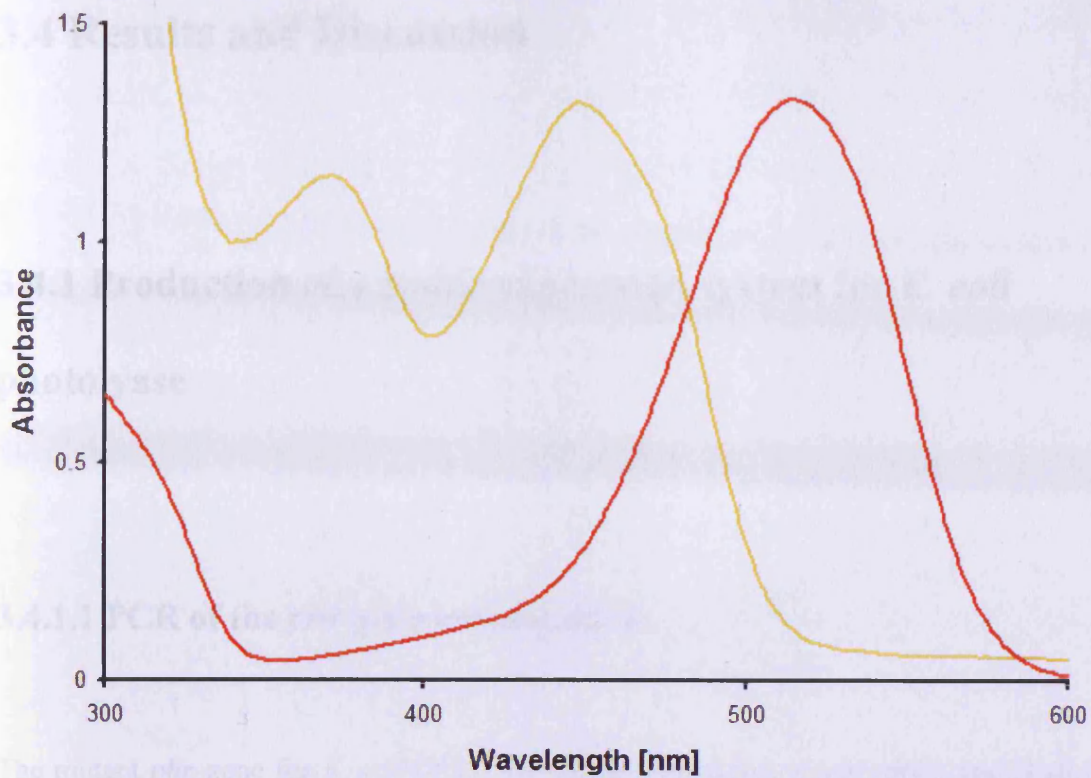


Figure 3.3: Direct comparison of the absorbance spectra of riboflavin (yellow signal) and roseoflavin (red signal).

3.4 Results and Discussion

3.4.1 Production of a stable expression system for *E. coli*

photolyase

3.4.1.1 PCR of the *phr* gene and digestion

The mutant *phr*-gene for *E. coli* CPD photolyase cloned into vector p602 and hosted in *B. subtilis* strain BR151 was constructed by Schleicher *et al.*, (2005) and was used as template for the upcoming PCR. This mutant photolyase is not able to bind the cofactor MTHF. Glutamate 109 is crucial for binding of MTHF to the protein as its carboxyl group participates in two H-bonds donated from the 2-amino group and the 3-imino group of the pterin moiety. A single amino acid substitution of glutamate 109 for alanine results in an MTHF-free, but still functional photolyase (Schleicher *et al.*, 2005). The mutant photolyase was used for following reasons. The strong absorbance of MTHF around 380 nm ($\lambda_{\max}=385$ nm; $\epsilon_{385\text{nm}}=25000$ M⁻¹ cm⁻¹) masks the absorption signal of reduced FAD ($\lambda_{\max}=380$ nm; $\epsilon_{380\text{nm}}=5680$ M⁻¹ cm⁻¹) and consequently interferes with numerous spectroscopic methods. Additionally, the low affinity of MTHF towards the protein results in partial loss of MTHF during purification leading to protein preparation containing a mixture of MTHF-free protein or enzyme with both cofactors in different batch-dependent ratios.

To obtain a system for the stable expression of *E. coli* CPD photolyase E109A a 1,475 bp fragment containing the mutant *phr* gene (size = 1475 bp) (*phr* gene, Locus: X57399; NCBI) was amplified by PCR from p602:*phr*E109A (Figure 3.4) and cloned directly into the expression plasmid pET-19b using restriction enzymes *Nde*I and *Bam*HI. The resulting expression plasmid pET-19b:*phr*E109A allows expression of the protein with an N-terminal 10 x His-tag, required for purification and reconstitution. *E. coli* BL21 (DE3) cells were transformed with pET-19b:*phr*.

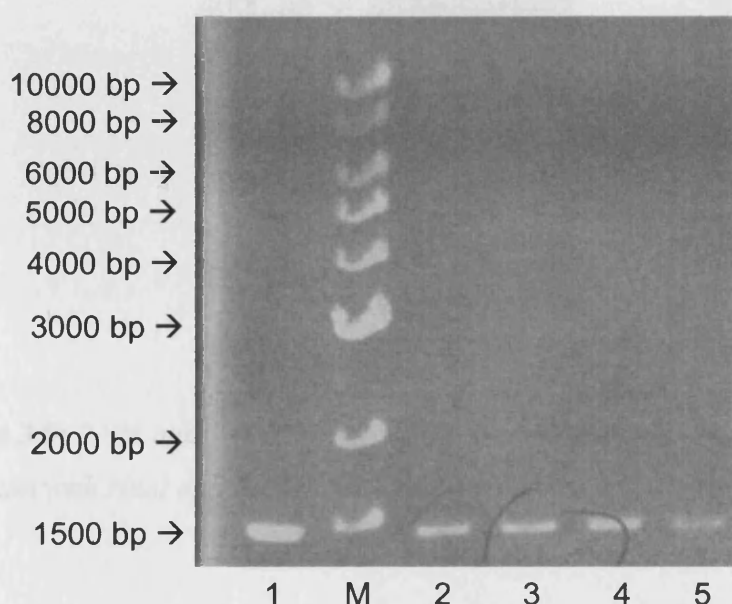


Figure 3.4: 0.8 % agarose gel of *phr* PCR products at approx. 1500 bp (Lane 1-5);
M = DNA marker

3.4.1.2 Isolation and digestion of expression vector pET-19b

The expression vector pET-19b supplied from Novagen[®] (5717 bp) was isolated from *E. coli* host XL-1 Blue using the QIAprep Spin Miniprep Kit (Qiagen). The plasmid

DNA was digested with restriction enzymes *NdeI* and *BamHI* to produce complementary overhangs suitable for ligation of vector and *phr* gene. The protein was expressed with an N-terminal tag of 10 histidines, which allows purification of the protein by metal chelate affinity chromatography. The linear vector is shown in Figure 3.5 and matches with the vector size given by the supplier.

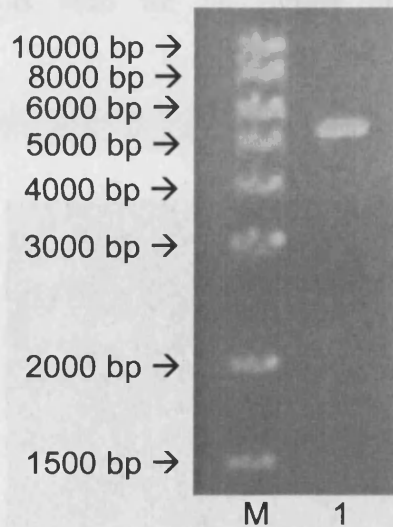


Figure 3.5: 0.8% agarose gel of the linearised vector pET-19b shown in Lane 1 after digestion with *NdeI* and *BamHI* with an approx. size of 5,7 kbp; M = DNA marker.

3.4.1.3 Ligation and transformation

The digested PCR fragment and the digested vector pET-19b were ligated in the molar ratio 3:1 respectively using the Quick Ligation kit from New England BioLabs[®] and transformed into XL1-Blue cells. Single colonies were picked and grown overnight at 37°C in Luria-Bertani medium, which contained the antibiotic ampicillin for selection. Plasmid-DNA was isolated and digested with *NdeI* and *BamHI*, resulting in two fragments of the expected sizes. The 0.8 % agarose gel

shown in Figure 3.6 contains the digested empty vector in Lane 1. Lane 2 and 3 contains digested vector with the excised mutant *phr* gene. Positive clones were sent for sequencing (Cogenics Lark Inc., Essex, UK) to verify the sequence identity of the PCR template with the sequence of the photolyase mutant gene. Constructs were transformed into the *E. coli* expression strain BL21 (DE3). The strain BL21 (DE3)-pET-19b-*phr*-5.2 was used for all further protein expression experiments of photolyase.

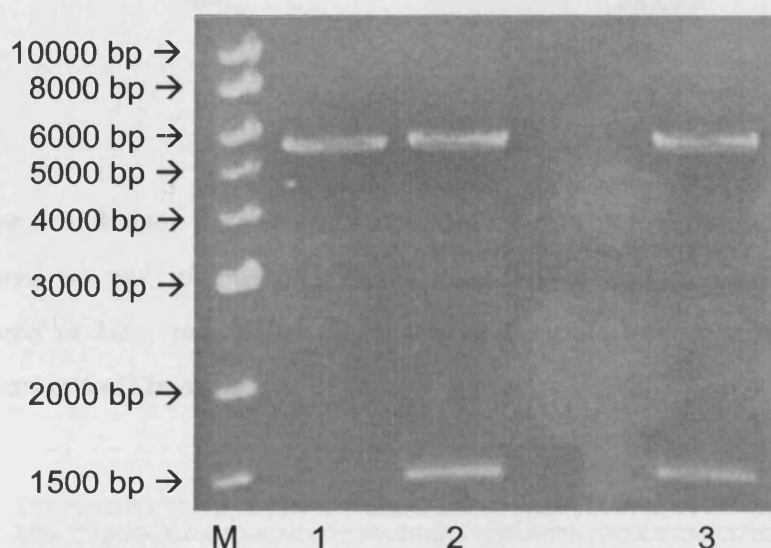


Figure 3.6: 0.8% agarose gel showing the empty vector pET-19b in lane 1 at approx 5.7 kbp after digestion with *NdeI* and *BamHI*. Lane 2 and 3 are showing the pET-19b-*phr*-5.2 plasmid after *NdeI* and *BamHI* digestion. M = DNA marker

The map of the vector pET-19b-*phr*-5.2 and the vector sequence are shown in Figure 3.7 and Figure 3.8 on the following pages.

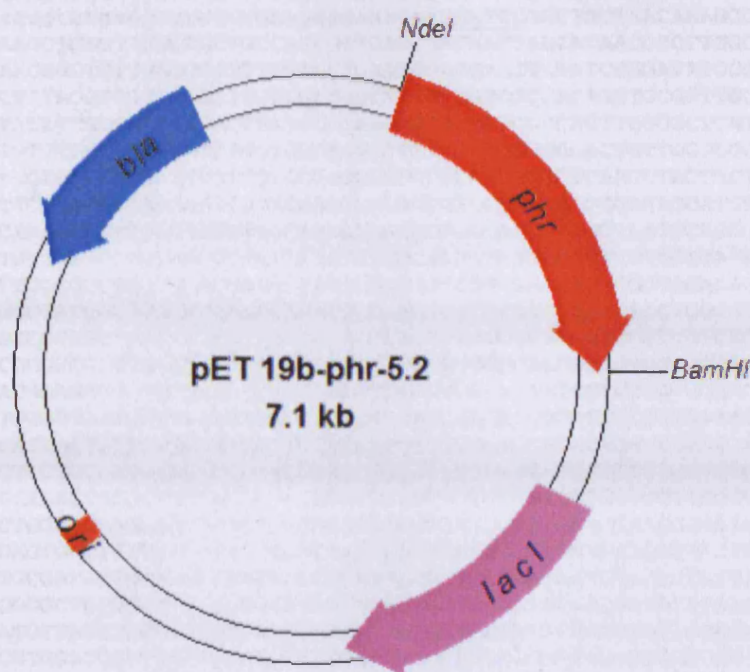


Figure 3.7: Vector map of *pET-19b-phr-5.2*; the *phr* gene coding for photolyase is coloured in red, the ampicillin-resistance gene coding for β -lactamase (*bla*) is coloured in blue, the *lacI* coding sequence is coloured in purple and the origin of replication (*ori*) in orange.

```

1      TTCTCATGTTTGACAGCTTATCATCGATAAGCTTTAATGCGGTAGTTTATCACAGTTAAA 60
61     TTGCTAACGCAGTCAGGCACCGTGTATGAAATCTAACAATGCGCTCATCGTCATCCTCGG 120
121    CACCGTCACCCTGGATGCTGTAGGCATAGGCTTGGTTATGCCGGTACTGCCGGCCCTCTT 180
181    AGATCTCGATCCC CGCAAATTAATACGACTCACTATAGGGAATTGTGAGCGGATAACAA 240
241    TTCCCCTCTAGAAATAATTTGTTTAACTTTAAGAAGGAGATATACCATGGGCCATCATC 300
301    ATCATCATCATCATCATCACAGCAGCGCCATATCGACGACGACGACAAGCATATGa 360
361    tgactaccatctggctctggtttcgccaggatttacgtctgcacgataatctcgactgg 420
421    ctgccgcctgccgaattcgtctgcacgcgtgctggcgtgtatatacgctacaccacgcc 480
481    agtggggcgacgcataacatgtcgccgcgtcaggctgaactatcaatgctcaactgaatg 540
541    ggctacaaatagcgtctgcggaaaaaggattcctttatgttccgtgaagtggatgact 600
601    ttgtcgccagtgtcgaaatagttaaacagggtgctgcggaacacagcgttaccacactgt 660
661    ttataactatcagatgaagtgaatgagcgggcgaggatgtggaagtgaagagcgc 720
721    tgcgtaacgtgggtgtgtaaggatttgatgacagcgtgatcctgccgcctggcgcggtga 780
781    tgaccggtaatcacgagatgtacaaagtcttacgcctttaagaatgctggctgaaac 840
841    ggctgcgggaagggatgccggagtgctgcctgcgcaaaaagttcgtagtagcggatcga 900
901    tagagccctcgccatccattacgctgaattatcctcgtcagtccttcgatactgcgcatt 960
961    ttccggtggaagaaaaagcggcgattgcgcaattacgccagttttgccagaacggtgccg 1020
1021  gagaatatgagcaacaacgagattttccggcagtggaaggcaccagccgtttgtcgcca 1080
1081  gcctggcaacgggcccgggttatcgctcgccagtgcttgcacgcttgttggtgtaacagc 1140
1141  cgcaggcgctggacgggtggggccggtagtgctggctaatgagctgatctggcgcgagt 1200
1201  ttaccgctacctgataacgtatcacccctcgttgtgtaaacatcgctccatattatgcct 1260
1261  ggaaggatcgtgtacagtggtcagagcaatccgcacatcttacaggcctggcaggaaggca 1320
1321  aaacgggataccgattgttgatgcccgtatgcgtcagcttaacagcactggctggatgc 1380
1381  ataacaggctacggatgattacagccagtttctggtgaaagatttattgatcgactggc 1440
1441  gcgaaggcgagcगतatctcatgtcgcagctgattgatgggtgatttggcagccaataacg 1500
1501  gtggctggcagtgggccgcttcaaccggaaccgatgcagcgcctgattttcgtattttca 1560
1561  acccgacaaccaggcgagaaatgtgatcatgaggcgagtttatccgccagtggttac 1620
1621  cggaaactgcgcgatgtgccagggaaagtggtgcatgagccgtggaagtgggcccagaaag 1680

```

Chapter 3: Cofactor exchange in DNA photolyase

1681 caggtgtgacgctggattatccgcaaccgatagtcgagcacaagaagcgagagtacaaa 1740
1741 cgttggcagcgtatgaggcggcgcggaaggggaaataaGGATCCGGCTGCTAACAAAGCC 1800
1801 CGAAAGGAAGCTGAGTTGGCTGCTGCCACCCTGAGCAATAACTAGCATAACCCCTTGGG 1860
1861 GCCTCTAAACGGGTCTTGGGGGTTTTTTCGTGAAAGGAGGAATATATCCGGATATCCC 1920
1921 GCCGATCCTCTACGCCGGACGCATCGTGGCCGGCATACCCGGGCCACAGGTGCGGTTCG 1980
1981 TGGCGCTATATCGCCGACATCACCAGTGGGGAAGATCGGGCTGCCACTTCGGGCTCAT 2040
2041 GAGCCCTTGTTCGGCGTGGGTATGGTGGCAGGCCCGTGGCCGGGGACTGTTGGGCGC 2100
2101 CATCTCCTTGCATGCACCATTCTTGGCGCGCGGTGCTCAACGGCTCAACCTACTACT 2160
2161 GGGCTGCTTCTAATGCAGGAGTCGCATAAGGGAGAGCGTCGAGATCCCGGACACCATCG 2220
2221 AATGGCGCAAACCTTTCGGGTATGGCATGATAGCGCCCGAAGAGAGTCAATTCAGGG 2280
2281 TGGTGAATGTGAAACCAGTAACGTTATACGATGTCGAGAGTATGCCGGTGTCTCTTATC 2340
2341 AGACCGTTTCCCGCGTGGTGAACCAGGCCAGCCAGTTCGCGAAAACGCGGAAAAAG 2400
2401 TGGAAAGCGCGATGGCGGAGCTGAATTACATTCCEAACCGGTGGCACAACAACCTGGCGG 2460
2461 GCAAACAGTCGTTGCTGATTGGCGTTGCCACCTCCAGTCTGGCCCTGCACGCGCCGTCGC 2520
2521 AAATGTGCGCGCGATTAATCTCGCGCCGATCAACTGGGTGCCAGCGTGGTGGTGTGCGA 2580
2581 TGGTAGAACGAAGCGCGCTCGAAGCCTGTAAAGCGCGGTGCACAATCTTCTCGCGCAAC 2640
2641 GCGTCAGTGGGCTGATCATTAACATATCCGCTGGATGACCAGGATGCCATTGCTGTGGAAG 2700
2701 CTGCCGCACTAATGTTCCGGCGTTATTTCTTGATGTCTCTGACCAGACACCCATCAACA 2760
2761 GTATTATTTCTCCCATGAAGACGGTACGCCACTGGGCGTGGAGCATCTGGTCGCATTGG 2820
2821 GTCACCAGCAAATCGCGCTGTTAGCGGGCCTTAAGTTCGTCTCGGCGCGTCTGCGTC 2880
2881 TGGCTGGCTGGCATAAATATCTCACTCGCAATCAAATTCAGCCGATAGCGGAACGGGAAG 2940
2941 GCGACTGGAGTGCCATGTCCGGTTTTCAACAAACCATGCAAATGCTGAATGAGGGCATCG 3000
3001 TTCCCACTGCGATGCTGTTGCCAACGATCAGATGGCGCTGGGCGCAATGCGCGCCATTA 3060
3061 CCGAGTCCGGGCTGCGCGTGGTGGCGGATATCTCGGTAGTGGGATACGACGATACCGAAG 3120
3121 ACAGCTCATGTTATATCCCGCGTTAACACCATCAAACAGGATTTTTCGCTGCTGGGGC 3180
3181 AAACACGCTGGACCGCTTGGTGAACCTCTCAGGGCCAGCGGTGAAGGCAATCAGC 3240
3241 TGTTCGCCGCTCACTGGTGAAGAAAGAAAACCACCCTGGCGCCCAATACGCAAACCGCT 3300
3301 CTCCCGCGCGTGGCGGATTCATTAATGCAGCTGGCAGCAGAGTTTCCCGACTGGAAA 3360
3361 GCGGGCAGTGGAGCGCAACGCAATTAATGTAAGTTAGCTCACTCATTAGGCACCGGGATCT 3420
3421 CGACCGATGCCCTTGAGAGCCTTCAACCCAGTCAGCTCCTTCCGGTGGGCGCGGGGCATG 3480
3481 ACTATCGTCGCGCATTATGACTGTCTTCTTTATCATGCAACTCGTAGGACAGGTGCCG 3540
3541 GCAGCGCTCTGGGTCAATTTTCGGCGAGGACCGCTTTCGCTGGAGCGCGAGTATCGGC 3600
3601 CTGTGCTTGGCGTATTCGGAATCTTGCACGCCCTCGCTCAAGCCTTTCGTCACTGGTCCC 3660
3661 GCCACCAAACGTTTCGGCGAGAAGCAGGCCATTATCGCCGGCATGGCGCCGACGCGCTG 3720
3721 GGCTACGTTCTGCTGGCGTTCGCGACGCGAGGCTGGATGGCTTCCCATTATGATTCTT 3780
3781 CTCGCTTCCGGCGGCATCGGGATGCCCGCGTTCGAGGCCATGCTGTCCAGGCAGGTAGAT 3840
3841 GACGACCATCAGGACAGCTTCAAGGATCGCTCGCGGCTCTTACCAGCCTAACTTCGATC 3900
3901 ACTGGACCGCTGATCGCTACGGCGATTTATCGCCGCTCGGCGAGCAGATGGAACGGGTTG 3960
3961 GCATGGATTGTAGGCGCCCTTATACCTTGTCTGCTTCCCGCGTTCGCTCGCGGTGCA 4020
4021 TGGAGCCGGCCACCTCGACCTGAATGGAAGCCGGCGCACCTCGCTAACGGATTACCA 4080
4081 CTCCAAGATTGGAGCCAATCAATTTCTTGGGAGAAGTGTGAATGCGCAAACCAACCCTT 4140
4141 GGCAGAACATATCCATCGCGTCCGCCATCTCCAGCAGCCGCACGCGGCGCATCTCGGGCA 4200
4201 GCGTTGGGTCTTGGCCACGGGTGCGCATGATCGTGTCTCTGTCGTTGAGGACCCGGCTAG 4260
4261 GCTGGCGGGTTGCCCTTACTGGTTAGCAGAATGAATCACCAGTACGCGAGCGAACGTGAA 4320
4321 GCGACTGCTGCTGCAAAAACGCTCTGCGACCTGAGCAACAACATGAATGGTCTTCGGTTCC 4380
4381 GTGTTTCGTAAAGTCTGGAAACGCGGAAGTCAGCGCCCTGCACCATTATGTTCCGGATCT 4440
4441 GCATCGCAGGATGCTGCTGGCTACCTGTGGAACACCTACATCTGTATTAACGAAGCGCT 4500
4501 GGCATTGACCCTGAGTGAATTTTCTCTGTTCCCGCGCATCCATACCGCCAGTTGTTTAC 4560
4561 CCTCACAAAGTTCAGTAACCGGGCATGTTTCATCATCAGTAACCCGTATCGTGAGCATCC 4620
4621 TCTCTCGTTTCATCGGTATCATTACCCCATGAACAGAAATCCCCCTTACACGGAGGCAT 4680
4681 CAGTGACCAAACAGGAAAAAACCGCCCTTAACATGGCCCGCTTATCAGAAAGCCAGACAT 4740
4741 TAACGCTTCTGGAGAACTCAACGAGCTGGACGCGGATGAACAGGCAGACATCTGTGAAT 4800
4801 CGCTTACAGACCACGCTGATGAGCTTTACCGCAGCTGCCCTCGCGGTTTCGGTGTGACG 4860
4861 GTGAAAACCTCTGACACATGCAGCTCCCGGAGACGGTACAGCTTGTCTGTAAGCGGATG 4920
4921 CCGGGAGCAGACAAGCCCGTCAGGGCGCGTCAGCGGGTGTGGCGGGTGTCCGGGCGCAG 4980
4981 CCATGACCCAGTACGCTAGCGATAGCGGAGTGTATACGGCTTAACTATGCGGCATCAGA 5040
5041 GCAGATTGACTAGAGTGCACCATATAGCGGTGTAATAACCGCACAGATGCGTAAGG 5100
5101 AGAAAAATACCGCATACGCGCTCTTCCGCTTCTCGCTCACTGACTCGCTGCGCTCGGTC 5160
5161 GTTCGGCTGCGGCGAGCGGTATCAGCTCACTCAAAGGCGGTAATACGGTTATCCACAGAA 5220
5221 TCAGGGGATAACCGCAGGAAAGAACATGTGAGCAAAAAGGCCAGCAAAAAGGCCAGGAACCGT 5280
5281 AAAAAAGCCCGCTTGTGCGGTTTTTCCATAGGCTCCGCCCCCTGACGAGCATCACAAA 5340
5341 AATCGACGCTCAAGTACAGAGGTGGCGAAACCCGACAGGACTATAAAGATACCAGGCGTTT 5400
5401 CCCCTGGAAGCTCCCTCGTGGCTCTCTCTGTTCCGACCTGCGGCTTACCGGATACCTG 5460
5461 TCCGCTTTCTCCCTTCGGGAAGCGTGGCGCTTTCATAGCTACGCTGTAGGTATCTC 5520
5521 AGTTCGGTGTAGGTGCTTCGCTCCAAGCTGGGCTGTGTGCACGAACCCCGTTACAGCCC 5580
5581 GACCGCTGCGCCTTATCCGGTAACTATCGTCTTGAGTCCAACCCGGTAAGACACGACTTA 5640
5641 TCGCCACTGGCAGCAGCCACTGGTAACAGGATTAGCAGAGCGAGGTATGTAGGCGGTGCT 5700
5701 ACAGAGTTCCTGAAGTGGTGGCCTAACTACGGCTACACTAGAAGGACAGTATTTGGTATC 5760

```

5761  TGCGCTCTGTGAAGCCAGTTACCTTCGGAAAAAGAGTTGGTAGCTCTTGATCCGGCAA 5820
5821  CAAACCACCGCTGGTAGCGGTGGTTTTTTTGTTTGAAGCAGCAGATTACGCGCAGAAAA 5880
5881  AAAGGATCTCAAGAAGATCCTTTGATCTTTTCTACGGGGTCTGACGCTCAGTGGAACGAA 5940
5941  AACTCAGCTTAAGGGATTTTGGTCATGAGATTATCAAAAAGGATCTTCACCTAGATCCTT 6000
6001  TTAAATTAAAAAATGAAGTTTTAAATCAATCTAAAGTATATATAGTAAACTTGGTCTGAC 6060
6061  AGTTACCAATGCTTAATCAGTGAGGCACCTATCTCAGCGATCTGTCTATTTCGTTCATCC 6120
6121  ATAGTTGCCTGACTCCCCGTCGTGTAGATAACTACGATACGGGAGGGCTTACCATCTGGC 6180
6181  CCCAGTGCTGAATGATACCGGAGACCCACGCTCACCGGCTCCAGATTTATCAGCAATA 6240
6241  AACCAGCCAGCCGGAAGGGCCGAGCGCAGAAGTGGTCTCGCAACTTTATCCGCCTCCATC 6300
6301  CAGTCTATTAATTGTTCGCGGGAAGCTAGAGTAAGTAGTTCGCCAGTTAATAGTTTGCCGC 6360
6361  AACCTGTGTGCCATTGCTGCAGGCATCGTGGTGTACGCTCGTCGTTGGTATGGCTTCA 6420
6421  TTCAGCTCCGGTTCCCAACGATCAAGGCGAGTTACATGATCCCCCATGTTGTGCAAAAAA 6480
6481  GCGGTTAGCTCCTTCGGTCTCCGATCGTTGTCAGAAGTAAGTTGGCCGCAGTGTATCA 6540
6541  CTCATGGTTATGGCAGCACTGCATAATTCTCTTACTGTCATGCCATCCGTAAGATGCTTT 6600
6601  TCTGTGACTGGTGAGTACTCAACCAAGTCATTCTGAGAATAGTGTATGCGGCGACCGAGT 6660
6661  TGCTCTTGCCCGCGTCAACACGGGATAATACCGCGCCACATAGCAGAACTTTAAAAGTG 6720
6721  CTCATCATTGGAAAACGTTCTTCGGGGCGAAAACCTCAAGGATCTTACCGCTGTTGAGA 6780
6781  TCCAGTTCGATGTAACCCACTCGTGCACCCAACCTGATCTTCAGCATCTTTACTTTCACC 6840
6841  AGCGTTTCTGGGTGAGCAAAAAACAGGAAGGCAAAATGCCGCAAAAAAGGGAATAAGGGCG 6900
6901  ACACGGAAATGTTGAATACTCATACTCTTCTTTTCAATATTATTGAAGCATTTATCAG 6960
6961  GGTTATTGTCTCATGAGCGGATACATATTTGAATGTATTTAGAAAAATAAACAAATAGGG 7020
7021  GTTCCGCGCACATTTCCCCGAAAAGTGCCACCTGACGTCTAAGAAACCATTATTATCATG 7080
7081  ACATTAACCTATAAAAAATAGGCGTATCACGAGGCCCTTTCGTCTTCAAGAA 7131

```

Figure 3.8: The vector sequence for the expression vector *pET-19b-phr-5.2*; Restriction sites *NdeI* and *BamHI* are underlined, the *phr* gene coding for photolyase is shown in small letters

3.4.1.4 Protein expression and protein purification

100 ml of overnight culture of BL21 (DE3)-*pET-19b-phr-5.2* cells were transferred into 5 l of 2 x YT-media. The cells were grown to an OD of 0.7-0.8 at 600 nm, induced with 1 mM IPTG and grown for additional 14 h at 20°C before harvesting. A 10 ml sample of non-induced cells and induced cells shortly before the harvesting were taken and analysed by SDS-PAGE. The SDS-PAGE gel in Figure 3.9 shows in lane 1 the non-induced cells. In lane 2 induced cells show a significant over expression of a protein around 50 kDa, which indicates photolyase overexpression ($M_r = 53,994$ Da for *E. coli* photolyase, Mu *et al.*, 2005).

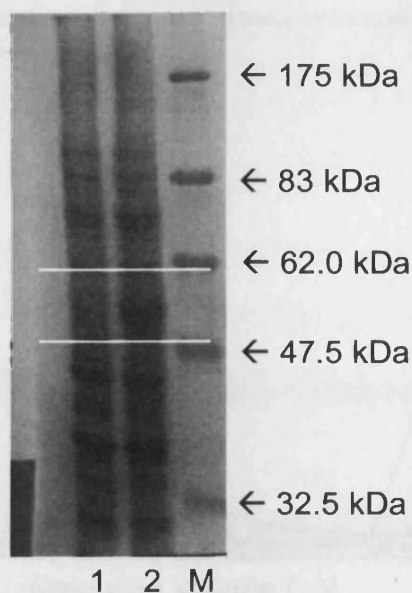


Figure 3.9: 12% SDS-PAGE of photolyase overexpression in BL21 (DE3). Lane 1: non-induced cells, Lane 2: induced cells after 14 h induction, photolyase overexpression band is marked between the white lines, M = protein marker

Protein purification was performed using a Ni-NTA-sepharose column (Ni-Sepharose resin from Amersham Biosciences, column volume 10 ml) using fast protein liquid chromatography (FPLC, AKTA system, Amersham Bioscience). Non-specific binding of most proteins was prevented by 100 mM imidazole in buffer A_{NiS} . Proteins were eluted with an increasing concentration of imidazole from 100 mM to 500 mM. The chromatogram in Figure 3.10 shows a single protein elution peak (B) starting with an imidazole concentration at approx. 110 mM. Fractions were collected (5 ml) and analysed by SDS-PAGE (Figure 3.11).

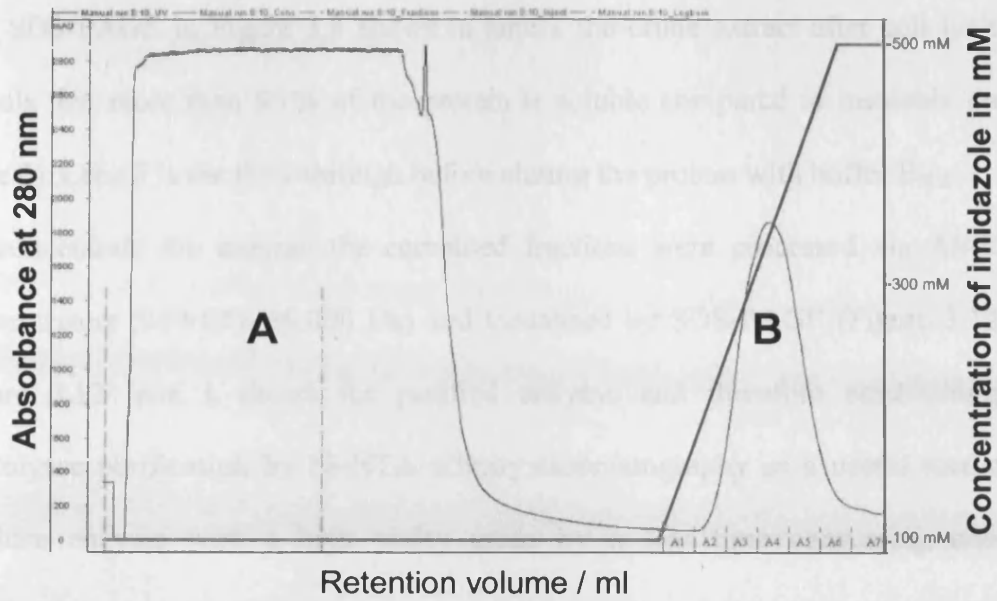


Figure 3.10: FPLC chromatogram of photolyase purification via Ni-NTA-Sepharose. A = unbound protein, flow through, B = photolyase elution peak; blue signal = absorbance at 280 nm, red signal = increasing concentration of imidazole in elution buffer in mM.

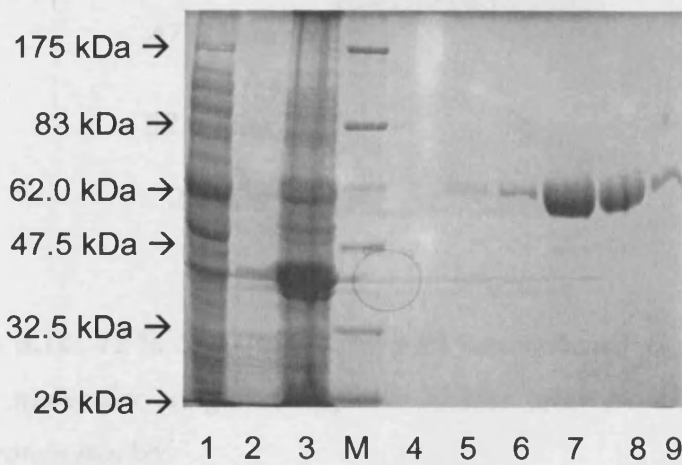


Figure 3.11: 12 % SDS PAGE gel after photolyase purification by Ni-NTA-Sepharose. Lane 1: crude extract, Lane 2: flow through; Lane 3: cell pellet; Lane 5-9: eluted fractions A1 – A6; M = protein marker

The SDS-PAGE in Figure 3.8 shows in lane 1 the crude extract after cell lysis and reveals that more than 50 % of the protein is soluble compared to insoluble protein (lane 3). Lane 2 is the flow-through before eluting the protein with buffer B_{NIS}.

To concentrate the enzyme the combined fractions were processed via AMICON concentrators (MWCO: 30.000 Da) and visualised by SDS-PAGE (Figure 3.12). In Figure 3.12 lane 1 shows the purified enzyme and therefore establishing the photolyase purification by Ni-NTA affinity chromatography as a useful method to produce enzyme with a high purity grade by a less time consuming one-step purification.

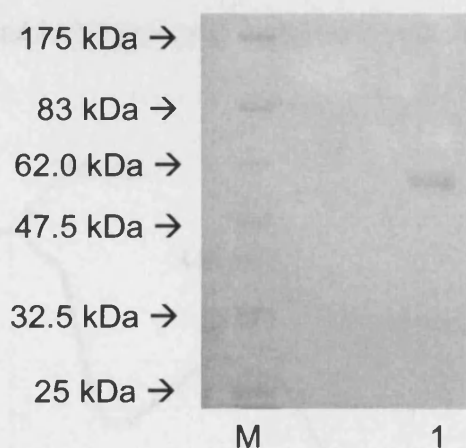


Figure 3.12: 12 % SDS-PAGE gel with concentrated *E. coli* photolyase in lane 1 with a molecular weight of approx. 53 kDa after Ni-NTA-Sepharose purification. *M* = protein marker

Photolyase concentration was estimated by UV/Vis spectroscopy based on the stoichiometric ratio of enzyme and FAD, which is 1:1 and with regards to the oxidation state of FAD. The spectrum shows significant absorption maxima that can be associated with different oxidation states of FAD in the enzyme. Absorption maxima at 580 nm and 620 nm are characteristic for the semiquinone form, FADH[•].

The absorption maximum at 445 nm indicates oxidation of FAD during aerobic protein purification. The absorption maximum at around 380 nm is present in all oxidation states of FAD. The different absorption maxima caused by different redox states of FAD have to be considered if the cofactor is used for calculating the total protein concentration (Jorns *et al.*, 1990) using Beer-Lambert's law. Measuring the absorption at 580 nm is used to calculate the concentration of enzyme with the cofactor in its radical form FADH^\bullet . The absorption at 443 nm indicates the concentration of FAD and FADH^\bullet . The absorption at 380 nm indicates the concentration of FAD, FADH^\bullet and FADH^- . The total enzyme concentration calculated from the UV/Vis spectrum shown in Figure 3.13 was 10.6 μM . Purified protein remains stable when stored in the dark under argon at -80°C .

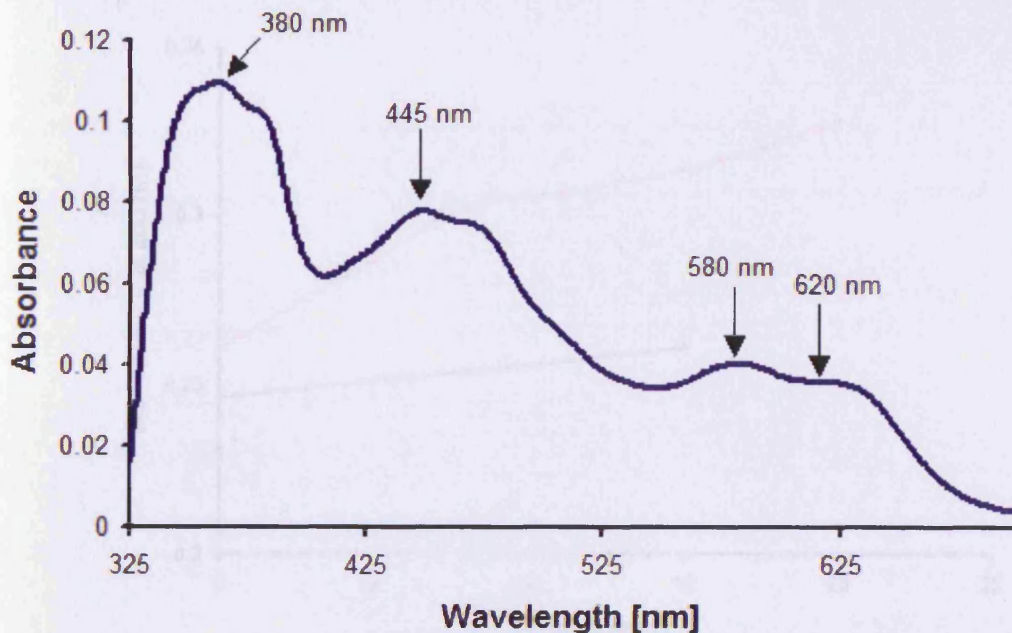


Figure 3.13: UV/Vis spectrum of *E. coli* DNA photolyase after Ni-NTA-Sepharose purification with significant absorption peaks

The DNA repair ability of purified photolyase was tested by transferring 53 nM enzyme (volume = 5 μ l) to 2.2 μ M UV-irradiated ssDNA oligo-(dT)₁₈, in reaction buffer (50 mM Tris-HCl, pH 7.0, 50 mM NaCl, 10 mM DTT 20% glycerol). The absorbance of the sample at 260 nm was measured and the sample was then kept for 15 min in a photon resistant container. After 15 min the absorbance at 260 nm was measured again. The photolyase-UV irradiated DNA mix was then exposed to white light (overhead strip lighting) for 20 min while the absorbance at 260 nm was measured after 5 min then after every 3 min . In Figure 3.14 the black signal, indicating for the absorbance at 260 nm of the sample measured before and after 15 minutes in the dark shows only a slight increase. A significant increase in absorbance at 260 nm (orange signal) is detected if the sample is irradiated with white light which indicates that thymine dimer repair is occurring.

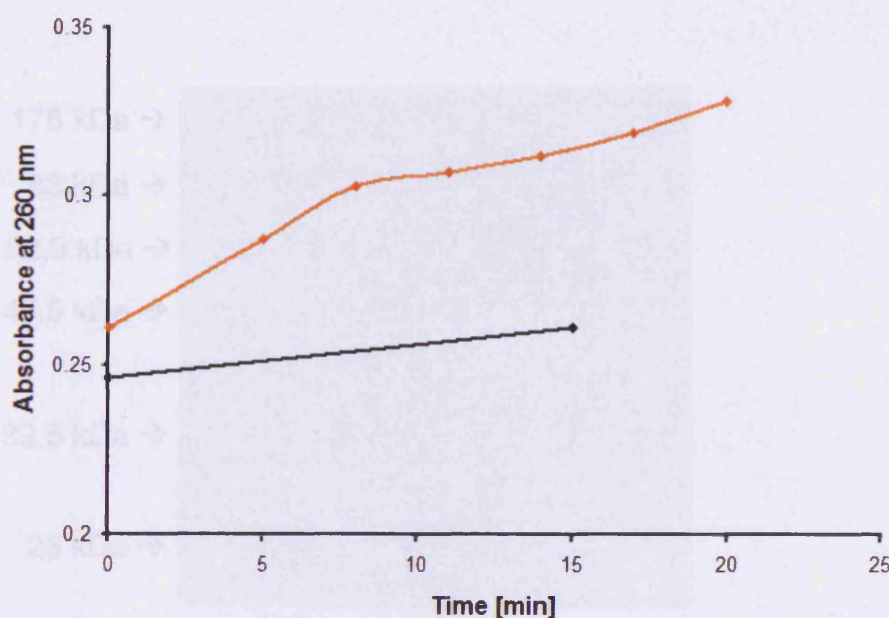


Figure 3.14: Time course of the photo repair of ssDNA oligo-(dT)₁₈ by photolyase. The black signal shows the absorbance at 260 nm for the sample before and after 15 min in the dark; the orange signal shows an increase in absorbance at 260nm after white light exposure.

3.4.2 Purification of FAD synthetase from *C. ammoniagenes*

Cells (10 g of wet cell mass) were harvested from 2 l of a culture of XL Blue-pMalribF-CA expressing the bi-functional enzyme FAD synthetase from *C. ammoniagenes*. The vector was prepared and made available by Christina Kemter in 2003 at Technical University Munich. The cloning procedure is published in Eisenreich *et al.*, 2004. Purification of the protein was accomplished in one step using an amylose column since the enzyme was expressed as a fusion protein with maltose binding protein. The enzyme was concentrated (final volume = 2 ml) to approx. 4.6 mM.

The SDS-PAGE image in Figure 3.15 shows in lane 1 the purified and concentrated FAD synthetase fused to the maltose binding protein.

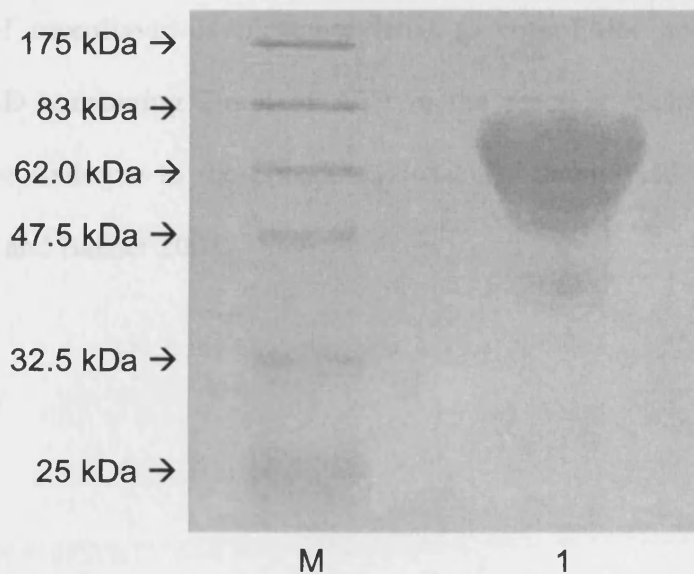
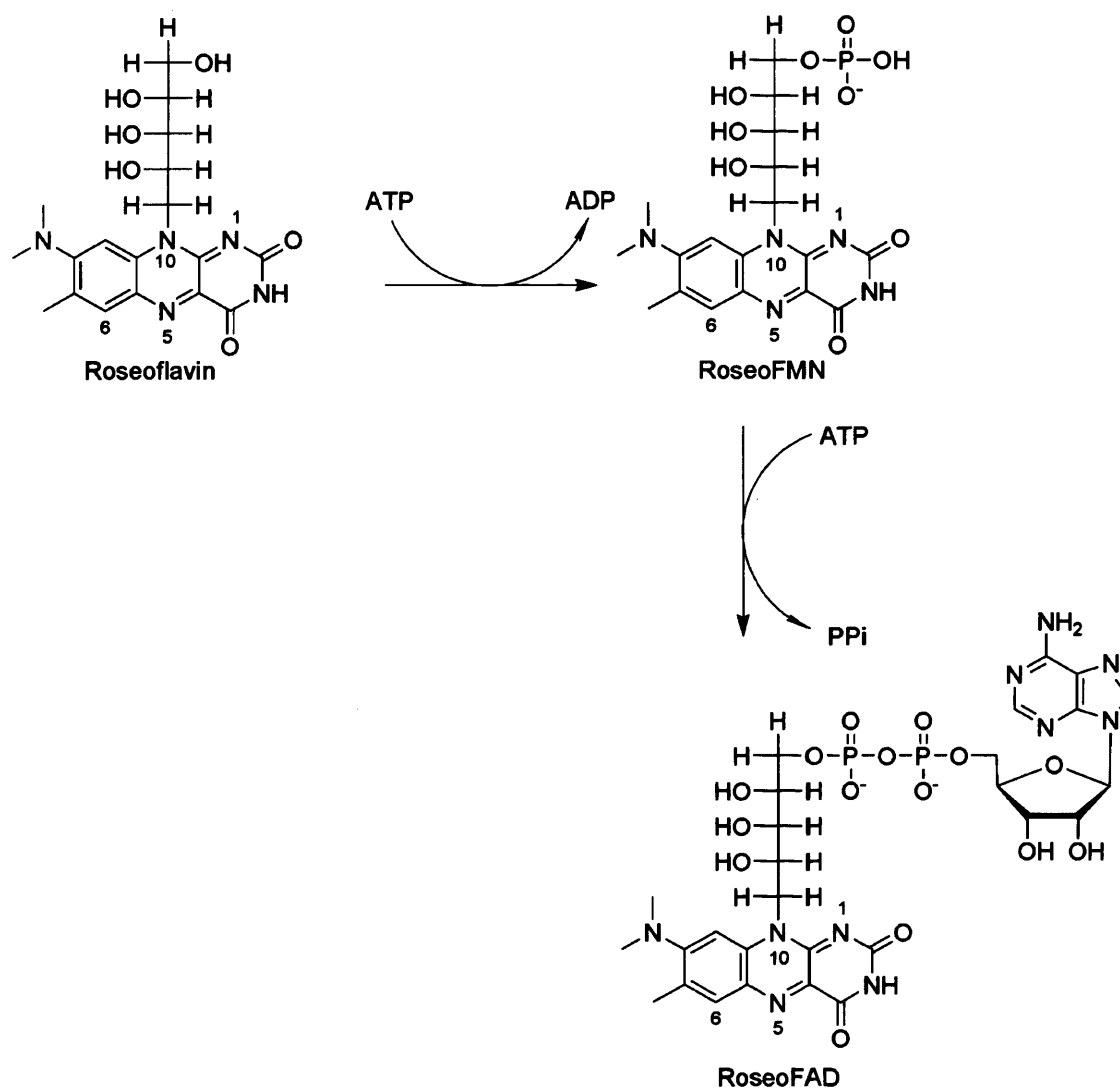


Figure 3.15: 12 % SDS-PAGE of FAD synthetase from *C. ammoniagenes* fused to maltose binding protein after purification via an amylose column in lane 1. M= protein marker

The size of the protein should be approx. 82 kDa (maltose binding protein ~ 44 kDa; FAD synthetase ~ 38 kDa) (Hagihara *et al.*, 1995). The lack of precision of the band size is due to the overload of the gel with protein. The enzyme fraction contains minor contaminations of background proteins. Neither background proteins nor the fusion with the maltose binding protein affects the catalytic activity of FAD synthetase, as the conversion of roseoflavin to roseoFAD described in the next section was successfully performed.

3.4.3 Catalytic conversion of roseoflavin to roseoFAD

The enzymatic conversion of roseoflavin to roseoFAD can be accomplished due to the fact that roseoflavin is recognised as substrate by FAD synthetase (Grill *et al.*, 2008). 1 mol of roseoflavin is phosphorylated to roseoFMN and then adenylylated to roseoFAD consuming 2 mol of ATP in the reaction (Scheme 3.1). This pathway would be analogue to the phosphorylation and adenylylation of riboflavin to FAD (Fischer and Bacher 2005).



Scheme 3.1: Pathway of the enzymatic conversion of roseoflavin to roseoFAD via roseoFMN catalysed by FAD synthetase from *C. ammoniagenes*

Enzymatic conversion of riboflavin to FAD was performed successfully in the past by Hagihara *et al.* (1995), Manstein and Pai (1986) and Efimov *et al.* (1998) to characterize the mechanism of FAD synthetase from *C. ammoniagenes* but also as an alternative to conventional organic synthesis in the preparation of coenzyme forms of riboflavin analogues (Eisenreich *et al.*, 2004).

The reaction was carried out by incubating 160 nmol roseoflavin and 5.28 μ mol ATP with 7.5 mg of FAD synthetase in 20 ml FAD-synthetase reaction buffer (50mM Tris-

HCl, pH 7.5. 15 mM MgCl₂) at 37°C for 14 h. RoseoFAD was further purified utilising a Q-Sepharose column to separate it from the FAD synthetase and by a florisil column (magnesium silica gel column) concentrated and lyophilised. The lyophilised roseoFAD (approx. 1 ng) was dissolved in sterile deionised H₂O (1 ml) and electrospray ionization mass spectrometry (ESI-MS) was performed to determine the molecular mass of the unknown compound if it corresponded to the molecular mass of roseoFAD. The mass spectrum in Figure 3.16 shows a signal at 813.3 m/z, which corresponds to the [M-H]⁻ of roseoFAD (calculated mass = 814.5 g/mol). The peaks found at 835.3 m/z, 857.3 m/z and 879.5 indicate for the sodium, disodium and trisodium adducts of roseoFAD with Na⁺-ions from the solvent bound to the negatively charged diphosphates of the ADP moiety of the flavin analogue.

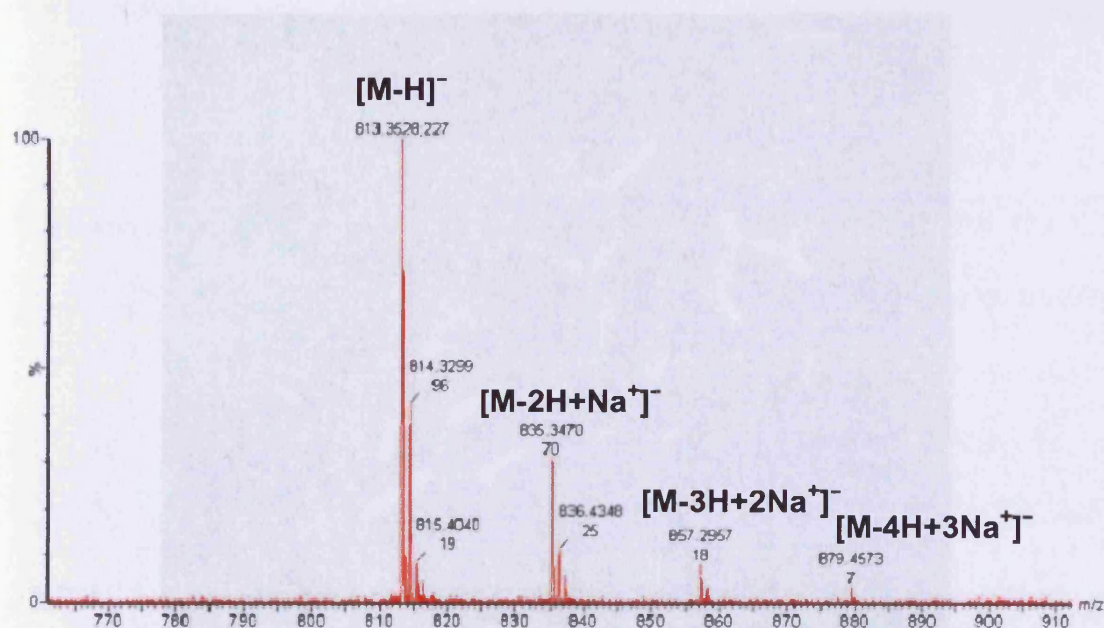


Figure 3.16: ESI-MS mass spectrum of roseoFAD after its catalytic conversion from roseoflavin, used in reconstitution experiments.

3.4.4 Reconstitution of *E. coli* photolyase with FAD and roseoFAD

Before the reconstitution of photolyase with roseoFAD was performed, necessary to the crystal structure of photolyase was consulted to verify if the dimethyl-amino group of roseoFAD would fit into the FAD binding pocket. Figure 3.17 is a model showing roseoFAD and the location of its dimethyl-amino group based on the position of the wild-type cofactor FAD inside DNA photolyase (Park *et al.*, 1995). The nearest neighbouring amino acid residues are 4-6 Å away, so a steric clash can be almost excluded.

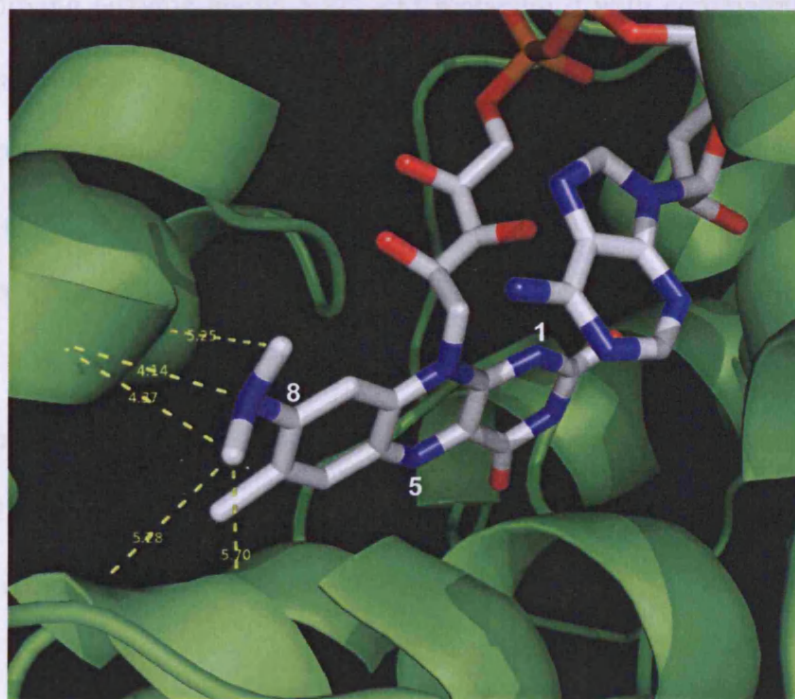


Figure 3.17: Model of the FAD binding site in DNA photolyase occupied by roseoFAD containing a dimethyl amino group on its C8. Nitrogens are coloured in blue, oxygens in red, phosphor orange, carbons in grey. Surrounding amino acid residues are shown as cartoons and are coloured in green (Park *et al.*, 1995) (PDB ID=1DNP).

3.4.4.1 Reconstitution of photolyase with FAD on Ni-NTA Sepharose column

Reconstitution of *E. coli* photolyase with FAD-analogue, roseoFAD, was initially carried out by immobilising the enzyme via its N-terminal 10 x His tag on a Ni-NTA Sepharose column. The enzyme was denatured with a high concentration of urea (8 M) while bound to the column, resulting in loss of non-covalently bound FAD. Cofactor-free enzyme would be reconstituted by removing urea while constantly washing the column with roseoFAD–buffer solution for at least 14 h. The enzyme should refold and by doing so assemble roseoFAD to the binding site of FAD. To establish this method for future denaturing and renaturing experiments it was tested first by removing enzyme bound FAD and replacing it with commercially available FAD (Sigma-Aldrich).

The crude protein extract was passed through the nickel column and washed till the absorbance at 280 nm was less than 0.1. The column was then washed with buffer A⁻, containing 8 M urea until wild-type FAD was removed. The column was constantly washed for 14h with buffer A⁻ containing 0.5 mM FAD. After eluting photolyase from the column (buffer B_{NIS}), collected fractions (volume 2 ml) were analysed by SDS-PAGE (Figure 3.18). Protein bands around 50 kDa, visible in lane 4 and 5 were taken as an indication that photolyase was eluted.

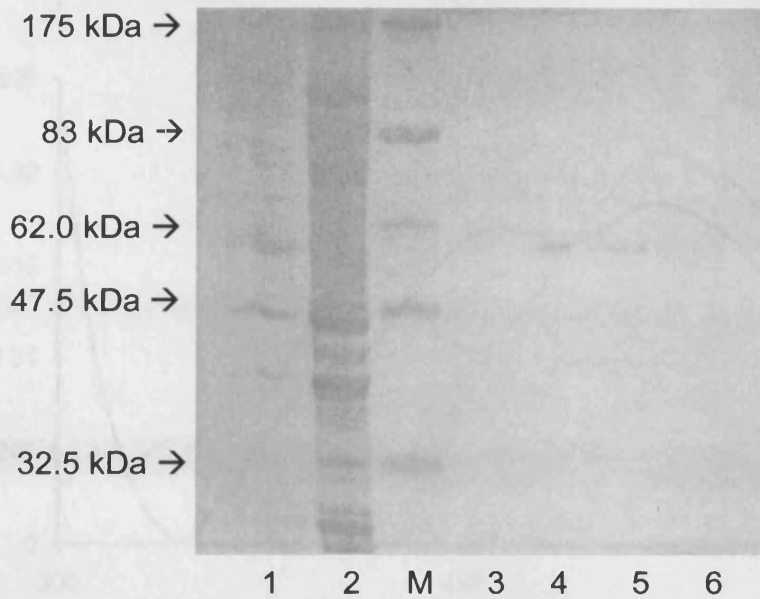


Figure 3.18: 12 % SDS-PAGE of photolyase after denaturation and reconstitution with FAD; Lane 1: crude extract, Lane 2: cell pellet, Lane 4-6: eluted fractions after reconstitution of photolyase with FAD after 14 h. M = protein marker

To identify whether photolyase was in fact reconstituted with FAD, fractions containing protein (fractions in lane 4 and 5, Figure 3.18) were combined and measured by UV/Vis spectroscopy to identify characteristic absorption signals of oxidised FAD when binding to photolyase.

Figure 3.19 shows the absorption signal (blue graph) of eluted enzyme fractions after FAD reconstitution compared to absorption signals obtained while measuring the same batch of FAD ($2 \mu\text{M}$ in buffer B_{NiS}) used for the reconstitution experiments (green graph). A direct comparison of both spectra shows considerable differences indicating that FAD was successfully incorporated into photolyase. Unstructured absorption bands around 370 nm and 450 nm are characteristic of free FAD in aqueous solution. While the absorption maximum around 450 nm for enzyme reconstituted in the presence of FAD is comparable with the maximum of free FAD, the absorption signal differs significantly around 370 nm.

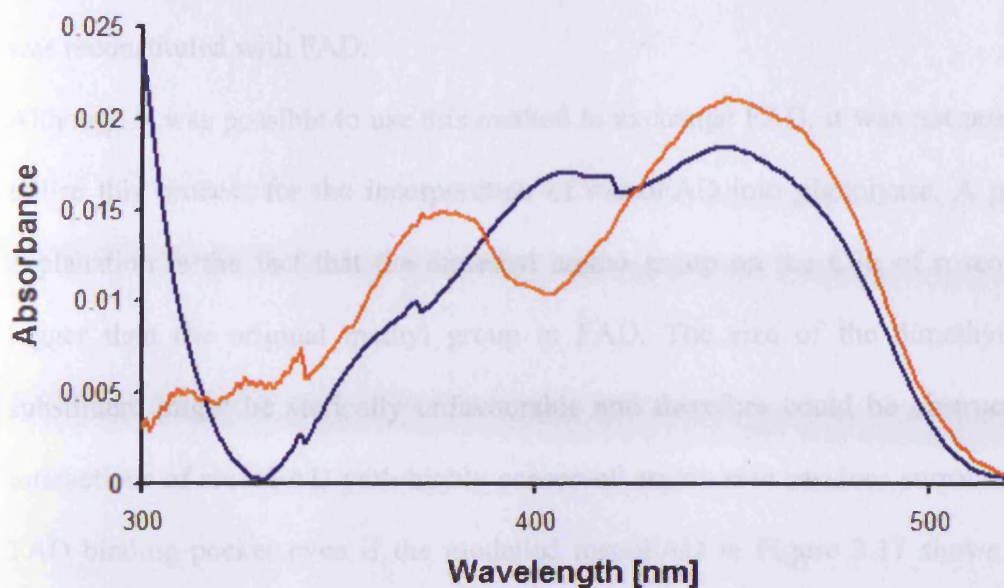


Figure 3.19: UV/Vis spectrum of photolyase reconstituted with FAD (blue signal) and spectrum of free FAD as reference (orange signal).

Free FAD has an absorption maximum at 370 nm; however the second absorption maximum of the sample-containing enzyme is around 400 nm, where the signal of free FAD is an absorption minimum. Due to the low concentration of FAD in the sample the characteristic shoulders at 430 nm and 480 nm that are usually observed when FAD binds enzyme (Jorns *et al.*, 1990) were not visible. It was not possible to obtain a more concentrated sample since protein aggregation was detected when the enzyme was concentrated via AMICON, despite the protein fraction being stored in buffer B_{NIS} containing 10 mM DTT under argon atmosphere. A subsequently performed UV/Vis spectrum showed only absorption signals of free FAD.

The spectrum of FAD bound to photolyase (Figure 3.19) was used to calculate the concentration of reconstituted protein, which was 1.7 μ M (volume 300 μ l) and equals 25 μ g. The initial concentration of 11 μ M photolyase (volume 17.5 ml) was calculated from the spectrum of free FAD after its extraction from the protein by urea. The initial

amount of enzyme was calculated to be 10 mg, which means that 0.25 % of protein was reconstituted with FAD.

Although it was possible to use this method to exchange FAD, it was not possible to utilise this process for the incorporation of roseoFAD into photolyase. A probable explanation is the fact that the dimethyl amino group on the C8 α of roseoFAD is bigger than the original methyl group in FAD. The size of the dimethyl amino substituent might be sterically unfavourable and therefore could be obstructive for interactions of roseoFAD with highly conserved amino acid residues surrounding the FAD binding pocket even if the modelled roseoFAD in Figure 3.17 shows that its rather unlikely. A further reason could be that proteins exposed to high concentrations of urea are sensitive to carbamylation. In aqueous solution and at room temperature urea can be decomposed to ammonium (NH₄⁺) and cyanate (OCN⁻), the corresponding base of isocyanic acid which affects amino acids such as arginine, lysine or cysteine.. Nitrogens in the side chains of lysine or arginine can act as nucleophiles (when not protonated) and attack the carbon of isocyanic acid leading to carbamylation. Derived from the crystal structure of *E. coli* photolyase (Park *et al.*, 1995) two highly conserved arginines are involved in directing FAD to its binding pocket. Arg 236 is interacting with one of the phosphate oxygens of the ADP moiety while in van der Waals contact to the isoalloxazine ring, Arg 344 forms a salt bridge with Asp 372. Carbamylation of these amino acids might inhibit the protein refolding process and therefore the incorporation of roseoFAD. Although denaturation-buffers, containing 8 M urea, were prepared directly before each experiment and used immediately, carbamylation of photolyase could not be totally excluded as the experiment was performed at room temperature as due to the high urea concentration of 8 M crystallisation would occur at lower temperatures.

3.4.4.2 Reconstitution of photolyase with roseoFAD via dialysis

The reconstitution of photolyase with roseoFAD via dialysis was performed as followed. The crude protein extract was passed over a Ni-NTA Sepharose fast flow drip column. The column was washed with buffer A⁻ until the absorbance at 280 nm was less than 0.1. The column was then washed with buffer A-urea, containing 8 M urea until all FAD was extracted from the enzyme. Photolyase was then eluted from the column under denatured conditions using buffer B-urea (500 mM imidazole and 8 M urea). The elution of apoenzyme from the Ni-NTA Sepharose column was controlled by SDS-PAGE (Figure 3.20). The UV/Vis spectrum (Figure 3.21) of eluted protein after AMICON concentration is showing no significant absorption above 350 nm, and therefore evidence for the absence of FAD in photolyase. 12 μM photolyase in buffer B-urea and 110 μM roseoFAD in a total volume of 600 μl were transferred to a cellulose ester dialysis tube with a molecular weight cut off of 100-500 Da. The concentration of urea in the dialysis buffer (buffer C_{Dy}) was decreased stepwise from 4 M to 2 M to 1 M to 0 M and each dialysis step was performed over a time scale of 5 h in the cold room and under argon atmosphere. A critical point was reached when the urea in the dialysis buffer was decreased from 2 M to 1 M. Precipitation of protein was detected. After the final dialysis step with buffer containing no urea, the protein was removed from the tubing and centrifuged with the attempt to separate remaining soluble protein from aggregated protein. The supernatant (2 ml) was transferred to spin column with a MWCO of 30,000 Da and washed with 20 ml of buffer C_{Dy} containing no urea concentration to remove unbound roseoFAD. However the absence of characteristic absorption signals in the UV/Vis spectrum of the supernatant shows that roseoFAD had not been incorporated.

Precipitation of photolyase at concentrations lower than 2 M urea and the absence of enzyme bound roseoFAD in the final dialysis batch indicate a low binding affinity of roseoFAD to apophotolyase and it highlights the necessity of FAD as a stabilising element in the tertiary structure of photolyase.

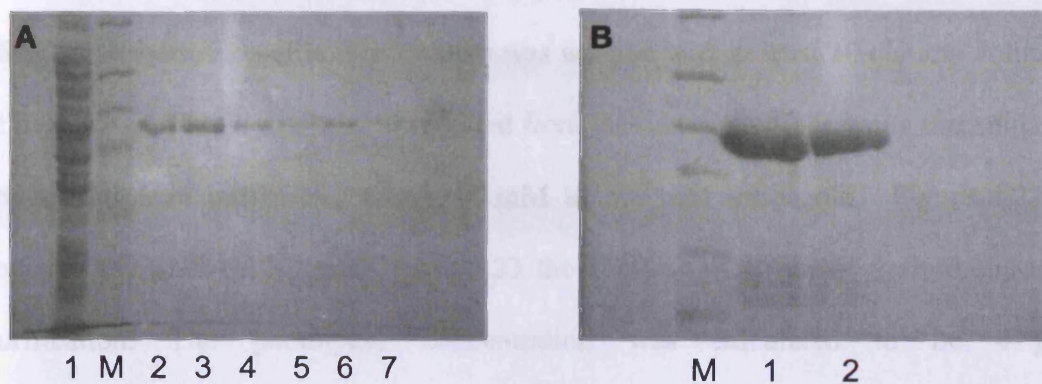


Figure 3.20: *A) 12 % SDS-PAGE of apophotolyase. Lane 1: crude lysate, lane 2-7 = fractions containing apophotolyase after elution from Ni-NTA-Sepharose column in elution buffer containing 8 M urea, M = protein marker B) 12 % SDS-PAGE of combined apophotolyase fractions in elution buffer, containing 8 M urea after AMICON concentration, lane 1 and 2 = apophotolyase containing fractions, M = protein marker*

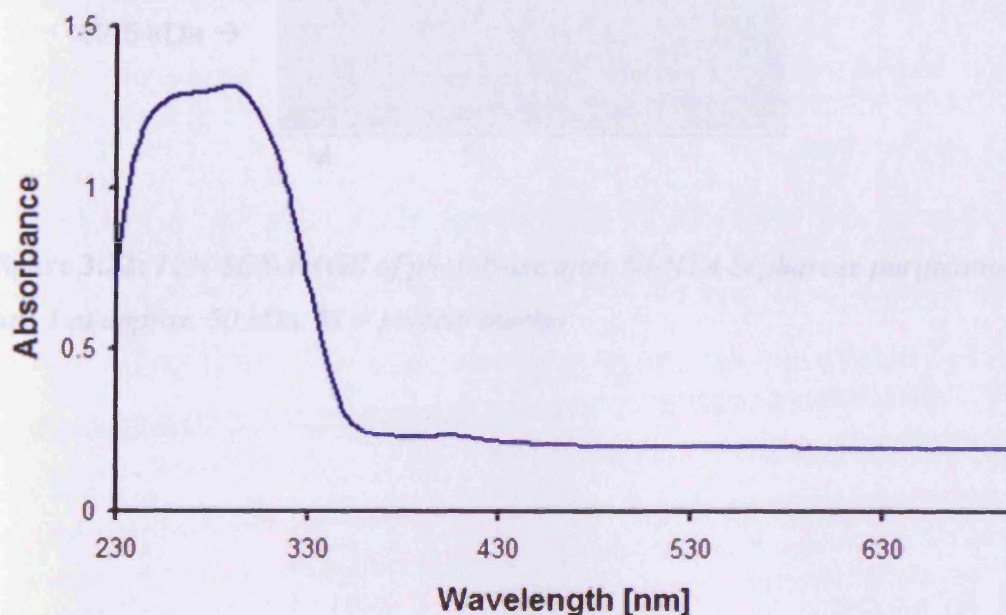


Figure 3.21: *UV/Vis spectrum of apophotolyase in elution buffer containing 8 M urea*

3.4.4.3 Reconstitution of photolyase with roseoFAD using Phenylsepharose 6 FF

Photolyase was purified by putting the photolyase containing crude extract onto a Ni-NTA sepharose column. The column was washed with at least 10 column volumes of buffer A_{Nis}. Photolyase was then eluted from the column by increasing the imidazole concentration in buffer B_{Nis} from 100 mM to 500 mM imidazole. Figure 3.22 is showing the SDS-PAGE and Figure 3.23 the UV/Vis spectrum of the protein after purification. The photolyase concentration was calculated to be 47 μ M (volume = 1 ml). The amount of enzyme was approx. 2.5 mg.

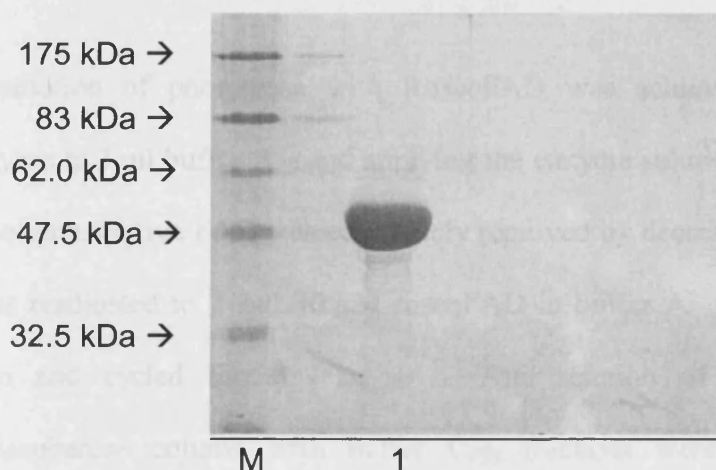


Figure 3.22: 12% SDS-PAGE of photolyase after Ni-NTA Sepharose purification in lane 1 at approx. 50 kDa. M = protein marker

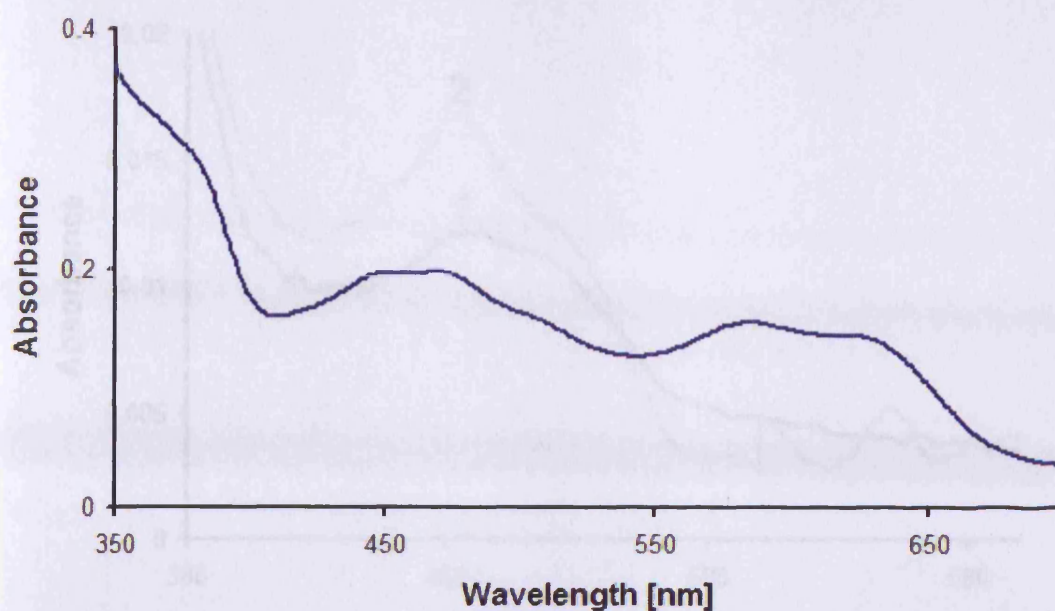


Figure 3.23: UV/Vis spectrum of *E. coli* photolyase after Ni-NTA-Sepharose purification.

Reconstitution of photolyase with RoseoFAD was achieved by diluting 31 μM photolyase in 3 ml buffer A_{PS} and applying the enzyme solution to a Phenylsepharose FF 6 column. Native FAD was completely removed by decreasing the pH to 3.5. The pH was readjusted to 7 and 40 μM roseoFAD in buffer A⁻ was passed through the column and cycled for at least 14 h. After elution of the protein from the Phenylsepharose column with buffer C_{PS}, fractions were analysed by UV/Vis spectroscopy to determine if the reconstitution of photolyase with roseoFAD was successful. Figure 3.24 on the next page shows the spectra of eluted photolyase fractions 1 and 2, with significant absorption signals between 400 nm and 600 nm with an absorption maximum around 485 nm.

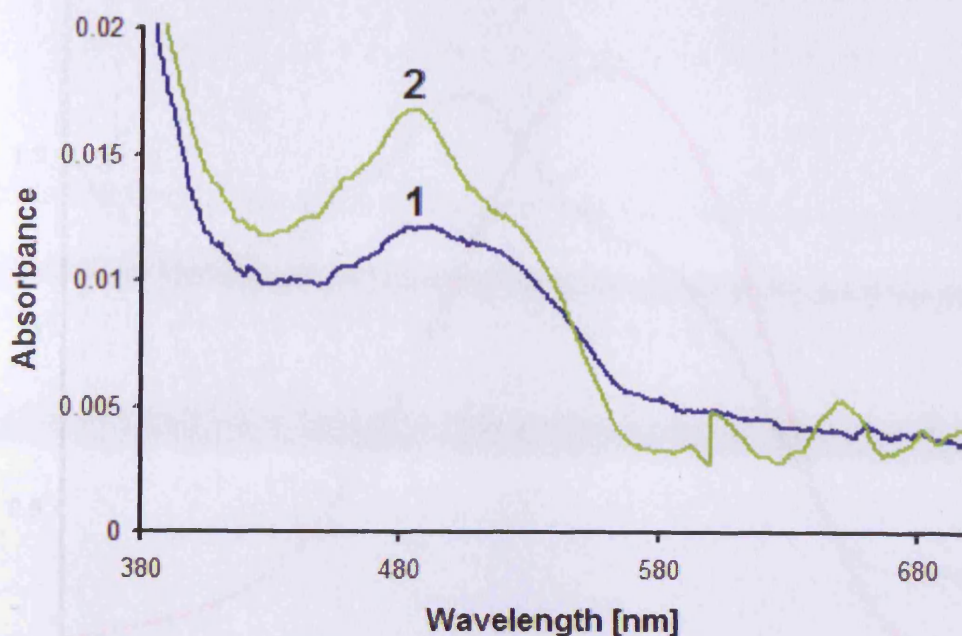


Figure 3.24: Absorption spectrum of photolyase fractions 1 and 2 after reconstitution with roseoFAD and after elution from the phenylsepharose column

Figure 3.25 on the next page compares the spectrum of free roseoFAD (red graph) with the spectrum of the eluted photolyase fraction 2 after the reconstitution with roseoFAD. It can be seen, that the absorption maximum at 505 nm observed in free roseoFAD (red signal) undergoes a hypsochromic shift by 20 nm when binding to photolyase (green signal), which then results in a new absorption maximum at around 485 nm. Two well pronounced shoulders at 450 nm and 461 nm are also detected, indicating for interaction of roseoFAD with the highly ordered protein structure of the enzyme and the anisotropic nature of the FAD binding pocket.

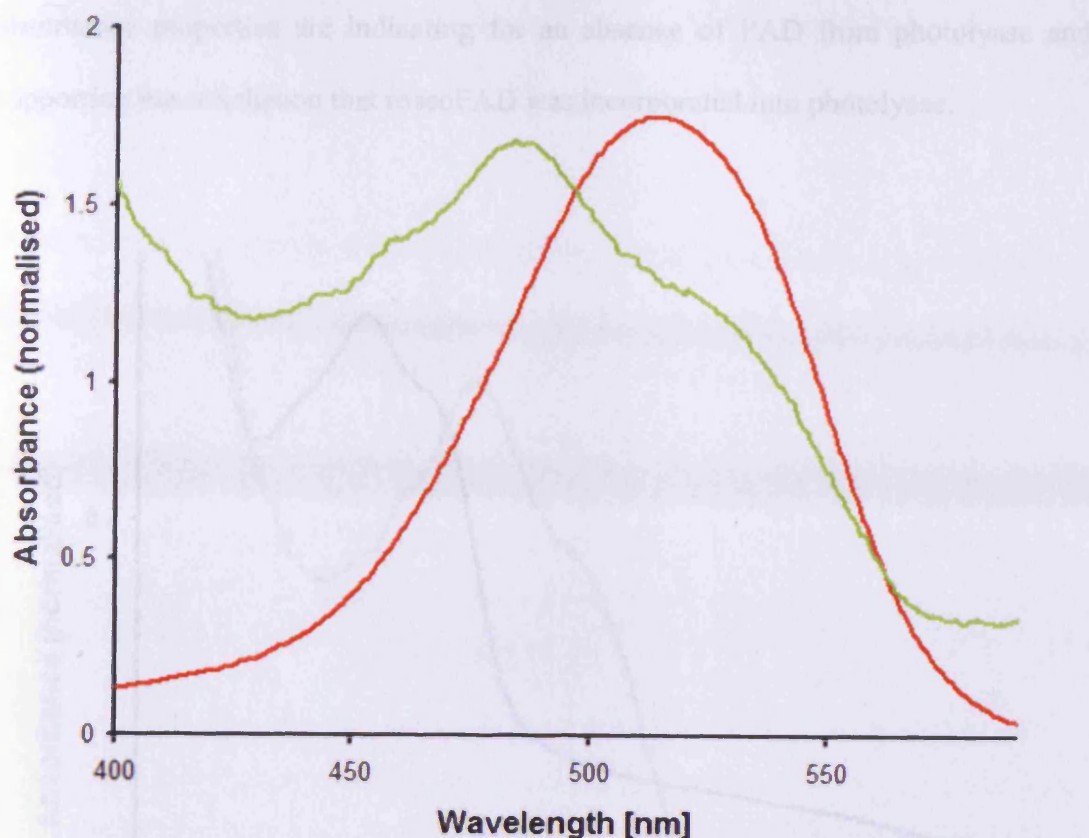


Figure 3.25: Absorption spectrum of free roseoFAD in its oxidised form (red signal) and when bound to photolyase (green).

A further evidence that photolyase was reconstituted with roseoFAD is provided if the UV/Vis spectrum of photolyase containing roseoFAD is compared to photolyase containing wild-type FAD in its oxidised form. As the reconstitution of photolyase was performed under aerobic conditions the enzyme contains roseoFAD in its oxidised form. Figure 3.26 is showing a spectrum of photolyase containing oxidised FAD (black graph). The spectrum reveals a significant absorption maximum around 450 nm with two pronounced shoulders at 430 nm and 470 nm. The spectrum of photolyase after the reconstitution with roseoFAD (green graph) differs from the wild-type photolyase significantly in its absorbance properties. When binding to photolyase roseoFAD is showing an absorbance maximum at 485 nm as well as two pronounced shoulders at 457 nm and 519 nm. These major differences in the

absorbance properties are indicating for an absence of FAD from photolyase and supporting the conclusion that roseoFAD was incorporated into photolyase.

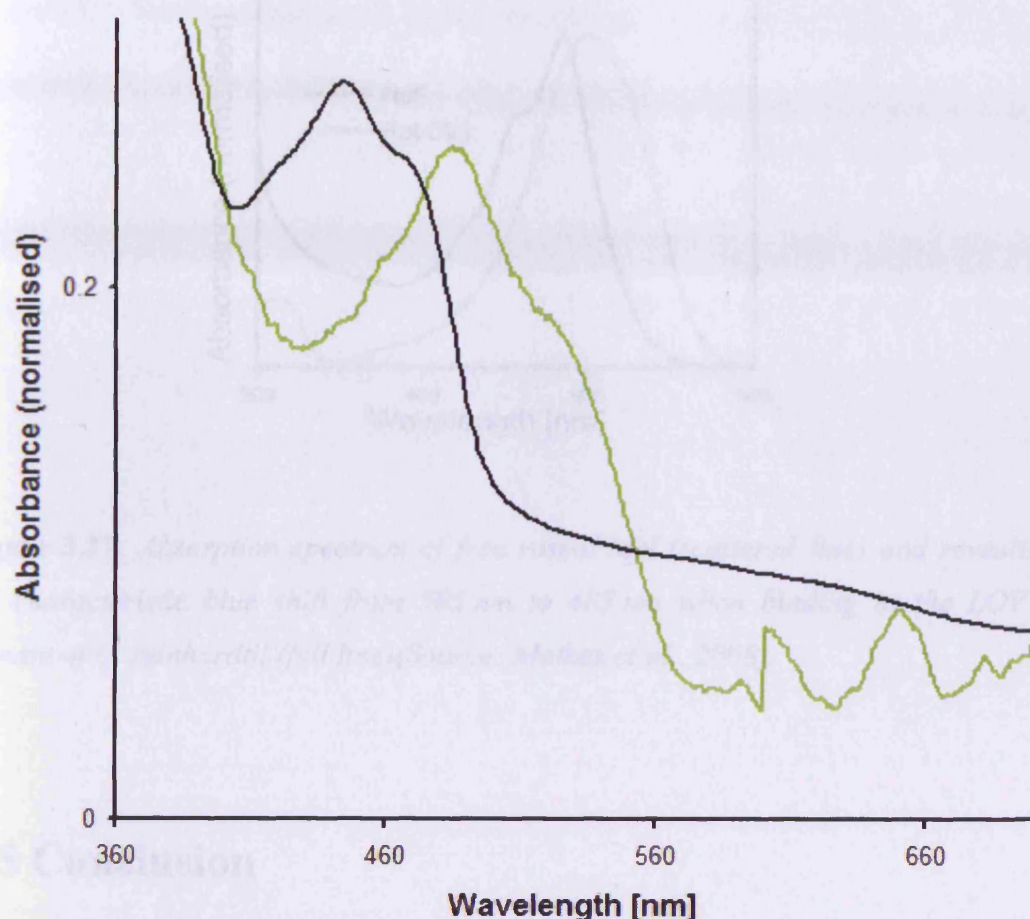


Figure 3.26: Comparison of the absorption spectrum of photolyase containing wild-type cofactor FAD in its oxidised form (black signal) and absorption spectrum of photolyase containing roseoFAD in its oxidised form (green signal).

A third evidence that photolyase was reconstituted with roseoFAD the work of Mathes *et al.* (2008), mentioned in 3.2, can be consulted. The UV/Vis spectrum (Figure 3.22) of roseoFMN replacing FMN in the LOV1 domain of phototropin in *C. reinhardtii* is showing significant similarities when comparing it with the spectrum of roseoFAD binding to photolyase (Figure 3.27). The absorption maximum of free

roseoFMN at 505 nm is blue-shifted to 485 nm when binding to the LOV1 domain.

This 20 nm blue shift is as well detectable when roseoFAD binds to photolyase.

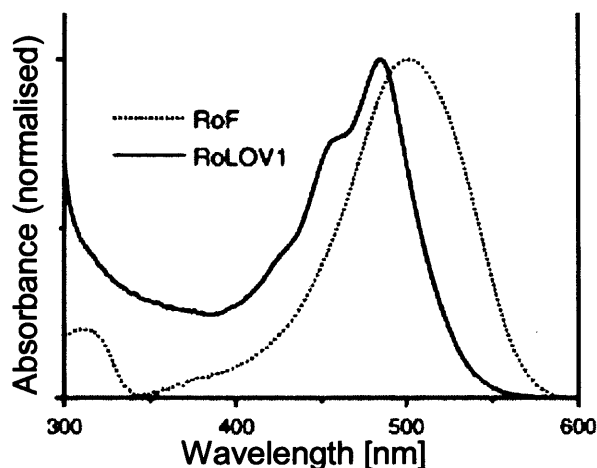


Figure 3.27: Absorption spectrum of free roseoFMN (scattered line) and revealing the characteristic blue shift from 505 nm to 485 nm when binding to the LOV 1 domain of *C. reinhardtii* (full line)(Source: Mathes et al., 2008).

3.5 Conclusion

In summary a stable expression system for *E. coli* photolyase was created. The amount of protein purified was between 2-5 mg from 5 l of cell culture. Photolyase was expressed with an additional N-terminal 10 x His-tag which not only allowed the effective purification of the protein by a single purification step using metal chelate affinity chromatography but should also establish an *in vitro*-method for exchange of FAD with roseoFAD. This method was successfully performed by extracting FAD from the enzyme and reconstituting the apoenzyme with FAD from a commercial source. The positive result was confirmed by UV/Vis spectroscopy. However this technique was not successful in replacing FAD with roseoFAD. The incorporation of

roseoFAD into the FAD binding site of apophotolyase was therefore achieved by reconstitution of apoenzyme via hydrophobic interaction chromatography. By decreasing the pH the protein was partly unfolded. Readjusting the pH in presence of roseoFAD led to binding of roseoFAD to photolyase. Cofactor exchange was confirmed by UV/Vis spectroscopy showing absorption signals that were associated with oxidised roseoFAD binding to photolyase. The signals share remarkable similarity with recently published data of roseoflavin derivatives binding to other flavin-dependent proteins (Mathes *et al.*, 2008). The method of roseoFAD integration into photolyase by pH change on a hydrophobic interaction column can therefore be considered as a promising technique for further cofactor-exchange experiments involving photolyase.

CHAPTER 4:

Surface Plasmon Resonance spectroscopy on

DNA photolyase

4.1. Work described in Chapter 4

The following chapter describes the detection of DNA repair by CPD photolyase in real-time which was investigated by using the spectroscopic method of surface plasmon resonance (SPR) in combination with evanescent wave cavity ring-down spectroscopy (EW-CRDS). The SPR and EW-CRDS equipment which was used for the experiments was designed by Dr. Andrew M. Shaw, University of Exeter (2004). SPR measurements were performed under the supervision and control of Dr. Maxim Rooth, University of Exeter, who kindly contributed the data. The gold nanoparticle modifications with self assembled monolayers (SAMs) for analysing the binding affinity of DNA and CPD photolyase to the SPR sensor chip were also prepared by Dr. Maxim Rooth, The SPR experiments required following arrangements. CPD photolyase from *E. coli* was overexpressed and purification of the enzyme was performed by using fast protein liquid chromatography (FPLC). DNA oligomers consisting of 18 thymidines were irradiated with UV-light to produce substrate for CPD photolyase. The binding of undamaged and damaged DNA to the SPR sensor chip was investigated and the signals were compared to signals obtained when binding single-stranded salmon DNA. The analysis of SPR signals resulting from photolyase binding to various self-assembled monolayers (SAMs) including calculations of the rate and binding constants for each monolayer were analysed to determine if these modified surfaces were suitable for further experiments. Finally, the CPD repair in UV damaged thymidine oligonucleotides by CPD photolyase was monitored in real-time and data were analysed in order to calculate the rate constants for DNA repair.

4.2 Introduction

Surface plasmon resonance spectroscopy (SPR) is a highly sensitive technique that can be used for studying macromolecular interactions (Flanagan and Pantell, 1984) (Karlson *et al.*, 1991) (Redman, 2007). In a SPR flow-cell one of the molecules of interest, termed ligand, is bound to the sensor surface, while the other, termed analyte, is free in solution and passes over the surface. Association and dissociation are measured in real-time by monitoring changes in the refractive index close to the sensor surface. SPR-analysis is not limited to proteins, as interactions between DNA-DNA, DNA-protein, lipid-protein and hybrid systems of biomolecules and non-biological surfaces can be investigated. SPR can be used in a variety of ways *e.g.* for the detection if two or more species bind to each other and how strong these interactions. Also the measurement of the actual association and dissociation rates can be performed. The labelling of participating compounds is not necessary and the interaction of biomolecules can be followed in real time. SPR was combined with evanescent cavity ring-down spectroscopy (EW-CRDS) in a self-designed apparatus built by Dr. Andrew M. Shaw (School of Biosciences, University of Exeter, 2004). Standard SPR-machines provided by companies such as BIAcore® are limited in function with respect to the intended experiment. The DNA repair by photolyase is initiated in the presence of near UV or blue light and standard SPR machines are lacking the ability of modification, for instance installing a blue light emitting diode (LED). The equipment for SPR measurements used in this chapter was self constructed and modified by the Physical Chemistry Department in Exeter. The modifications made it possible to utilise two spectroscopic methods, SPR and EW-CRDS, for the detection of DNA repair by photolyase.

4.3 Surface Plasmon Resonance spectroscopy (SPR)

The physical basis of SPR derives from the phenomenon of total internal reflection (TIR). When a light beam passes from a material with a high refractive index n_1 (e.g. glass) into a material with a lower refractive index n_2 (e.g. water) some light is refracted at the interface. If the angle at which light strikes the interface is greater than a critical angle θ_c , total internal reflection occurs in which the light beam is not refracted but instead propagates back into the high refractive index medium (Figure 4.1).

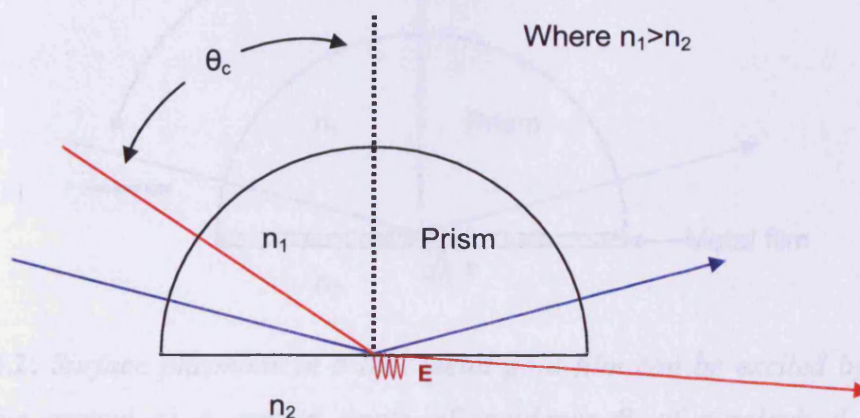


Figure 4.1: A light beam (red arrow) propagates from a high refractive index medium n_1 into a lower refractive medium n_2 (with $n_1 > n_2$) by a certain angle of incidence smaller than the critical angle θ_c . Total internal reflection (TIR) occurs when a light beam (blue arrow) strikes the interface of a medium with low refractive index at an angle greater than the critical angle θ_c ; n_1 is the refractive index of the glass prism, n_2 is the refractive index of the exit medium, E is the evanescent field wave.

The reflected light beam does not lose net energy across the TIR interface but will leak an electrical field into the lower refractive index medium, named evanescent field wave (E). The amplitude of the evanescent field wave exponentially decays with growing distance from the interface. If the extinction coefficient of the lower

refractive index medium is not zero the evanescent field wave transfers the matching photon energy to the medium. Since the surface of the material with the high refractive index, in this case glass, is coated with a thin layer of a noble metal such as gold, the p-polarized (p = planar) component of the evanescent field wave penetrates the metal layer and excites electromagnetic surface plasmons within the metal film (Figure 4.2). For plasmon excitation by a photon the energy and the momentum of both have to be conserved.

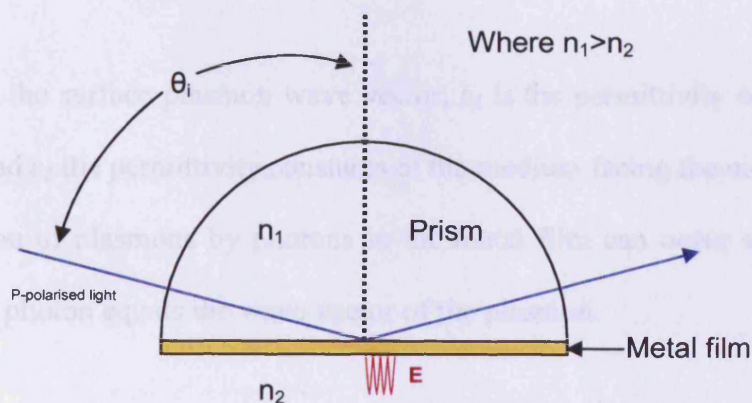


Figure 4.2: Surface plasmons in a thin metal gold film can be excited by incoming light (blue arrow) at a certain angle of incidence θ_i of p-polarized light at a glass/metal interface creating TIR which results in an enhanced evanescent field wave E .

The wave vector of the incident light is given by following equation:

$$K_i = \left(\frac{2\pi}{\lambda} \right) n \sin \theta_i$$

Equation 4.1

Where K_i is a component of the incident light wave vector that is parallel to the prism interface, θ_i is the incident light angle, λ is the wavelength of the incident light and n the refractive index (RI) of the prism.

The wave vector of the plasmon can be described by following equation:

$$K_p = \left(\frac{2\pi}{\lambda} \right) \sqrt{\frac{\epsilon_1 \epsilon_2}{\epsilon_1 + \epsilon_2}} \quad \text{Equation 4.2}$$

Where K_p is the surface plasmon wave vector, ϵ_1 is the permittivity constants of the metal film and ϵ_2 the permittivity constants of the medium facing the metal.

The excitation of plasmons by photons in the metal film can occur when the wave vector of the photon equals the wave vector of the plasmon:

$$K_i = K_p \quad \text{Equation 4.3}$$

The wave vector of the incoming light can be modified to match the plasmon wave vector by varying the angle of incidence θ_i .

Matching both wave vectors result in resonant absorption of energy that can be detected by a decrease in the intensity of the reflected light. Interactions occur on the surface of the sensor *e.g.* by binding biomolecules to the gold film changes the refractive index within the evanescent field wave and therefore alters the angle of incidence to create surface plasmon resonance. This change can be detected as response signals, and by monitoring the SPR-angle as a function of time it is possible to measure kinetic events of biomolecule interaction. The technique is *e.g.* used in the

BIACORE-system, which works at a fixed wavelength and utilizes photodetectors that allow tracking the angle of the reflectance minimum (<http://www.protein.iastate.edu/seminars/BIACore/TechnologyNotes/TechnologyNote1.pdf>, 2001).

4.4 Combination of SPR with evanescent wave cavity ring-down spectroscopy (EW-CRDS)

SPR spectroscopy was combined with evanescent wave cavity ring-down spectroscopy (EW-CRDS). EW-CRDS is a direct laser absorption technique introduced by O'Keefe and Deacon (1988), which is significantly more sensitive than conventional absorption spectroscopy. This technique is largely based upon the measurement of the rate of absorption rather than the magnitude of absorption of a light pulse confined in a closed optical cavity with a high Q-factor (O'Keefe and Deacon, 1988). The advantage results from the intrinsic insensitivity of CRDS to light source intensity fluctuations, and the long effective path lengths (up to tens of kilometres) that can be realized in stable optical cavities. Normally, a CRDS experiment involves a short light pulse that is trapped in a stable optical cavity between two highly reflecting mirrors (99.95 %). The light, which enters the cavity on one side, "rings" back and forth between the two mirrors many times. The time behaviour of the light intensity inside the cavity can be monitored by the small fraction of light that is transmitted through one of the mirrors. If the loss factor in the cavity is the reflectivity loss of the mirrors it can be shown that the light intensity

inside the cavity decays exponentially in time by a decay constant, named ring-down time τ (Engeln *et al.*, 1997). By introducing a TIR element into the cavity, *i.e.* a gold-coated glass prism, the laser beam (at a certain angle) is total internal reflected and the evanescent wave is generated, which decays exponentially from the interface with a characteristic penetration depth. Molecules, which are present within this evanescent field, change the refractive index (RI) of the sensor surface as they absorb radiation from the cavity thereby causing a change in the ring-down time.

Figure 4.3 represents the design of the EW-CRDS apparatus that was used for SPR experiments.

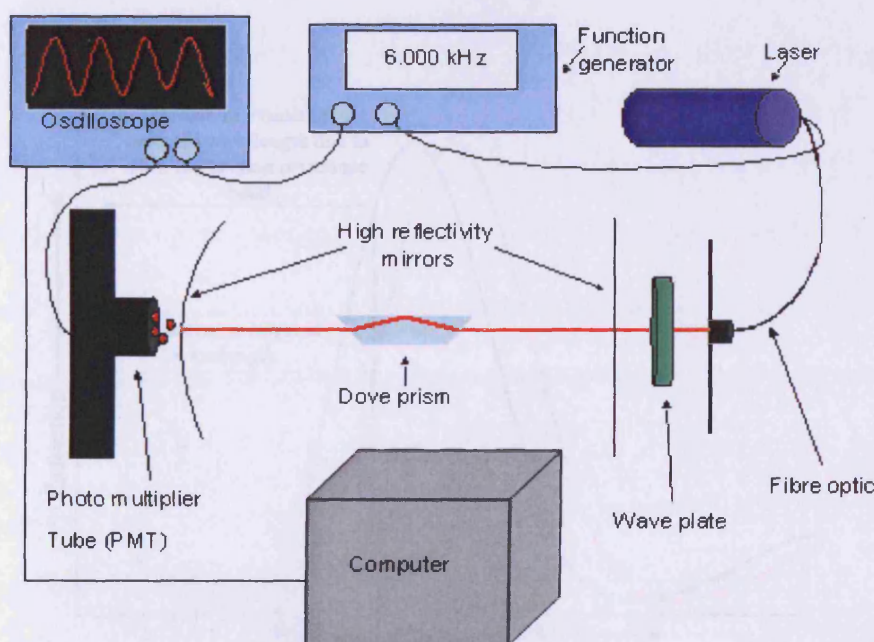


Figure 4.3: The EW-CRDS apparatus designed for SPR experiments (Dr. Andrew M. Shaw, Exeter)

An additional modification with respect to conventional SPR equipment was the replacement of the thin gold film with gold nanoparticles (gold colloids) adsorbed to the Dove prism to generate a sensor surface of the flow cell. The binding of *e.g.* biomolecules to gold nanoparticles, is measured by monitoring changes in the RI

close to the sensor surface. Any binding or adsorption process creating a change in surface RI may be measured. The change can be understood as an increase or decrease in the extinction of the particles on the surface. The evanescent field wave travels for a short distance into the medium from the gold nanoparticles and therefore the resonant frequency of the surface plasma wave (and thus the extinction of the gold nanoparticles) is sensitive to the local refractive index above the particle causing a shift in the spectrum of the plasmon. If the surface is immersed in aqueous buffer solution containing *e.g.* protein, its binding to the surface causes an increase in refractive index, which is detected by a shift in the SPR and a change in extinction of the nanoparticles (Figure 4.4).

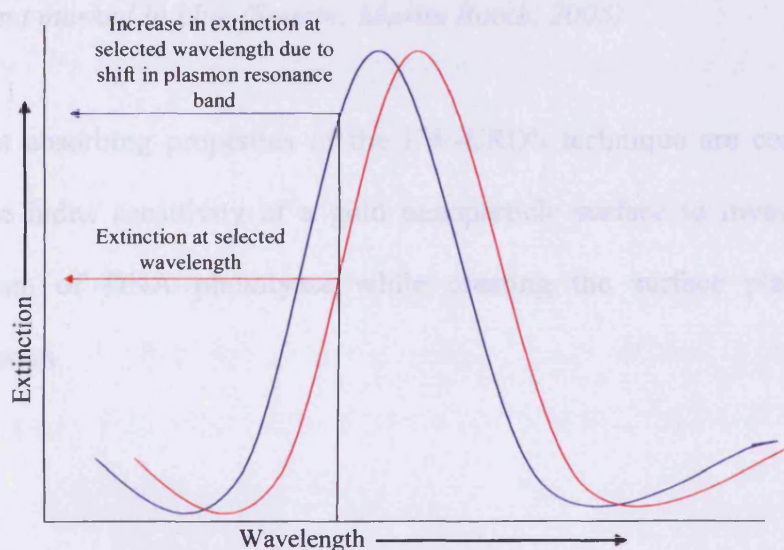


Figure 4.4: The Spectrum is showing a shift in the surface plasmon band affecting the particle extinction at a specific wavelength (Source: Maxim Rooth, 2006)

The binding efficiency of biomolecules to noble metal surfaces such as gold nanoparticles, can be enhanced by activating the metal surface with self-assembled monolayers (SAMs) (Disley *et al.*, 1998). SAMs are highly ordered organic monolayers that self-assemble to solid surfaces. They consist of alkyl-thiols of the

formula $\text{HS}[\text{CH}_2]_n\text{X}$ in which the thiol group binds covalently to the gold surface, while the alkyl moiety can carry various substituents X that can interact with molecules participating in SPR experiments. Figure 4.5 shows the surface of the dove prism coated with gold particles where molecules can bind.

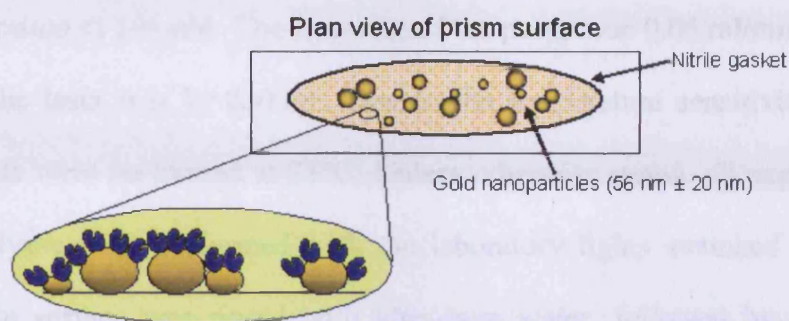


Figure 4.5: The prism surface coated with gold nanoparticles adhering one type of interactant marked in blue (Source: Maxim Rooth, 2005)

The light absorbing properties of the EW-CRDS technique are combined with the refractive index sensitivity of a gold nanoparticle surface to investigate the repair mechanism of DNA photolyase while creating the surface plasmon resonance phenomenon.

4.5 SPR experiments with CPD photolyase and DNA

The SPR and EW-CRDS equipment used was designed and made available by Dr. Andrew M. Shaw, Exeter (2004). SPR measurements were performed under the supervision and control of Dr. Max Rooth who kindly contributed the data. The gold nanoparticle surface was modified with three different SAMs (self assembled

monolayers) to analyse the binding affinity of CPD photolyase to the SPR sensor chip. SAMs used were thioctic acid, 4-aminothiophenol and cysteine and were also prepared by Dr. Max Rooth, Exeter.

CPD photolyase was thawed on ice in the dark and subsequently transferred to 5 ml of sterile filtered and degassed SPR-buffer containing 10 mM DTT to gain a final enzyme concentration of 166 nM. The flow rate of the pump was 0.06 ml/min and the wavelength of the laser was $\lambda = 830$ nm. Due to the temperature sensitivity of the laser, experiments were performed at 25°C. Unless otherwise stated, all experiments involving photolyase were performed with the laboratory lights switched off. The gold nanoparticle surface was rinsed with ultra-pure water, followed by a 100 % ethanol to establish the refractive index sensitivity. SPR-buffer was injected into the system to obtain a stable baseline. Photolyase was added until the baseline became stable again. The system was rinsed with SPR-buffer to remove non-specific bound enzyme until the reading stabilised. UV irradiated DNA was injected across the surface until a stable signal was observed. The surface was then washed again with SPR-buffer to remove weakly bound/excess DNA. The catalytic process of DNA repair was started by illuminating the surface ($\lambda_{\text{max}} = 460$ nm) with a blue light emitting diode (LED), which was built into the flow cell. The blue light radiation continued until the signal became stable.

4.5.1 Binding of DNA to the SPR sensor chip

The binding ability of native and UV-damaged ssDNA oligo-(pT)₁₈ to a sensor chip covered with gold nanoparticles was investigated by detecting changes in the SPR

response signal (Figure 4.6). The binding of either UV-damaged ssDNA oligo-(pT)₁₈ or undamaged ssDNA oligo-(pT)₁₈ leads to a decrease in the refractive index resulting in a negative SPR signal response. Absorption or scatter processes at the laser wavelength from molecules or particles present within the evanescent field remove radiation from the cavity decreasing the ring-down time τ . The change in τ is directly related to the extinction of the species and the concentration profile of the species at the interface. The correlation of changes in the refractive index and in extinction is described in detail in 4.4. The signal response for undamaged and damaged DNA when binding to the gold surface differ in that form that the refractive index for undamaged DNA is more negative than for UV-damaged DNA. The detection of a decreased extinction signal, referred to as “blue-shift”, is an unusual feature as the binding of an analyte SPR surface would normally result in an increase in the local refractive index and therefore in an increase in extinction. The binding of the oligonucleotides to a plain gold sensor surface is not permanent due to the fact that the signal levels back to its starting point when the gold surface was rinsed with SPR-buffer.

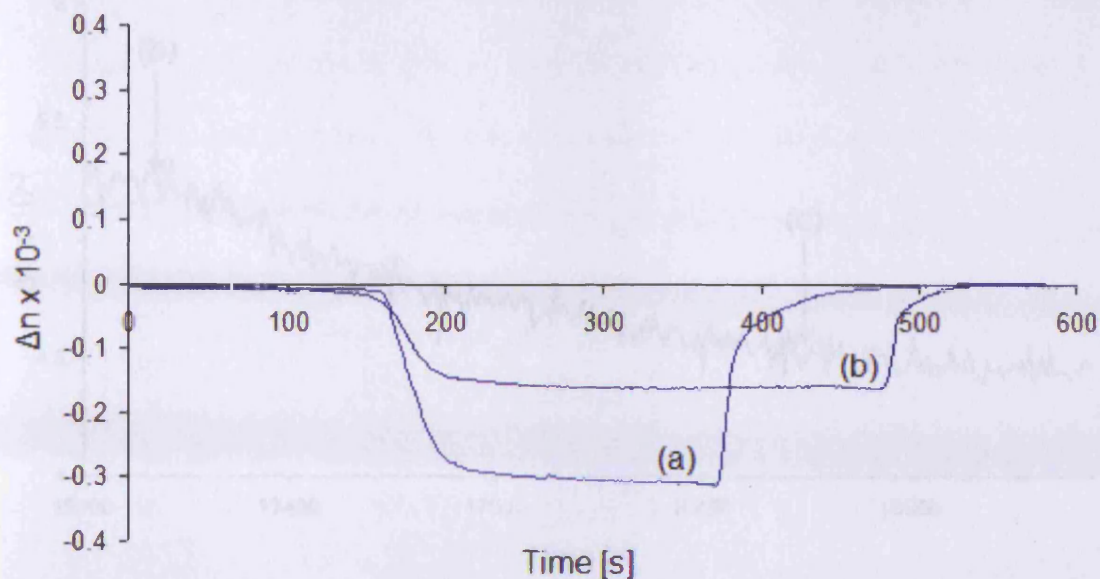


Figure 4.6: SPR sensogram for the binding of (a) undamaged ssDNA oligo-(pT)₁₈ and (b) UV damaged ssDNA oligo-(pT)₁₈ to an unmodified gold nanoparticle surface is showing a different decrease in the refractive index for undamaged and damaged oligonucleotides. The binding to gold nanoparticles is not permanent as the oligonucleotides can be washed off by SPR-buffer.

The binding ability of UV-damaged ssDNA oligo-(pT)₁₈ to the SPR surface was also tested by activating gold nanoparticles with a self-assembled monolayer of cysteine. Experiments were performed in SPR-buffer at pH 7 and the negatively charged DNA backbone electrostatically interacts with the positively charged ammonium group of the cysteines, immobilised on the SPR surface. It can be seen in Figure 4.7 that the damaged DNA binds to the cysteine SAM and produces a reduction of the refractive index in the plasmon field resulting in a decrease of extinction (blue-shift).

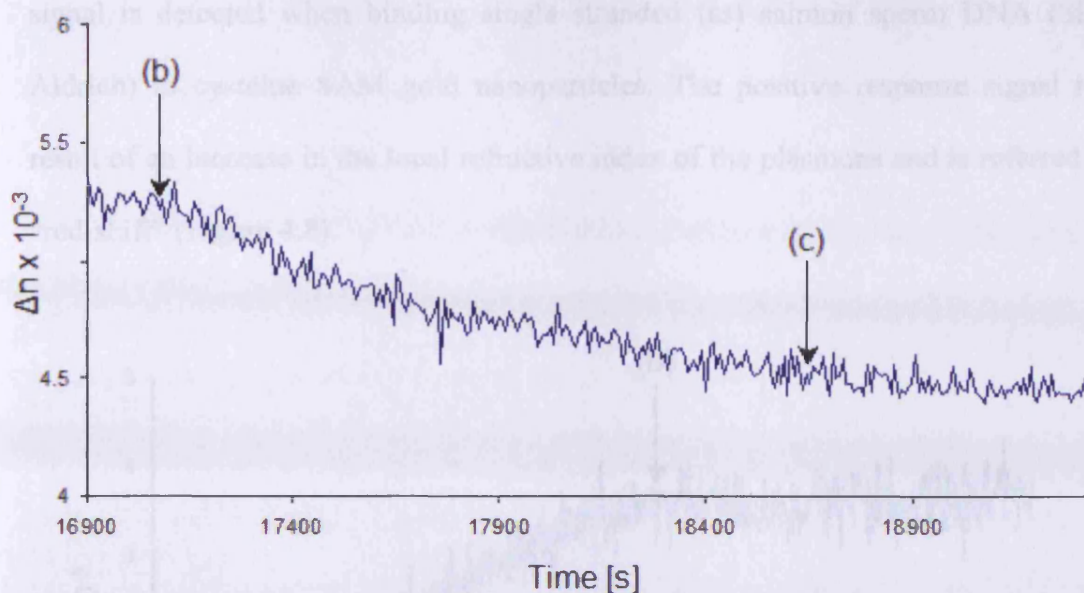


Figure 4.7: SPR sensogram of UV-damaged ssDNA oligo-(pT)₁₈ binding to a cysteine SAM surface is showing a decrease in the refractive index. The binding of the oligonucleotides remains stable when the surface is rinsed with SPR-buffer. (b) marks the injection point of damaged DNA and at point (c) the system is flushed with SPR buffer

In contrast to UV-damaged ssDNA oligo-(pT)₁₈ binding to plain gold nanoparticles, DNA bound to the cysteine monolayer remains consistent. After rinsing the surface with SPR-buffer no increasing SPR signal is recorded that can be associated with loss of DNA. Also the change of the refractive index is of one order of magnitude larger compared to DNA binding to plain gold colloids.

Inverted shifts in the refractive index, while binding ssDNA oligo-(pT)₁₈ to gold colloids were a reproducible characteristic and were detected in all further experiments including the binding of oligonucleotides to photolyase.

To identify if the appearance of a negative shift in the refractive index is only characteristic for short thymidine oligonucleotides the interaction of single stranded polynucleotides within the local plasmon field was investigated. A positive SPR

signal is detected when binding single stranded (ss) salmon sperm DNA (Sigma-Aldrich) to cysteine SAM gold nanoparticles. The positive response signal is the result of an increase in the local refractive index of the plasmons and is referred to as “red-shift” (Figure 4.8).

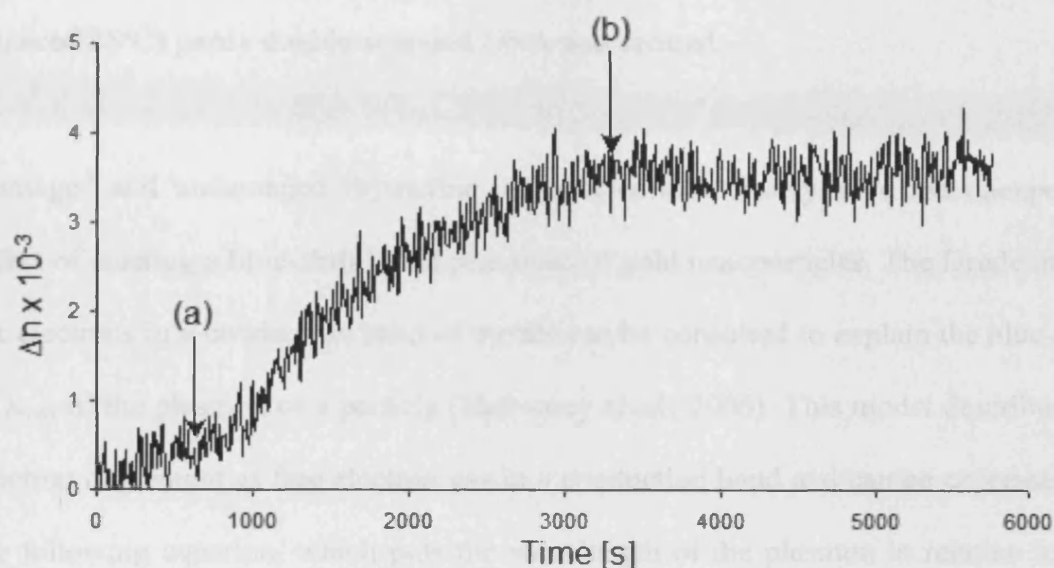


Figure 4.8: SPR sensogram after binding single stranded salmon sperm DNA to a cysteine SAM gold nanoparticle surface, which results in an increase in the refractive index. Where (a) is the injection point for the single stranded salmon sperm DNA and (c) for the injection point of SPR-buffer

An explanation for the positive signal can be that molecular weights and/or base sequences of long polynucleotides might influence the refractive index in a different manner when interacting with gold nanoparticles than short oligonucleotides. Secondly, the commercially acquired salmon sperm DNA might contain contaminations that are responsible for the increase in the refractive index. However it is difficult to maintain DNA single stranded for a longer period of time. Intramolecular double strand formation due to H-bond interaction of complementary parts of the DNA can be the reason for the appearance of secondary structures such as hairpin loops, stem loops and also tertiary structures *i.e.* double helix. The production

of single stranded DNA is usually performed heating double stranded DNA to generate single strands, which are immediately snap frozen. After defrosting, the ssDNA should be used immediately to avoid annealing of complementary parts. It is possible that during the slow injection of ssDNA into the SPR flow cell (flowrate = 0.06 ml/min) at room temperature (the temperature sensitivity of the laser required 25°C) partly double stranded DNA was created.

Damaged and undamaged thymidine oligonucleotides clearly have the unexpected effect of creating a blue-shift in the plasmons of gold nanoparticles. The Drude model for electrons in a conduction band of metals can be consulted to explain the blue-shift in λ_{\max} of the plasmon of a particle (Mulvaney *et al.*, 2006). This model describes the electron movement as free electron gas in a conduction band and can be expressed by the following equation, which puts the wavelength of the plasmon in relation to the electron density in the conduction band:

$$\frac{\Delta N}{2N} = -\frac{\Delta \lambda}{\lambda} \qquad \text{Equation 4.4}$$

Where N equals the electron density in the conduction band and λ is the maximum wavelength of the plasmon. If an increase in electron density within the conduction band occurs it causes a decrease in the wavelength, which results in a blue-shift of the plasmon. While binding to the gold surface poly-T oligonucleotides donate electrons to the conduction band, which explains the observed decrease in extinction (blue-shift) of the radiation at the interrogation wavelength. It can be observed from signals shown in Figure 4.6 that the damaged and undamaged oligonucleotides differ from each other in their electron donating properties. The blue-shift created by the damaged oligonucleotides (Figure 4.6) is approximately half the value for undamaged

oligonucleotides. The fact that electron density of the phosphate backbone does not change during thymine dimer formation suggests that changes in the ring structure caused by the dimerisation of two pyrimidines could be responsible for the smaller charge donating capacity of the damaged DNA. The electrons in a pyrimidine ring are conjugated and responsible for the planar structure of a thymine, while the cyclobutane ring in a thymine dimer is puckered due to loss of the aromaticity of the pyrimidine, whereby each atom involved lies out of plane compared to the other three by 0.5 Å (Camerman and Camerman, 1970). These structural changes possibly influence the electron density in the molecules, which explains the different observed response signals when binding either intact or UV damaged oligonucleotides to the gold surface. Additionally the condensation of DNA into surface structures is a complex process as it depends on factors like the ionic strength of the buffer solution or the presence of multivalent ions as well as the enhanced charge distribution at a charged interface (Schwinefus and Bloomfield, 2000).

4.5.2 DNA photolyase-binding to gold nanoparticles with different self-assembled monolayers

Performing binding studies on photolyase-DNA interaction by SPR spectroscopy firstly requires the immobilisation of high concentrations of enzyme to the gold nanoparticle sensor surface as well as the production of strong changes in SPR signals related to enzyme-substrate interaction for a more precise analysis. The binding efficiency of photolyase to three different SAMs was investigated and compared to the binding efficiency of enzyme to plain gold nanoparticles. The three SAMs

generated on gold colloids were L-cysteine, 4-aminothiophenol (4-ATP) and thioctic acid (TOA) (Figure 4.9) and were prepared by Dr. Maxim Rooth, Exeter.

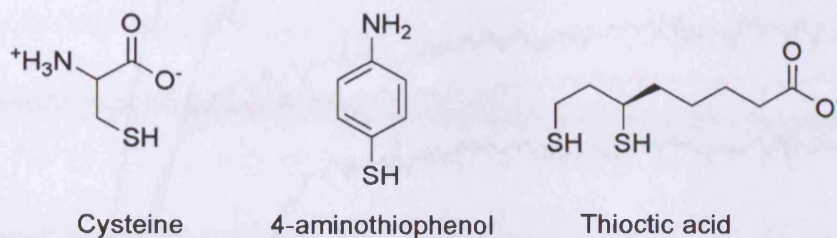


Figure 4.9: L-cysteine, 4-aminothiophenol (4-ATP) and thioctic acid (TOA) used for self-assembled monolayers on gold nanoparticles.

SPR response signals of photolyase binding to each SAM surface are shown in Figure 4.10. SPR responses of photolyase binding to plain gold colloids is shown in Figure 4.11.

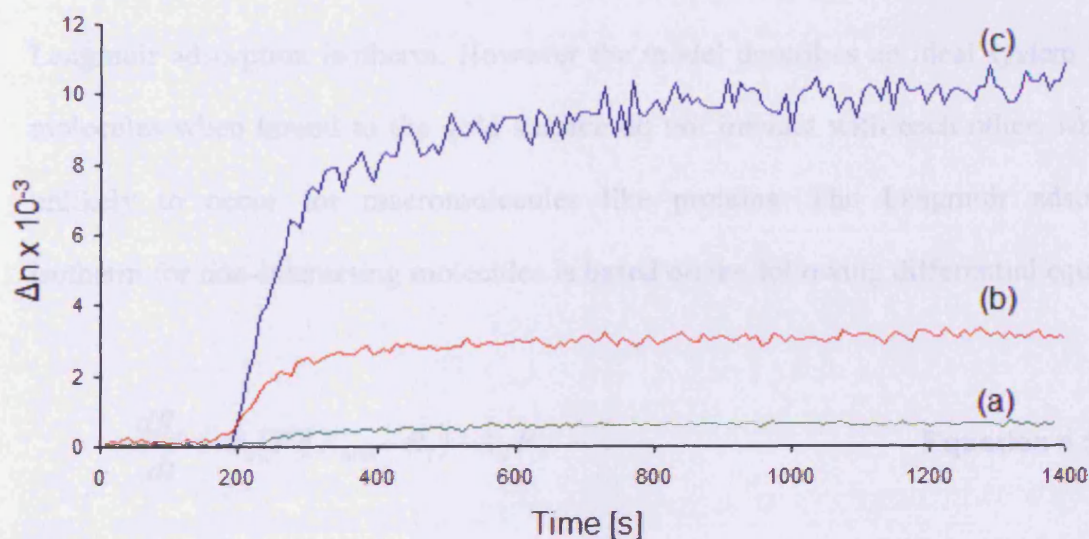


Figure 4.10: The SPR sensogram is showing the response of the binding of photolyase to three different SAM functionalised gold surfaces; (a) 4-aminothiophenol, (b) thioctic acid and (c) L-cysteine.

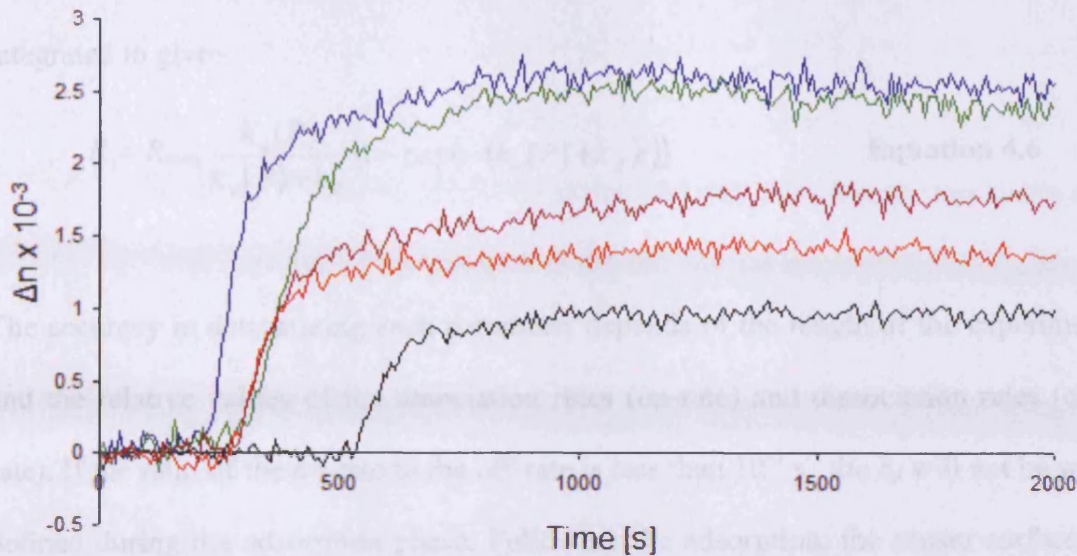


Figure 4.11: The SPR sensograms for photolyase binding to plain gold nanoparticles. Differences in the response signals are linked to the diverseness of the gold nanoparticle adsorption to the glass prism, which affects the binding ability of photolyase.

The adsorption of a molecule to the gold surface can be described by the conventional Langmuir adsorption isotherm. However the model describes an ideal system where molecules when bound to the gold surface do not interact with each other, which is unlikely to occur for macromolecules like proteins. The Langmuir adsorption isotherm for non-interacting molecules is based on the following differential equation:

$$\frac{dR_t}{dt} = k_a[P](R_{\max} - R_t) - k_d R_t \quad \text{Equation 4.5}$$

Where R_t is the response for the refractive index at time t and k_a is the adsorption rate constant. P is the concentration of either DNA or enzyme in solution, R_{\max} is the

The interpretation of the association rate constants presented in Table 4.1 leads to the conclusion that binding of the enzyme to a charged SAM is of a magnitude faster than binding to plain gold nanoparticles. The dissociation constant K_d for photolyase bound to plain gold nanoparticles is of one magnitude higher compared to the K_d for each SAM. As the experiments were performed at pH 7 the carboxyl group of thioctic acid is deprotonated and the amino group of 4-aminothiophenol protonated while the L-cysteine SAM provides both, positive charged amino groups and negatively charged carboxyl groups, which favour electrostatic interactions with opposite charged regions on the enzyme surface. These interactions of enzyme molecules with charged SAMs may be preferred and are responsible for the tighter binding of photolyase to a SAM activated sensor surface. The maximum signal change R_{max} is significantly higher for binding protein to a cysteine SAM compared to the other two SAMs and approximately one order of magnitude bigger compared to signal of photolyase binding to plain gold colloids. Due to the fact that rate constants and equilibrium constants of photolyase binding to gold nanoparticles modified with different SAMs are approximately of the same magnitude the R_{max} value was the decisive factor to utilise the cysteine SAMs for further experiments. Despite the enhanced binding of photolyase to a cysteine SAM due to electrostatic interaction there is the possibility of protein molecules binding to the surface in less favourable orientations. The substrate binding site of photolyase is narrowed by arginine residues 226, 342 and 397, which are providing a trace of positive electrostatic potential (Park *et al.*, 1995). The positively charged amino groups of arginines can interact with the negatively charged carboxyl groups of the cysteine SAM in which case the active site of the protein would be almost inaccessible for substrate. The binding of photolyase to plain gold nanoparticles can be explained by covalent bond formation between the surface

exposed thiol-groups of cysteine residues and the gold particles. Photolyase contains seven cysteines, with three of them C23, C125 and C168 surface exposed and therefore accessible to interact with the gold.

4.5.3 Photolyase–DNA binding and DNA repair detection by SPR and EW-CRDS in real time

DNA binding and repair experiments with photolyase in the radical form

The binding of UV-damaged ssDNA oligo-(pT)₁₈ to photolyase with its cofactor in the radical form, FADH[•], was investigated by SPR. During the experiments the redox state of the enzyme was kept in its radical form by protecting the sensor chip from light to eliminate the possibility of reduction of photolyase. After the equilibration of the sensor surface by rinsing with SPR-buffer, photolyase (166 nM) was injected at point (a) as shown in Figure 4.12.

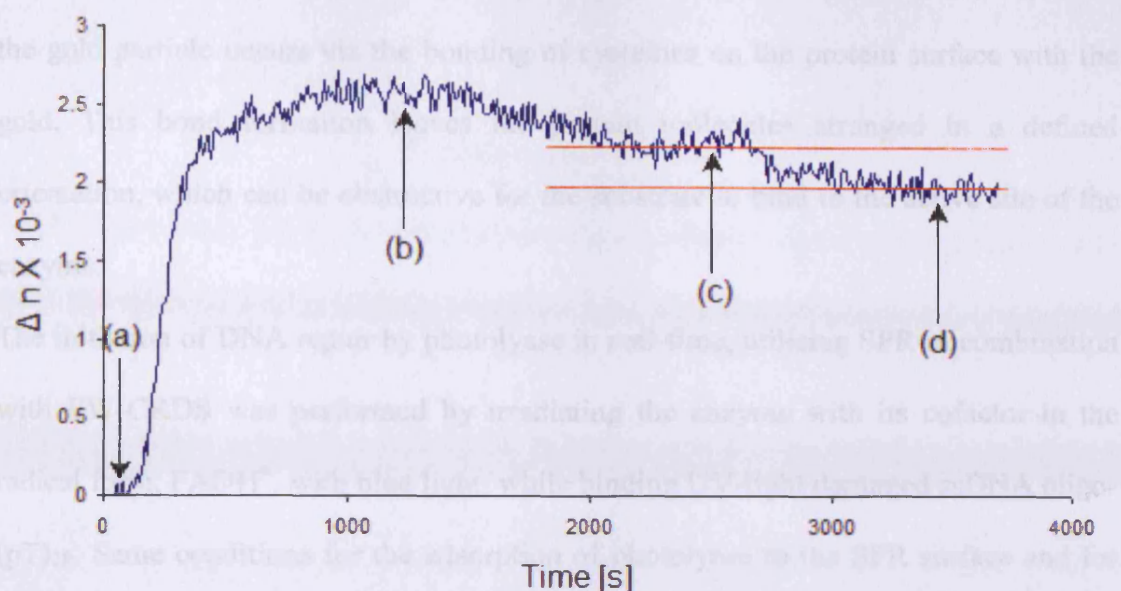


Figure 4.12: The SPR sensogram of UV-light damaged ssDNA oligo-(pT)₁₈ binding to photolyase. (a) is the injection point of photolyase, (c) is the injection point for the UV damaged oligonucleotides, (b) and (d) are assigned to washing steps of the SPR sensor surface with SPR-buffer. The horizontal red lines are marking the discrepancy of the signal observed before the injection of DNA and after.

The increase in the refractive index indicates the binding of enzyme to the gold colloids. At point (b) the system was rinsed again with SPR-buffer to remove unspecifically bound enzyme in order to achieve a stable baseline. The UV-damaged ssDNA oligo-(pT)₁₈ (2.2 μM) were injected at point (c), which subsequently resulted into the characteristic decrease of the refractive index, which was also observed for the binding of short oligonucleotides to the gold nanoparticles and is described in 4.5.1. At point (d) the system was washed again with SPR-buffer. Since the signal remained unchanged, the conclusion can be drawn that damaged DNA is bound by photolyase in the radical form and remains bound to the enzyme in the absence of light. The observed inverted signal however might not be only due to the formation of a photolyase-DNA complex but can also result of unspecific adsorption of DNA to

the enzyme. For this method used, it is unavoidable, as the binding of the enzyme to the gold particle occurs via the bonding of cysteines on the protein surface with the gold. This bond formation leaves the protein molecules arranged in a defined orientation, which can be obstructive for the substrate to bind to the active site of the enzyme.

The initiation of DNA repair by photolyase in real-time, utilising SPR in combination with EW-CRDS was performed by irradiating the enzyme with its cofactor in the radical form, FADH^\bullet , with blue light, while binding UV-light damaged ssDNA oligo-(pT)₁₈. Same conditions for the adsorption of photolyase to the SPR surface and for binding of damaged DNA to the immobilised enzyme were applied as mentioned in the previous experiment. The SPR sensogram for the DNA repair by photolyase is shown in Figure 4.13.

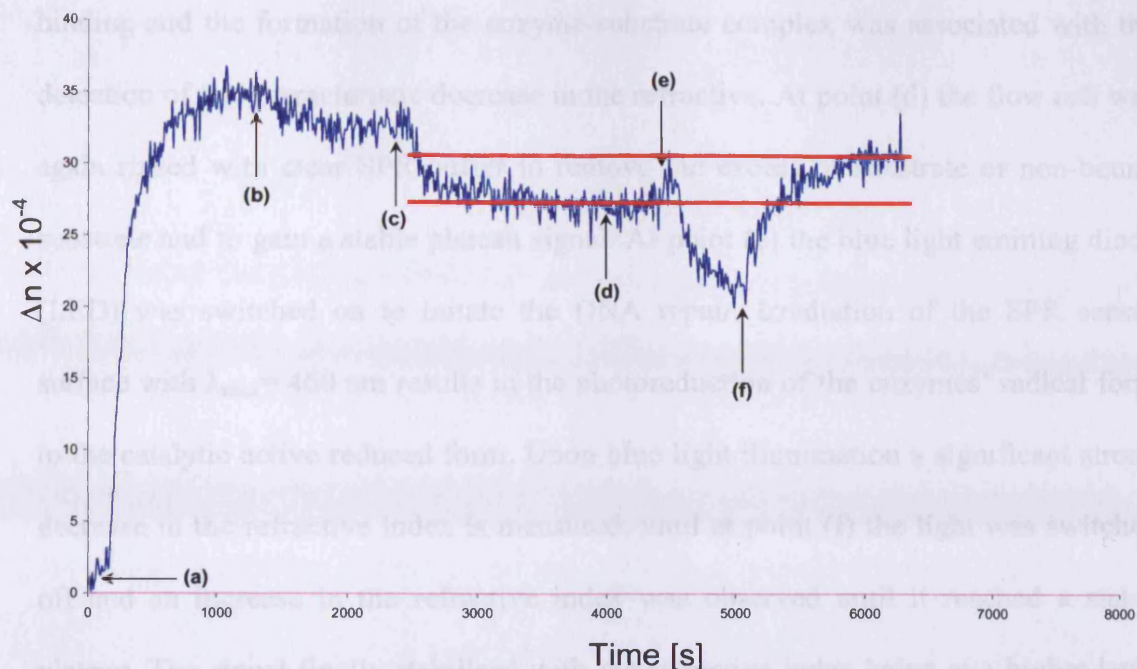


Figure 4.13: The SPR sensogram for the photo-repair of UV light irradiated ssDNA oligo-(pT)₁₈ by photolyase. Where (a) is binding of enzyme to gold nanoparticles, (b) rinsing the flow cell with SPR-buffer, (c) injection of irradiated ssDNA oligo-(pT)₁₈ to the system, (d) rinsing the flow cell with SPR-buffer, (e) start of blue-light irradiation and (f) end of blue-light irradiation. The horizontal red lines are marking the difference of the signal associated with the binding of damaged DNA and starting at point (c) and the final stable signal after the blue light was switched off.

For better interpretation of the observed changes in the refractive index, the SPR signal is divided into five segments between (a) and (f) with each segment explained as follows. At point (a) photolyase, containing FAD in its radical state FADH[•], with a concentration of 166 nM was injected into the flow cell resulting in an increase in the refractive index due to the immobilisation of enzyme to the gold nanoparticles. At point (b) clear SPR-buffer was injected into the flow cell to wash off unspecific bound enzyme eventually resulting in a stable plateau signal, indicating a saturation of protein on the sensor surface. At point (c) the substrate, UV irradiated ssDNA oligo-(pT)₁₈, with a concentration of 2.2 μ M was injected into the flow cell. The DNA

binding and the formation of the enzyme-substrate complex was associated with the detection of the characteristic decrease in the refractive. At point (d) the flow cell was again rinsed with clear SPR-buffer to remove the excess of substrate or non-bound substrate and to gain a stable plateau signal. At point (e) the blue light emitting diode (LED) was switched on to initiate the DNA repair. Irradiation of the SPR sensor surface with $\lambda_{\max} = 460$ nm results in the photoreduction of the enzymes' radical form to the catalytic active reduced form. Upon blue light illumination a significant strong decrease in the refractive index is measured, until at point (f) the light was switched off and an increase in the refractive index was observed until it reached a stable plateau. The signal finally stabilised with the refractive index being at a higher level compared to the height of the signal after the damaged DNA bound to the enzyme. In Figure 4.13 this is marked by the two horizontal red lines, which differ in their height. This increase in the refractive index is associated with the release of DNA due to the fact that DNA repair by photolyase occurred and product was released.

The same experimental conditions were applied to photolyase binding to gold nanoparticles functionalised with a cysteine SAM. The sensogram is shown in Figure 4.14. The strong inverted peak associating with photolyase-DNA interaction in the previous sensogram (Figure 4.13) after starting the blue light illumination could not be observed. However the increase in the refractive index after the blue light was switched on (e) still indicates for a DNA repair and product release.

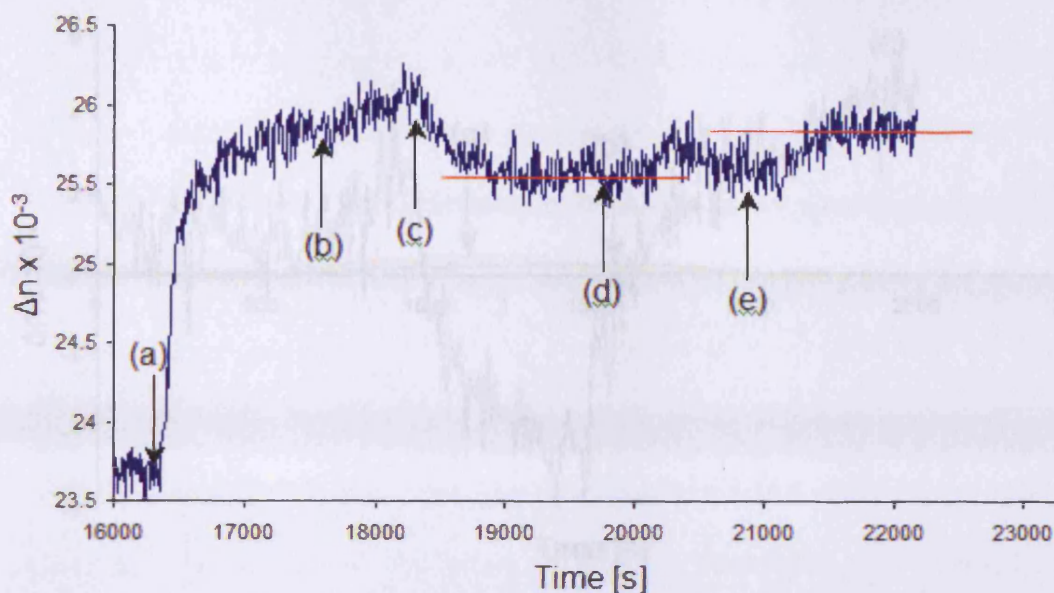


Figure 4.14: The SPR sensogram of DNA repair by photolyase when binding UV-damaged ssDNA oligo-(pT)₁₈ to gold nanoparticles functionalised with cysteine SAM. Point (a) marks the injection of photolyase, at (b) the surface is rinsed with SPR-buffer, (c) marks the injection point for the UV-damaged ssDNA oligo-(pT)₁₈, at (d) the surface was rinsed with SPR-buffer and point (e) marks the start of blue light irradiation. The horizontal red lines are marking the difference of the signal associated with the binding of damaged DNA and starting at point (c) and the signal change after the blue light was switched off.

To explain the detection of the strong inverted shift of the SPR signal between point (e) and (f) in Figure 4.13 the potential heating effect induced by the blue LED was tested in following control experiments. An empty SPR sensor chip consisting of a new prism coated with gold nanoparticles and a sensor chip charged with the protein bovine serum albumin (BSA) were irradiated with blue light. The SPR signals obtained were compared to the signal of photolyase bound to UV-damaged DNA during the irradiation with blue light from Figure 4.13. The sensogram is shown in Figure 4.15.

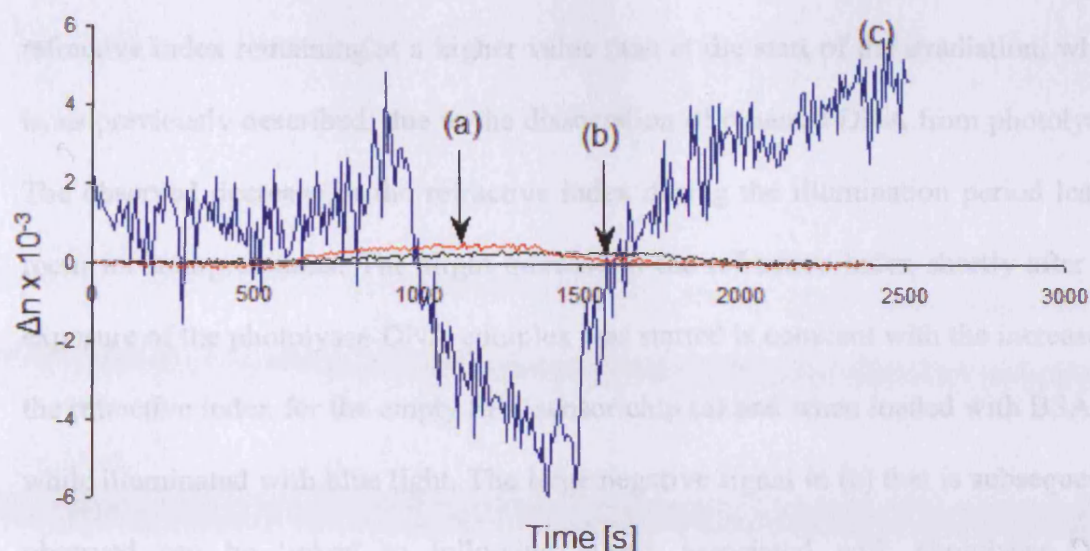


Figure 4.15: The SPR Sensogram is showing changes in the refractive index produced by the heating effect of the blue LED used during the SPR experiments. Two different modified SPR surfaces were irradiated; with the observed signals corresponding to (a)(red signal) BSA bound to gold nanoparticles and (b)(black signal) an empty gold nanoparticle surface. The signals were compared to the SPR response of (c) blue light irradiated photolyase while binding to UV-damaged DNA from Figure 4.19

Upon illumination by blue LED, a small increase in the refractive index is visible for the empty gold nanoparticle surface ((b) in Figure 4.15) as well as for the surface charged with BSA ((a) in Figure 4.15). This indicates that the local heating of the blue LED is affecting the extinction of the surface plasmons, which results in the observed higher refractive index. After the blue light is switched off, the signals return in both cases, (a) and (b), back to their starting points. The heating effects are minimal being of one magnitude smaller than the signal change after illumination of photolyase bound the damaged DNA ((c) in Figure 4.15) and in the opposite direction. While irradiating the photolyase-DNA complex with blue light, a brief increase of the refractive index is detectable followed immediately by a large negative shift that was

persistent until the blue light was turned off. The signal became stable with the refractive index remaining at a higher value than at the start of the irradiation, which is, as previously described, due to the dissociation of repaired DNA from photolyase. The observed decrease in the refractive index during the illumination period leaves room for interpretations. The slight increase in the refractive index shortly after the exposure of the photolyase-DNA complex was started is coherent with the increase of the refractive index for the empty SPR sensor chip (a) and when loaded with BSA (b) while illuminated with blue light. The large negative signal in (c) that is subsequently observed can be linked to following events associated with photolyase-DNA interaction during light exposure. The enzyme contains semi reduced FADH^\bullet and is therefore not capable of DNA repair. The cofactor remains in its radical form until photoreduction by illumination with the blue LED in presence of a reducing agent (*i.e.* DTT in the SPR-buffer) takes place. As long as blue light is present the enzyme, containing reduced FADH^- , is capable of DNA repair by transferring electrons from the cofactor to the dimer. The reduction of the cofactor and the flow of electrons to the substrate can be the reason for the strong inverted signal observed. As previously explained regarding equation 4.4, an increase in electron density affects the plasmon resonance by decreasing the local refractive index for gold nanoparticles when binding ssDNA oligo-(pT)₁₈. This can be applied to the photolyase-DNA complex, assuming that the flow of electrons during the repair mechanism increases the electron density close to the SPR sensor surface. Taking the short-time increase in the refractive index in signal (c) in the beginning of illumination into consideration it is possible that a heating effect like in signal (a) and (b) could occur, but is finally over-compensated by the signal for the decrease in the refractive index due to the increase in electron density close to the surface. Upon repetition of the experiment of DNA

repair by photolyase (Figure 4.16) the previously observed negative shift in the refractive index during illumination with blue light was not detected, although experimental conditions were kept equal.

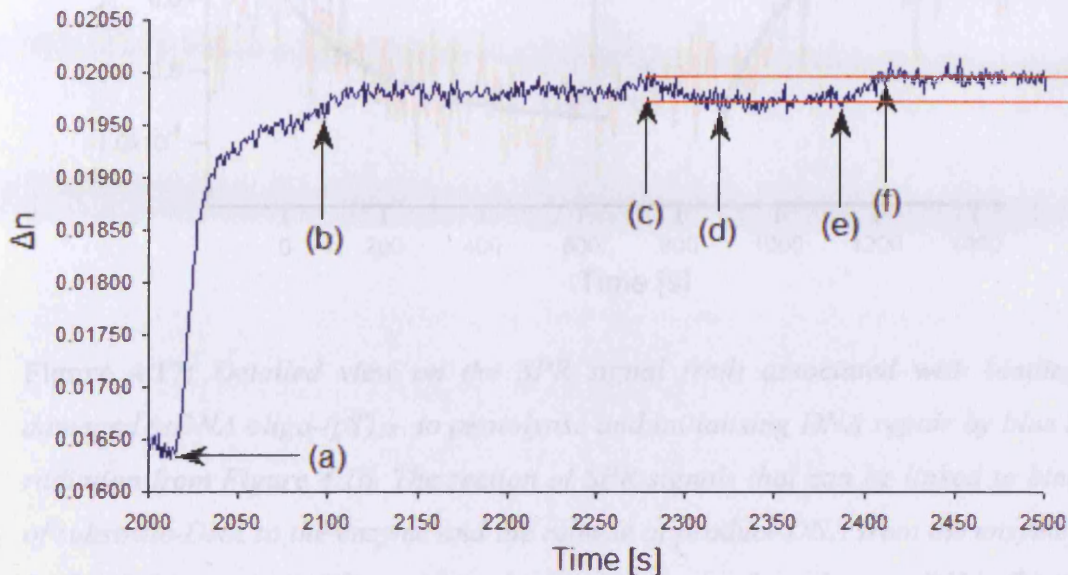


Figure 4.16: SPR sensogram of a repeated experiment showing the photo-repair of UV light irradiated ssDNA oligo-(pT)₁₈ by photolyase. (a) is the adsorption of enzyme to gold nanoparticles, (b) the flow cell was rinsed with SPR-buffer, (c) adding irradiated ssDNA oligo-(pT)₁₈ to the enzyme, (d) rinsing the flow cell with SPR-buffer, (e) start of blue-light illumination and (f) end of blue-light irradiation. The horizontal red lines are marking the discrepancy of the signal associated with the binding of damaged DNA beginning at point (c) and the final signal after point (f) when the blue light was switched off.

The SPR signals from the sensogram in Figure 4.16 specifically associated with the steps of DNA binding to enzyme, activation of DNA repair by irradiation and the subsequently release of repaired DNA is shown in Figure 4.17.

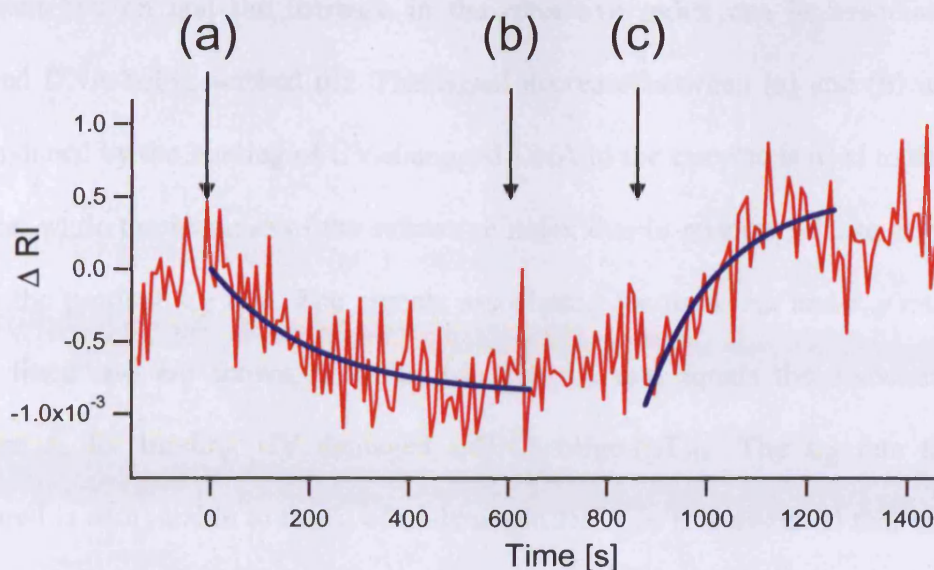


Figure 4.17: Detailed view on the SPR signal (red) associated with binding of damaged ssDNA oligo-(pT)₁₈ to photolyase and initialising DNA repair by blue light radiation from Figure 4.16. The section of SPR signals that can be linked to binding of substrate-DNA to the enzyme and the release of product-DNA from the enzyme can be fitted (blue curve). Where (a) is the injection point for substrate DNA, (b) is the injection point of clear SPR-buffer and (c) the point where the blue LED was switched on.

The negative signal developing at (a) in Figure 4.17 clearly indicates a change in the refractive index and is associated with substrate binding to photolyase. After approx. 10 min the system was washed with fresh SPR-buffer for approx. 4 min, with subsequent results slight increase of the signal caused by the removal of unbound substrate. The following stable signal in the refractive index represents photolyase saturated with substrate-DNA. A significant increase in the refractive index is immediately detected when the SPR sensor surface is radiated with blue light (c), however the strong inverted signal as in Figure 4.13 is not detected. The signal finally reaches a plateau comparable to the starting point by (a) prior to substrate DNA addition. This signal response infers that DNA repair was initiated when the blue LED

was switched on and the increase in the refractive index can be associated with repaired DNA being washed off. The signal decrease between (a) and (b) in Figure 4.17 induced by the binding of UV-damaged DNA to the enzyme is used to derive the k_{on} rate, while the increase of the refractive index due to product release at point (c) yields the product k_{off} rate. The signals associating for these k_{on} and k_{off} rates were curve fitted and are shown in Table 4.2. The k_{on} rate equals the association rate constant k_a for binding UV damaged ssDNA oligo-(pT)₁₈. The k_{off} rate that was measured is comparable to the k_d of undamaged DNA as it is assumed that blue light irradiation triggered the repair mechanism and the dissociation of product is observed due to the lower affinity of the enzyme to undamaged DNA.

Process	$k_{on} / \text{M}^{-1} \text{s}^{-1}$	K_d
Damaged DNA binding to photolyase (radical)	$3.2 \pm 0.2 \times 10^3$	<100 nM
Dissociation of repaired DNA	k_{off} / s^{-1} $6 \pm 2 \times 10^{-2}$	>6 mM

Table 4.2: The association rate constant k_{on} and equilibrium dissociation constant K_d (based on the detection limit for $k_{off} < 1 \times 10^{-4} \text{ s}^{-1}$) for the binding of UV-light damaged ssDNA oligo-(pT)₁₈ to photolyase in the radical form is listed as well as the dissociation rate constant k_{off} and the equilibrium dissociation constant K_d of DNA after initialising the repair by illumination with blue light (Rooth *et al.* manuscript in preparation)

The determined values from Table 4.2 were compared to rate and equilibrium constants given in the literature. Sancar *et al.* (1987) utilised nitrocellulose filter binding assays and flash photolysis to estimate equilibrium and rate constants.

Photodamaged pBR322 vector-DNA as used as substrate and the binding to photolyase in the radical form (termed blue photolyase) or oxidised form (termed “yellow” photolyase) was investigated. Husain and Sancar (1987) used the “gel retardation” assay to analyse the rate and equilibrium constants for the binding and repair of a 43 base pair duplex containing one thymine dimer in a central location. The measured values for calculating the equilibrium association constant K_a for substrate-DNA and photolyase depends on the experimental method, but are roughly comparable. Utilising the “nitrocellulose filter binding”-assay, Sancar *et al.* (1987) calculated $K_a = 6.0 \pm 2.1 \times 10^7 \text{ M}^{-1}$ and $K_a = 4.7 \pm \times 10^7 \text{ M}^{-1}$ with the “Flash Photolysis”-method. Husain and Sancar (1987) published a $K_a = 2.6 \times 10^8 \text{ M}^{-1}$ by utilising the gel retardation method. As $K_d = 1/K_a$ the equilibrium constant for the binding of damaged DNA to photolyase during the SPR experiments is also in the nanomolar range. The uncertainty in the K_d of damaged DNA calculated from the SPR experiments derives from the k_{off} being below the detection limit and also of different binding conditions of photolyase for damaged DNA. This may originate from variations in the orientation of photolyase while adsorbed to the gold surface and therefore can affect the availability of the enzymes active site. Uncertainty may also arise from the variability in the number and conformation of thymine dimers present in the 18-T oligomer, which affects the affinity of the substrate for the enzyme. Figure 4.18 is showing variations in the response signals for the binding of damaged DNA to photolyase and for these reasons variations in the curve fitting.

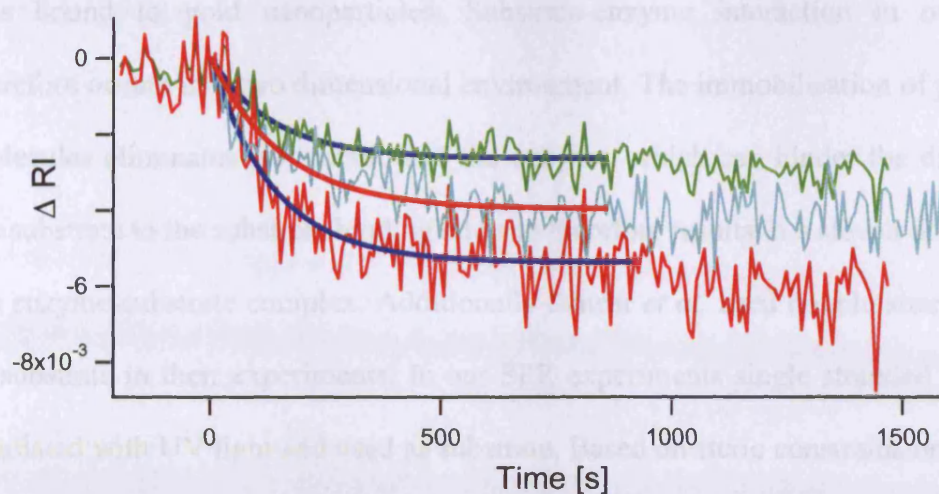


Figure 4.18: The SPR sensogram is showing different changes in the refractive index when UV-damaged ssDNA oligo-(pT)₁₈ binds to photolyase depending on the character of the substrate as well as on the accessibility of the enzyme for the substrate, which leads to a variability in the fitted curves.

SPR measurements using a BIAcore 1000 SPR machine were undertaken by Torizawa *et al.* (2004) to determine the binding constants for *T. thermophilus* photolyase binding to a single stranded 15-oligomer containing a single thymine dimer while varying the NaCl concentration in the reaction buffer. The association constant for the binding of the oligomers to the enzyme in presence of 50 mM NaCl in the reaction buffer is $K_a = 2.8 \times 10^8 \text{ M}^{-1}$ and therefore concordant to the equilibrium constant derived from our SPR measurements with 50 mM NaCl in SPR-buffer.

The association rate constant k_{on} using flash photolysis (Sancar *et al.*, 1987) was calculated to be $1.4\text{--}4 \times 10^6 \text{ M}^{-1} \text{ s}^{-1}$ and is therefore three orders of magnitude faster than the $k_{on} = 3.2 \pm 0.2 \times 10^3 \text{ M}^{-1} \text{ s}^{-1}$ observed in our SPR experiments. The discrepancy in the association rate constant can be explained by taking following reasons into consideration. Sancar *et al.* (1987) incubated photolyase and substrate prior to their experiment in buffer solution whereas photolyase in our experiments

was bound to gold nanoparticles. Substrate-enzyme interaction in our system therefore occurs in a two dimensional environment. The immobilisation of photolyase molecules eliminates free rotation of the enzyme, which can hinder the diffusion of the substrate to the substrate binding site and therefore results in a slower formation of the enzyme-substrate complex. Additionally Sancar *et al.* used double stranded DNA as substrate in their experiments. In our SPR experiments single stranded DNA was irradiated with UV light and used as substrate. Based on steric constraints only the *cis-syn* thymine dimer is formed in double stranded DNA (Kim *et al.*, 1993), however Kim *et al.* (1993) have shown that as well as to the *cis-syn* isomer the *trans-syn* isomer can form in single stranded DNA when irradiated with UV-light (ratio of 7:1 for the *cis-syn* isomer). Photolyase binds to the *trans-syn* isomer with about 10^4 -fold lower affinity than the *cis-syn* isomer, however the photochemical repair efficiency is comparable to that of the *cis* isomer (Kim *et al.*, 1993).

The k_{off} rate for the release of repaired DNA after illumination with blue light has a value of $6 \pm 2 \times 10^{-2} \text{ s}^{-1}$, with an estimated equilibrium constant K_d of $> 6\text{mM}$.

The literature value of the equilibrium constant for non-substrate DNA and photolyase interaction, published by Husain and Sancar, (1987) is $3.47 \times 10^3 \text{ M}^{-1}$. The difference of one order of magnitude between this value and our estimated value derives from the method Sancar and Husain utilised to measure the binding of undamaged DNA to photolyase. They measured the affinity of the enzyme to non-substrate DNA indirectly by measuring inhibition of the specific complex formation while adding non-substrate DNA in excess to enzyme and substrate DNA.

We also attempt to detect repair of UV-damaged ssDNA oligo-(pT)₁₈ by binding first the substrate DNA to gold nanoparticles modified with a cysteine SAM. The

possibility of adsorption and immobilisation of DNA to a SPR surface containing cysteine SAM is shown in Figure 4.7. Monitoring the binding of photolyase (radical form) to surface-bound damaged DNA and the following activation of the DNA repair is shown in Figure 4.19.

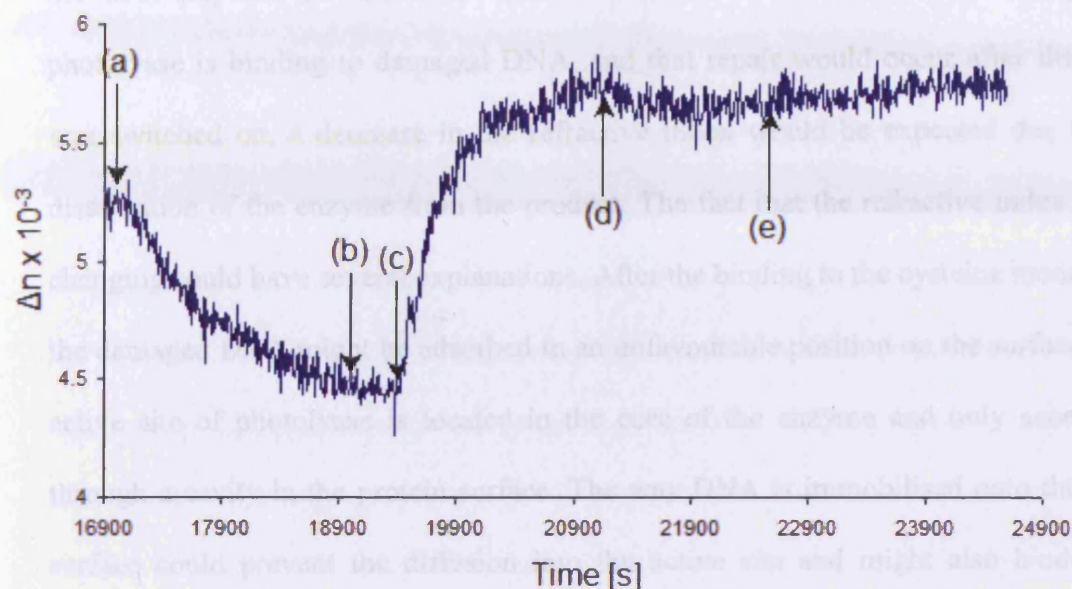


Figure 4.19: The SPR sensogram of DNA repair by photolyase binding UV-damaged ssDNA oligo-(pT)₁₈ first to gold nanoparticles modified with a cysteine SAM and then injecting photolyase to the system. (a) is the point of injection of damaged DNA, (b) the washing step with SPR-buffer, (c) the injection point of photolyase, (d) the second washing step and point (e) is the start of blue light illumination.

At point (a) the UV-damaged DNA was injected to the system visible by creating the characteristic decrease in the refractive index. After adjusting a stable signal by rinsing the system with SPR-buffer (b) photolyase was injected at (c) in an attempt to bind to damaged DNA by creating the enzyme-substrate complex. The adsorption of the enzyme is detectable by an increase in the refractive index. After a second washing step at point (d) to remove un-bound protein, the illumination of the surface with blue light was started at point (e). The negative signal shift developing after the

injection of DNA clearly corresponds to the DNA adsorbing to the gold nanoparticles. The binding is consistent, as the signal remained steady when rinsing the surface with buffer. The increase in the refractive index after the injection of photolyase indicates for an adsorption to the surface saturated with substrate DNA. However no change in the SPR response is detectable after illumination of the surface. Assuming that photolyase is binding to damaged DNA, and that repair would occur after the light was switched on, a decrease in the refractive index would be expected due to the dissociation of the enzyme from the product. The fact that the refractive index is not changing could have several explanations. After the binding to the cysteine monolayer the damaged DNA might be adsorbed in an unfavourable position on the surface. The active site of photolyase is located in the core of the enzyme and only accessible through a cavity in the protein surface. The way DNA is immobilised onto the SPR surface could prevent the diffusion into the active site and might also hinder the enzymes ability to bind the damaged DNA strand properly. A way to improve the accessibility of single stranded DNA on a SPR sensor was presented by Ladder *et al.* (2004). They immobilised biotinylated single stranded DNA through a streptavidin bridge to a mixed SAM of biotinylated alkanethiol and oligo(ethylene glycol). A further explanation is the formation of protein multilayers when photolyase is injected into the SPR flow cell due to unspecific protein-protein interaction despite the ionic strength of 50 mM NaCl in SPR buffer. This unwanted event is also possible by binding first the enzyme to the sensor surface and then injecting the substrate DNA, however it is in this case possible that some photolyase molecules are adsorbed in such a manner that the substrate binding site remains accessible that substrate can be bound and repaired product released. In the former case multilayers of enzyme would

block the dissociation of the product. It is therefore better to revert to the previous binding order with protein adsorbing first to the surface and than DNA.

DNA binding and repair experiments with photolyase in the oxidised form

The DNA repair ability of photolyase, containing its cofactor FAD in the oxidised form, was tested by adsorbing the enzyme to gold nanoparticles binding UV-damaged ssDNA oligo-(pT)₁₈ and illumination with blue light.

FAD oxidises upon extended storage of photolyases under non-reducing conditions and in contact with air. The change in oxidation states of FAD in photolyase can be observed by colour changes of the protein solution and by UV/Vis spectroscopy. The oxidised enzyme appears yellow, however oxidation leads also to aggregation of protein in which following purification steps were necessary to recover soluble photolyase. Yellow photolyase was centrifuged (10 min, 16,000 \times g, 4°C) to separate soluble protein from aggregated protein. The supernatant was transferred into a Microcon centrifugal filter device (Millipore) with a MWCO of 30,000 Da to separate photolyase from free FAD by centrifugation. During the centrifugation steps the retentate was diluted with SPR-buffer containing no DTT to exchange the storage buffer C_{Ds} and to remove traces of DTT. UV/Vis spectroscopy confirmed the presence of photolyase bound to FAD in its oxidised form, while a spectrum of the flow through showed signals indicating for free FAD. The sensogram of oxidised photolyase interacting with damaged DNA with a FAD cofactor in its oxidised form binding UV-damaged ssDNA oligo-(pT)₁₈ and the initiation of the DNA repair by blue light illumination is shown in Figure 4.20.

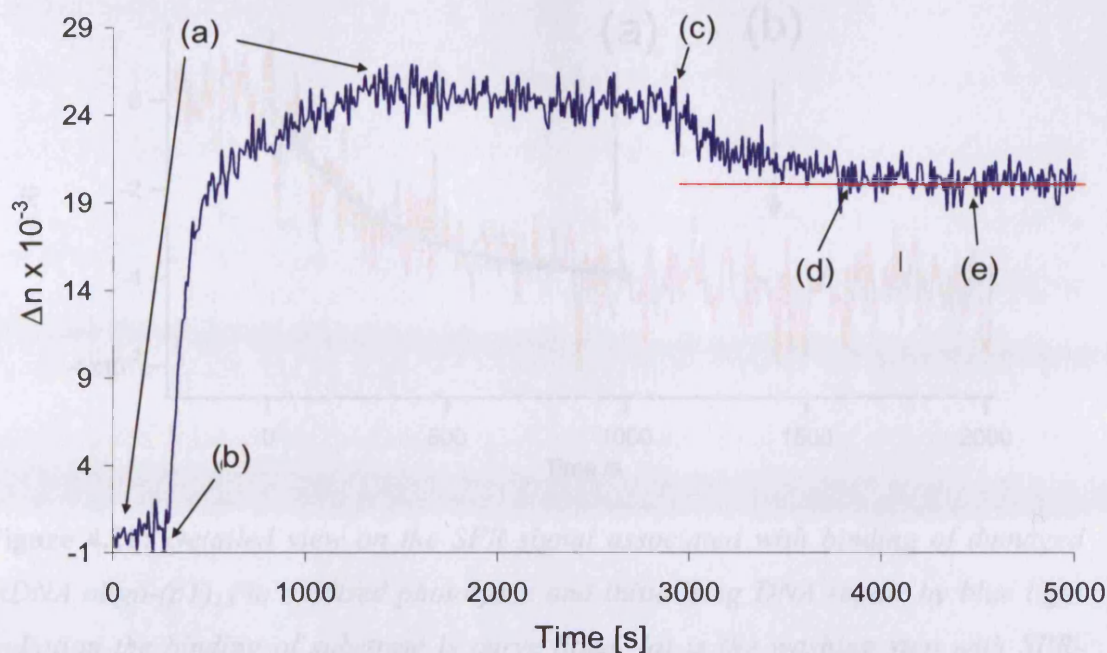


Figure 4.20: The sensogram of photolyase with FAD in its oxidised form binding to UV-damaged ssDNA oligo-(pT)₁₈ and illumination with blue light. Where (a) corresponds to washing steps with SPRE-buffer (containing no DTT), (b) is the injection point of photolyase, (c) is the injection point of damaged DNA, (a) marks the beginning of illumination and at point (e) the light was switched off. The SPR signal does not change during illumination with blue light.

The SPR signal responses are comparable to the previous experiments involving the adsorption after the injection of oxidised photolyase at point (b) the increase in the refractive index indicates for the adsorption of photolyase to the gold nanoparticles. The injection of damaged DNA to the system at (c) results in the already characterised decrease in the refractive index. After the washing step at (d) the blue light illumination was started at (e). Irradiation has not effect on the refractive index, as signal changes in the previous experiments were observed after the blue light was switched on. Taking in consideration that the photoreduction of the enzyme via blue light requires the presence of a reducing agent in the buffer suggest that DNA is not dissociating from the enzyme due to non-repair of the thymine dimers.

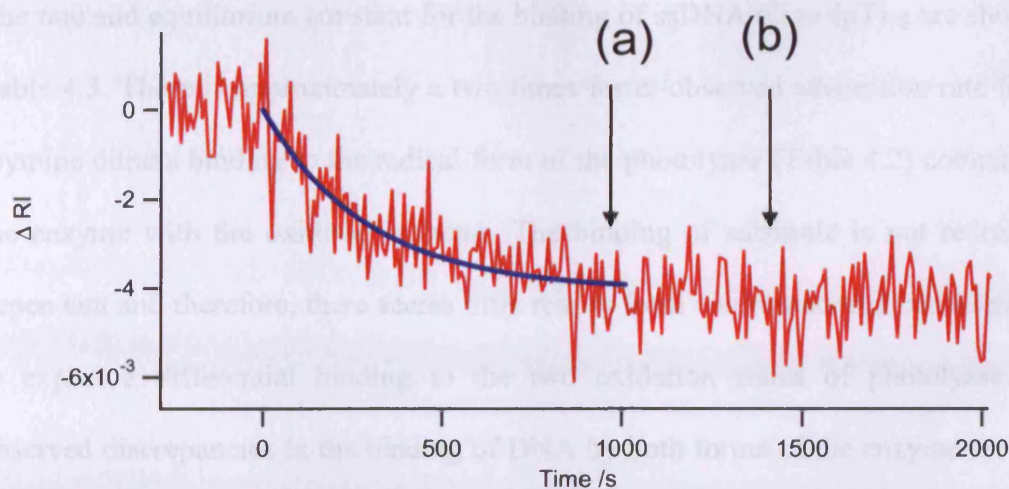


Figure 4.21: Detailed view on the SPR signal associated with binding of damaged ssDNA oligo-(pT)₁₈ to oxidised photolyase and initialising DNA repair by blue light radiation the binding of substrate is curve fitted. (a) is the washing step with SPR-buffer, (b) starting point of blue light irradiation .

Figure 4.21 is showing the section of the signal response after the binding of DNA, with the decrease in the refractive index curve fitted and during the blue light irradiation. If compared to Figure 4.17 the start of the blue light illumination clearly does not result in a signal response.

Process	$k_{on} / \text{M}^{-1} \text{s}^{-1}$	K_d
Damaged DNA binding to photolyase (oxidised)	$1.6 \pm 0.2 \cdot 10^3$	<100 nM

Table 4.3: The association rate constant k_a and equilibrium dissociation constant K_d for the binding of UV-light damaged ssDNA oligo-(pT)₁₈ to photolyase in the oxidised state (detection limit for $k_{off} < 1 \times 10^{-4} \text{ s}^{-1}$) (Rooth et al. manuscript in preparation).

The rate and equilibrium constant for the binding of ssDNA oligo-(pT)₁₈ are shown in Table 4.3. There is approximately a two times faster observed adsorption rate for the thymine dimers binding to the radical form of the photolyase (Table 4.2) compared to the enzyme with the oxidised cofactor. The binding of substrate is not redox-state dependant and therefore, there seems little reason from conformational considerations to expect a differential binding to the two oxidation states of photolyase. The observed discrepancies in the binding of DNA by both forms of the enzyme are most likely due to the effectiveness in the coupling of the plasmon field to either the radical or oxidised form and damaged poly-T combined molar polarisabilities. The derived K_d for the oxidised form of the enzyme is concordant to the equilibrium constant published by Sancar *et al.*, (1987), which is $K_a = 4.8 \times 10^7 \text{ M}^{-1}$.

4.6 Conclusion

SPR in combination with EW-CRDS was successfully used to investigate the reaction mechanism of DNA repair by photolyase. The binding ability and signal response of purified enzyme to the SPR sensor chip was tested by modifying the gold nanoparticle surface with self-assembled monolayers (SAMs). The production of thymine dimers as substrate for photolyase was effectively performed by the irradiation of thymidine oligonucleotides with UV-light. The formation of photoproducts could be followed photospectrometrically by measuring the decrease in absorbance during UV-light exposure. The binding of native and damaged oligonucleotides to the SPR sensor chip produced negative SPR signal responses as a reproducible characteristic for all following experiments. Changes in the SPR signals were used to estimate the

association rate constants of photolyase binding to each SAM modified surface. The binding of UV-light damaged DNA to photolyase and the repair process was observed after blue light exposure. From the obtained signal changes, which can be directly linked to photolyase–DNA interaction, it was possible to calculate the associate rate constant of DNA binding to photolyase and the dissociation rate constant for the release of repaired DNA. Further the dissociation constant of the photolyase-DNA complex was calculated. The results were found to be concordant to published data. SPR combined with EW-CRDS was therefore successfully introduced as a sensitive and accurate method in observing enzyme-substrate interaction.

CHAPTER 5:

General conclusions and future work

Photolyase is involved in the DNA repair mechanism that opposes the harmful effects of UV-light on DNA. It is utilised by the majority of organisms but is not present in higher mammals such as humans. Photolyase is very distinct in its substrate specificity and is highly efficient in catalysing DNA repair. However even after more than 50 years since its discovery. The mechanism of repair is still not fully clear. DNA-repair by photolyase is carried out by a single electron transfer from its reduced cofactor FAD to the substrate. Two routes of electron transfer are postulated but neither have been proven. One hypothesis involves a direct electron transfer via the C8 α -methyl group from the FAD's isoalloxazine ring; the second hypothesis suggests an indirect electron transfer involving the adenine moiety. In order to investigate the electron-transfer the modification of the catalytic cofactor FAD with respect to its C8 α -methyl group and the comparison of the action spectrum of wild-type enzyme and modified enzyme is of interest. An aspect of the present thesis was the development of an *in vitro* method that would make it possible to exchange the wild-type cofactor FAD in photolyase for the FAD analogue roseoFAD, which contains a dimethyl amino group in place of a methyl group on its C8 atom. RoseoFAD was biochemically synthesised from its precursor roseoflavin by enzymatic conversion utilising a FAD-synthetase displacing time consuming and expensive conventional organic synthesis. The successful reaction was confirmed by mass spectroscopy. The exchange of FAD by roseoFAD was successfully achieved by denaturing the enzyme via pH change while bound to a hydrophobic interaction column. Readjusting the pH to its previous value and subsequently washing the column with roseoFAD resulted into binding of roseoFAD to the protein. This method was found to be more successful than the dialysis method or the cofactor exchange on a Ni-NTA column where high concentrations of urea were used to denature the enzyme. It should also be

mentioned that the redox state of the FAD analogue that is incorporated might be of importance to guarantee a successful reconstitution. All attempts to incorporate roseoFAD were performed under aerobic or mild anaerobic conditions and with the cofactor derivative in its oxidised form. It is however possible that the reduced state of roseoFAD would bind better as it more closely corresponds to the reduced state of FAD. Unfortunately the reconstitution could only be achieved in low yields and the roseoFAD modified photolyase was unstable and degraded quickly into aggregated protein and free roseoFAD. The following work to increase the yield of modified enzyme and to improve its stability is necessary. That could include the reconstitution of photolyase with roseoFAD under anaerobic conditions. However substituents on the C8 atom of the isoalloxazine ring do not inhibit the incorporation of FAD analogues and the original methyl group of FAD is not relevant for keeping FAD bound photolyase. For future work, the DNA-repair efficiency of reconstituted photolyase should be compared to that of the wild-type enzyme. EPR and ENDOR spectroscopy can be utilised to detect if the dimethyl amino substituent influences the formation of the FADH^\bullet radical during catalysis and therefore characterising the importance or the negligence of the C8 α -methyl group for the DNA repair.

Surface Plasmon Resonance (SPR) is an established spectroscopy method to investigate the interaction of biomolecules. Signal changes observed can be used to association and dissociation of two molecules in the dependence of time. Therefore it is possible to calculate the rate constants for association (k_{on}) and dissociation (k_{off}) as well as the equilibrium constants K_d or K_a . The combination of SPR with Evanescent Wave Cavity Ring-down spectroscopy was introduced to increase the sensitivity with

respect to the obtained SPR signals by increasing the path length of the incoming light beam. The binding of photolyase to the gold nanoparticles was ensured by treating the gold colloids with self-assembled monolayers (SAMs) with the intention to increase protein binding and hence the signal response. The advantage over conventional SPR machines was also the set up of the self-constructed SPR equipment, which allowed a grade of modification such as the installation of a blue light diode (LED) to activate the DNA repair. The resulting signals were aligned to the action spectrum of photolyase and the calculated rate and equilibrium constants showed remarkable agreement with published values. The data presented in this study were obtained by using UV-light damaged single stranded poly-T oligonucleotides as substrate. A wider range of substrates should be used in future experiments including double stranded DNA or a random DNA oligonucleotides containing only one thymine dimer. SPR measurements could also be performed, by using photolyase, which contains FAD-analogues. The comparison of signal responses for wild-type enzyme and modified enzyme as well as the calculation of rate and equilibrium constants can be consulted to investigate which atoms in the FAD molecule might influence the substrate binding and if DNA repair is inhibit and if so, to which extend.

References:

Ahmad M, Jarillo JA, Klimczak LJ, Landry LG, Peng T, Last RL, Cashmore AR (1997) An enzyme similar to animal type II photolyases mediates photoreactivation in Arabidopsis. *Plant Cell* **9**: 199-207

Aubert C, Vos MH, Mathis P, Eker APM, Brettel K (2000) Intraprotein radical transfer during photoactivation of DNA photolyase. *Nature* **405**: 586-590

Baer ME, Sancar GB (1993) The role of conserved amino acids in substrate-binding and discrimination by photolyase. *J. Biol. Chem.* **268**: 16717-16724

Beukers R, Berends W (1960) Isolation and identification of the irradiation product of thymine. *Biochim. Biophys. Acta.* **41**: 550-551

Beukers R, Eker APM, Lohman PHM (2008) 50 years thymine dimer. *DNA Repair* **7**: 530-543

Blackburn GM, Davies RJH (1966) Structure of DNA-derived thymine dimer. *Biochem. Biophys. Res. Commun.* **22**: 704-706

Byrdin M, Eker APM, Vos MH, Brettel K (2003) Dissection of the triple tryptophan electron transfer chain in Escherichia coli DNA photolyase: Trp382 is the primary donor in photoactivation. *Proc. Nat. Acad. Sci. U.S.A.* **100**: 8676-8681

Camerman N, Camerman A (1970) Crystal and molecular structure of photodimer-A of 1,3-dimethylthymine (isomer in irradiated deoxyribonucleic acid). *J. Am. Chem. Soc* **92**: 2523-2527

Carell T, Burgdorf LT, Kundu LM, Cichon M (2001) The mechanism of action of DNA photolyases. *Current Opinion in Chemical Biology* **5**: 491-498

Cooke G, Legrand YM, Rotello VM (2004) Model systems for flavoenzyme activity: an electrochemically tuneable model of roseoflavin. *Chemical Communications*: 1088-1089

Crick FH, Brenner S, Watson R, Barnett L (1961) General nature of genetic code for proteins. *Nature* **192**: 1227-1232

Disley DM, Cullen DC, You HX, Lowe CR (1998) Covalent coupling of immunoglobulin G to self-assembled monolayers as a method for immobilizing the interfacial-recognition layer of a surface plasmon resonance immunosensor. *Biosens. Bioelectron.* **13**: 1213-1225

- Efimov I, Kuusk V, Zhang XP, McIntire WS (1998) Proposed steady-state kinetic mechanism for *Corynebacterium ammoniagenes* FAD synthetase produced by *Escherichia coli*. *Biochemistry* **37**: 9716-9723
- Eisenreich W, Kemter K, Bacher A, Mulrooney SB, Williams CH, Muller F (2004) C-13-, N-15- and P-31-NMR studies of oxidized and reduced low molecular mass thioredoxin reductase and some mutant proteins. *Eur. J. Biochem.* **271**: 1437-1452
- Eker APM, Yajima H, Yasui A (1994) DNA photolyase from the fungus *Neurospora crassa* - purification, characterisation and comparison with other photolyase. *Photochem. Photobiol.* **60**: 125-133
- Engeln R, Berden G, vandenBerg E, Meijer G (1997) Polarization dependent cavity ring down spectroscopy. *J. Chem. Phys.* **107**: 4458-4467
- Fischer M, Bacher A (2005) Biosynthesis of flavoenzymes. *Nat. Prod. Rep.* **22**: 324-350
- Flanagan MT, Pantell RH (1984) Surface-plasmon resonance and immunosensors. *Electron. Lett.* **20**: 968-970
- Fujihashi M, Numoto N, Kobayashi Y, Mizushima A, Tsujimura M, Nakamura A, Kawarabayasi Y, Miki K (2007) Crystal structure of archaeal photolyase from *Sulfolobus tokodaii* with two FAD molecules: Implication of a novel light-harvesting cofactor. *J. Mol. Biol.* **365**: 903-910
- Goodhead DT (1989) The initial physical damage produced by ionizing radiations. *International Journal of Radiation Biology* **56**: 623-634
- Goosen N, Moolenaar GF (2008) Repair of UV damage in bacteria. *DNA Repair* **7**: 353-379
- Grill S, Busenbender S, Pfeiffer M, Kohler U, Mack M (2008) The bifunctional flavokinase/flavin adenine dinucleotide synthetase from *Streptomyces davawensis* produces inactive flavin cofactors and is not involved in resistance to the antibiotic roseoflavin. *J. Bacteriol.* **190**: 1546-1553
- Gunz D, Hess MT, Naegeli H (1996) Recognition of DNA adducts by human nucleotide excision repair - Evidence for a thermodynamic probing mechanism. *J. Biol. Chem.* **271**: 25089-25098
- Hagihara T, Fujio T, Aisaka K (1995) Cloning of FAD synthetase gene from *Corynebacterium ammoniagenes* and its application to FAD and FMN production. *Appl. Microbiol. Biotechnol.* **42**: 724-729
- Harm W, Harm H, Rupert CS (1968) Analysis of photoenzymatic repair of UV lesions in DNA by single light flashes .II. *In vivo* studies with *Escherichia coli* cells and bacteriophage. *Mutation Research* **6**: 371-385

- Heelis PF, Kim ST, Okamura T, Sancar A (1993) The photo repair of pyrimidine dimers by DNA photolyase and model systems. *J. Photochem. Photobiol., B* **17**: 219-228
- Henry AA, Jimenez R, Hanway D, Romesberg FE (2004) Preliminary characterization of light harvesting in E-coli DNA photolyase. *Chembiochem* **5**: 1088-1094
- Hess MT, Schwitter U, Petretta M, Giese B, Naegeli H (1997) Bipartite substrate discrimination by human nucleotide excision repair. *Proc. Nat. Acad. Sci. U.S.A.* **94**: 6664-6669
- Hirouchi T, Nakajima S, Najrana T, Tanaka M, Matsunaga T, Hidema J, Teranishi M, Fujino T, Kumagai T, Yamamoto K (2003) A gene for a Class II DNA photolyase from *Oryza sativa*: cloning of the cDNA by dilution-amplification. *Molecular Genetics and Genomics* **269**: 508-516
- Horvath I, Tihanyi K, Szeberenyi S, Otani S (1979) Effect of roseoflavin on microsomal drug-metabolizing enzyme-system. *Febs Letters* **98**: 49-52
- Hsu DS, Zhao XD, Zhao SY, Kazantsev A, Wang RP, Todo T, Wei YF, Sancar A (1996) Putative human blue-light photoreceptors hCRY1 and hCRY2 are flavoproteins. *Biochemistry* **35**: 13871-13877
- Hu H (1990) Effects of ultraviolet-radiation. *Medical Clinics of North America* **74**: 509-514
- Husain I, Sancar A (1987) Binding of *Escherichia coli* DNA photolyase to a defined substrate containing a single T reversible T dimer. *Nucleic Acids Res.* **15**: 1109-1120
- Jiricny J (1998) Replication errors: cha(lle)nging the genome. *Embo Journal* **17**: 6427-6436
- Jorns MS, Wang BY, Jordan SP, Chanderkar LP (1990) Chromophore function and interaction in *Escherichia coli* DNA photolyase – reconstitution of the apoenzyme with pterin and or flavin derivatives. *Biochemistry* **29**: 552-561
- Kao JLF, Nadji S, Taylor JS (1993) Identification and structure determination of a third cyclobutane photodimer of thymidyl-(3'- 5')-thymidine – the *trans-syn*-II product. *Chem. Res. Toxicol.* **6**: 561-567
- Kao YT, Saxena C, Wang LJ, Sancar A, Zhong DP (2005) Direct observation of thymine dimer repair in DNA by photolyase. *Proc. Nat. Acad. Sci. U.S.A.* **102**: 16128-16132
- Karle IL, Wang SY, Varghese AJ (1969) Crystal and molecular structure of a thymine-thymine adduct. *Science* **164**: 183-184

- Karlsson R, Michaelsson A, Mattsson L (1991) Kinetic – analysis of monoclonal antibody-antigen interactions with a new biosensor based analytical system *J. Immunolo. Met.* **145**: 229-240
- Kasai S, Miura R, Matsui K (1975) Chemical structure and some properties of roseoflavin. *Bull. Chem. Soc. Jpn.* **48**: 2877-2880
- Kavakli IH, Sancar A (2004) Analysis of the role of intraprotein electron transfer in photoreactivation by DNA photolyase in Vivo. *Biochemistry* **43**: 15103-15110
- Kay CWM, Feicht R, Schulz K, Sadewater P, Sancar A, Bacher A, Mobius K, Richter G, Weber S (1999) EPR, ENDOR, and TRIPLE resonance spectroscopy on the neutral flavin radical in *Escherichia coli* DNA photolyase. *Biochemistry* **38**: 16740-16748
- Kelner A (1949) Effect of visible light on the recovery of *Streptomyces griseus* conidia from ultraviolet irradiation injury. *Proc. Nat. Acad. Sci. U.S.A.* **35**: 73-79
- Kim ST, Heelis PF, Okamura T, Sancar A (1991) Determination of rates and yields of interchromophore energy transfer and intermolecular electron transfer in *Escherichia coli* photolyase by time-resolved fluorescence and absorption spectroscopy. *Photochem. Photobiol.* **53**: 11262-11270
- Kim ST, Li YF, Sancar A (1992) The third chromophore of DNA photolyase – Trp-277 of *Escherichia coli* DNA photolyase repairs thymine dimers by direct electron-transfer. *Proc. Nat. Acad. Sci. U.S.A.* **89**: 900-904
- Kim ST, Sancar A (1993) Photochemistry, photophysics, and mechanism of pyrimidine dimer repair by DNA photolyase. *Photochem. Photobiol.* **57**: 895-904
- Klar T, Kaiser G, Hennecke U, Carell T, Batschauer A, Essen LO (2006) Natural and non-natural antenna chromophores in the DNA photolyase from *Thermus thermophilus*. *Chembiochem* **7**: 1798-1806
- Komori H, Masui R, Kuramitsu S, Yokoyama S, Shibata T, Inoue Y, Miki K (2001) Crystal structure of thermostable DNA photolyase: Pyrimidine-dimer recognition mechanism. *Proc. Nat. Acad. Sci. U.S.A.* **98**: 13560-13565
- Laemmli UK (1970) Cleavage of structural proteins during assembly of head of bacteriophage-T4. *Nature* **227**: 680-&
- Lahue RS, Au KG, Modrich P (1989) DNA mismatch correction in a defined system. *Science* **245**: 160-164
- Leclerc JE, Borden A, Lawrence CW (1991) The thymine-thymine pyrimidine-pyrimidone(6-4) ultraviolet-light photoproduct is highly mutagenic and specifically induces 3' thymine-to-cytosine transitions in *Escherichia coli*. *Proc. Nat. Acad. Sci. U.S.A.* **88**: 9685-9689

- Lee JH, Hwang GS, Choi BS (1999) Solution structure of a DNA decanter duplex containing the stable 3' T center dot G base pair of the pyrimidine(6-4)pyrimidone photoproduct (6-4) adduct : Implications for the highly specific 3' T -> C transition of the (6-4) adduct. *Proc. Nat. Acad. Sci. U.S.A.* **96**: 6632-6636
- Ley RD (1993) Photoreactivation in humans. *Proc. Nat. Acad. Sci. U.S.A.* **90**: 4337-4337
- Li YF, Kim ST, Sancar A (1993) Evidence for lack of DNA photoreactivating enzyme in humans. *Proc. Nat. Acad. Sci. U.S.A.* **90**: 4389-4393
- Li YF, Sancar A (1990) Active-site of *Escherichia coli* DNA photolyase - mutations at Trp277 alter the selectivity of the enzyme without affecting the quantum yield of photorepair. *Biochemistry* **29**: 5698-5706
- Lindahl T, Wood RD (1999) Quality control by DNA repair. *Science* **286**: 1897-1905
- Lipman RSA, Jorns MS (1992) Direct evidence for singlet singlet energy-transfer in *Escherichia coli* DNA photolyase. *Biochemistry* **31**: 786-791
- MacFarlane AW, Stanley RJ (2003) Cis-Syn thymidine dimer repair by DNA photolyase in real time. *Biochemistry* **42**: 8558-8568
- Manstein DJ, Pai EF (1986) Purification and characterization of FAD synthetase from *Brevibacterium ammoniagenes*. *J. Biol. Chem.* **261**: 6169-6173
- Massey V (1995) Flavoprotein structure and mechanism - introduction. *FASEB J.* **9**: 473-475
- Massey V (2000) The chemical and biological versatility of riboflavin. *Biochem. Soc. Trans.* **28**: 283-296
- Mathes T, Vogl C, Stolz J, Hegemann P (2009) In vivo generation of flavoproteins with modified cofactors. *J. Mol. Biol.* **385**: 1511-1518
- Maul MJ, Barends TRM, Glas AF, Cryle MJ, Domratcheva T, Schneider S, Schlichting I, Carell T (2008) Crystal structure and mechanism of a DNA (6-4) photolyase. *Angew. Chem. Int. Ed.* **47**: 10076-10080
- Mees A, Klar T, Gnau P, Hennecke U, Eker APM, Carell T, Essen LO (2004) Crystal structure of a photolyase bound to a CPD-like DNA lesion after in situ repair. *Science* **306**: 1789-1793
- Modrich P (1991) Mechanisms and biological effects of mismatch repair. *Annu. Rev. Gen.* **25**: 229-253
- Modrich P, Lahue R (1996) Mismatch repair in replication fidelity, genetic recombination, and cancer biology. *Annu. Rev. Biochem.* **65**: 101-133

- Moertl S, Fischer M, Richter G, Tack J, Weinkauff S, Bacher A (1996) Biosynthesis of riboflavin. Lumazine synthase of *Escherichia coli*. *J. Biol. Chem.* **271**: 33201-33207
- Molina MJ, Rowland FS (1974) Stratospheric sink for chlorofluoromethanes - chlorine atomic-catalysed destruction of ozone. *Nature* **249**: 810-812
- Mu WM, Zhang DF, Xu L, Luo ZF, Wang YZ (2005) Activity assay of his-tagged *E. coli* DNA photolyase by RP-HPLC and SE-HPLC. *J. Biochem. Bioph. Methods* **63**: 111-124
- Mullis KB, Faloona FA (1987) Specific synthesis of DNA *in vitro* via a polymerase-catalysed chain reaction. *Methods Enzymol.* **155**: 335-350
- Mulvaney P, Perez-Juste J, Giersig M, Liz-Marzan LM, Pecharroman C (2006) Drastic surface plasmon mode shifts in gold nanorods due to electron charging. *Plasmonics* **1**: 61-66
- O'Connor KA, McBride MJ, West M, Yu H, Trinh L, Yuan K, Lee T, Zusman DR (1996) Photolyase of *Myxococcus xanthus*, a gram-negative eubacterium, is more similar to photolyases found in archaea and "higher" eukaryotes than to photolyases of other eubacteria. *J. Biol. Chem.* **271**: 6252-6259
- O'Neil LL, Grossfield A, Wiest O (2007) Base flipping of the thymine dimer in duplex DNA. *J. Phys. Chem. B* **111**: 11843-11849
- Okeefe A, Deacon DAG (1988) Cavity ring-down optical spectrometer for absorption measurements using pulsed laser sources. *Rev. Sci. Instrum.* **59**: 2544-2551
- Otani S, Takatsu M, Nakano M, Kasai S, Miura R, Matsui K (1974) Roseoflavin, a new antimicrobial pigment from *Streptomyces*. *J. Antibiot.* **27**: 88-89
- Otto MK, Jayaram M, Hamilton RM, Delbruck M (1981) Replacement of riboflavin by an analog in the blue-light photoreceptor of *Phycomyces*. *Proc. Nat. Acad. Sci. U.S.A.* **78**: 266-269
- Park H, Zhang KJ, Ren YJ, Nadji S, Sinha N, Taylor JS, Kang CH (2002) Crystal structure of a DNA decamer containing a cis-syn thymine dimer. *Proc. Nat. Acad. Sci. U.S.A.* **99**: 15965-15970
- Park HW, Kim ST, Sancar A, Deisenhofer J (1995) Crystal-structure of DNA photolyase from *Escherichia coli*. *Science* **268**: 1866-1872
- Payne G, Wills M, Walsh C, Sancar A (1990) Reconstitution of *Escherichia coli* photolyase with flavins and flavin analogs. *Biochemistry* **29**: 5706-5711
- Peng W, Shaw BR (1996) Accelerated deamination of cytosine residues in UV-induced cyclobutane pyrimidine dimers leads to CC->TT transitions. *Biochemistry* **35**: 10172-10181

- Petersen JL, Lang DW, Small GD (1999) Cloning and characterization of a class II DNA photolyase from *Chlamydomonas*. *Plant Molecular Biology* **40**: 1063-1071
- Prytkova TR, Beratan DN, Skourtis SS (2007) Photoselected electron transfer pathways in DNA photolyase. *Proc. Nat. Acad. Sci. U.S.A.* **104**: 802-807
- Ramsey AJ, Alderfer JL, Jorns MS (1992) Energy transduction during catalysis by *Escherichia coli* DNA photolyase. *Biochemistry* **31**: 7134-7142
- Ramsey AJ, Jorns MS (1992) Effect of 5-deazaflavin on energy transduction during catalysis by *Escherichia coli* DNA photolyase. *Biochemistry* **31**: 8437-8441
- Redman JE (2007) Surface plasmon resonance for probing quadruplex folding and interactions with proteins and small molecules. *Methods* **43**: 302-312
- Rupert CS (1962) Photoenzymatic repair of ultraviolet damage in DNA .I. Kinetics of reaction. *Journal of General Physiology* **45**: 703-724
- Rupert CS, Goodgal SH, Herriott RM (1958) Photoreactivation *in vitro* of ultraviolet inactivated *Hemophilus influenzae* transforming factor. *J. Gen. Physiol.* **41**: 451-471
- Sancar A (1994) Structure and function of DNA photolyase. *Biochemistry* **33**: 2-9
- Sancar A (2003) Structure and function of DNA photolyase and cryptochrome blue-light photoreceptors. *Chemical Reviews* **103**: 2203-2237
- Sancar A (2008) Structure and Function of Photolyase and *in Vivo* Enzymology: 50th Anniversary. *J. Biol. Chem.* **283**: 32153-32157
- Sancar A, Sancar GB (1988) DNA-repair enzymes. *Annual Review of Biochemistry* **57**: 29-67
- Sancar GB (1990) DNA photolyases - physical-properties, action mechanism, and roles in dark repair. *Mutation Research* **236**: 147-160
- Sancar GB, Jorns MS, Payne G, Fluke DJ, Rupert CS, Sancar A (1987a) Action mechanism of *Escherichia coli* DNA photolyase .3. Photolysis of the enzyme-substrate complex and the absolute action spectrum. *J. Biol. Chem.* **262**: 492-498
- Sancar GB, Smith FW, Reid R, Payne G, Levy M, Sancar A (1987b) action mechanism *Escherichia coli* DNA photolyase.1. Formation of the enzyme-substrate complex. *J. Biol. Chem.* **262**: 478-485
- Sancar GB, Smith FW, Sancar A (1985) Binding of *Escherichia coli* DNA photolyase to UV-irradiated DNA. *Biochemistry* **24**: 1849-1855
- Scharer OD (2003) Chemistry and biology of DNA repair. *Angew. Chem. Int. Ed.* **42**: 2946-2974

- Schleicher E, Hessling B, Illarionova V, Bacher A, Weber S, Richter G, Gerwert K (2005) Light-induced reactions of *Escherichia coli* DNA photolyase monitored by Fourier transform infrared spectroscopy. *FEBS J.* **272**: 1855-1866
- Schwinefus JJ, Bloomfield VA (2000) The greater negative charge density of DNA in Tris-borate buffers does not enhance DNA condensation by multivalent cations. *Biopolymers* **54**: 572-577
- Seeberg E, Eide L, Bjoras M (1995) The base excision-repair pathway. *Trends Biochem. Sci.* **20**: 391-397
- Setlow RB, Carrier WL (1966) Pyrimidine dimers in ultraviolet-irradiated DNAs. *J. Mol. Biol.* **17**: 237-&
- Srinivasan V, Schnitzlein WM, Tripathy DN (2001) Fowlpox virus encodes a novel DNA repair enzyme, CPD-photolyase, that restores infectivity of UV light-damaged virus. *J. Viro.* **75**: 1681-1688
- Takahashi S, Nakajima N, Saji H, Kondo N (2002) Diurnal change of cucumber CPD photolyase gene (CsPHR) expression and its physiological role in growth under UV-B irradiation. *Plant and Cell Physiology* **43**: 342-349
- Tamada T, Kitadokoro K, Higuchi Y, Inaka K, Yasui A, deRuiter PE, Eker APM, Miki K (1997) Crystal structure of DNA photolyase from *Anacystis nidulans*. *Nature Structural Biology* **4**: 887-891
- van Oers MM, Lampen MH, Bajek MI, Vlak JM, Eker APM (2008) Active DNA photolyase encoded by a baculovirus from the insect *Chrysodeixis chalcites*. *DNA Repair* **7**: 1309-1318
- Varghese AJ, Wang SY (1967) Ultraviolet irradiation of DNA *in vitro* and *in vivo* produces a 3rd thymine-derived product. *Science* **156**: 955-957
- Wang CI, Taylor JS (1992) *In vitro* evidence that UV-induced frameshift and substitution mutations at T-tracts are the result of misalignment-mediated replication past a specific thymine dimer. *Biochemistry* **31**: 3671-3681
- Weber S (2005) Light-driven enzymatic catalysis of DNA repair: a review of recent biophysical studies on photolyase. *Biochim. Biophys. Acta, Bioenerg.* **1707**: 1-23
- Weber S, Mobius K, Richter G, Kay CWM (2001a) The electronic structure of the flavin cofactor in DNA photolyase. *J. Am. Chem. Soc.* **123**: 3790-3798
- Weber S, Richter G, Schleicher E, Bacher A, Mobius K, Kay CWM (2001b) Substrate binding to DNA photolyase studied by electron paramagnetic resonance spectroscopy. *Biophys. J.* **81**: 1195-1204
- Welsh KM, Lu AL, Clark S, Modrich P (1987) Isolation and characterization of the *Escherichia coli* muth gene-product. *J. Biol. Chem.* **262**: 15624-15629

Xu L, Mu WM, Ding YW, Luo ZF, Han QK, Bi FY, Wang YZ, Song QH (2008) Active site of *Escherichia coli* DNA photolyase: Asn378 is crucial both for stabilizing the neutral flavin radical cofactor and for DNA repair. *Biochemistry* **47**: 8736-8743

Xu L, Zhang DF, Mu WM, van Berkel WJH, Luo ZF (2006) Reversible resolution of flavin and pterin cofactors of His-tagged *Escherichia coli* DNA photolyase. *Biochim. Biophys. Acta, Proteins Proteomics* **1764**: 1454-1461

Yajima H, Inoue H, Oikawa A, Yasui A (1991) Cloning and functional characterization of a eukaryotic DNA photolyase gene from *Neurospora crassa*. *Nucleic Acids Res.* **19**: 5359-5362

Yasuhira S, Yasui A (1992) Visible light-inducible photolyase gene from the goldfish *Carassius auratus*. *J. Biol. Chem.* **267**: 25644-25647

Yasui A, Eker APM, Yasuhira S, Yajima H, Kobayashi T, Takao M, Oikawa A (1994) A new class of DNA photolyases present in various organisms including aplacental mammals. *EMBO J.* **13**: 6143-6151

Yasui A, Laskowski W (1975) Determination of number of photoreactivating enzyme molecules per haploid *Saccharomyces* cell. *Int. J. Radiat. Biol.* **28**: 511-518

